2014 Spring

"Advanced Physical Metallurgy"

- Bulk Metallic Glasses -

06.12.2014

Eun Soo Park

Office: 33-313
Telephone: 880-7221
Email: espark@snu.ac.kr
Office hours: by appointment

8.2 Deformation Behavior

Deformation behavior of Metallic glass

8.2.2 Homogeneous Deformation

- high temp. (>$0.7T_g$) and in the SCLR/ high strain rate
- Viscous flow → significant plasticity

  : achieve net-shape forming capability
- Newtonian (high temp. & low stress) vs non-Newtonian (high temp. & applied stress) : associated with the precipitation of nanocrystals

⇩

Homogeneous deformation

8.2.1 Inhomogeneous Deformation

- Low temp. (<$0.5T_g$)/ high stress
- Localized shear band/ 45° to the loading axis
- Strain softening: deformed at lower stress and higher rate

⇩

Catastrophically Failure

Flow Mechanisms

❖ Basic Modes of Deformation

- Homogeneous Flow
  - Each volume element undergoes the same strain.

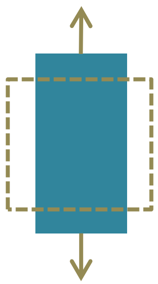

- Inhomogeneous Flow
  - Strain is concentrated in a few thin shear bands.

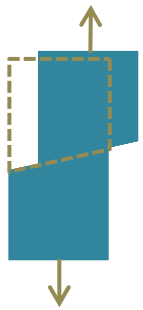

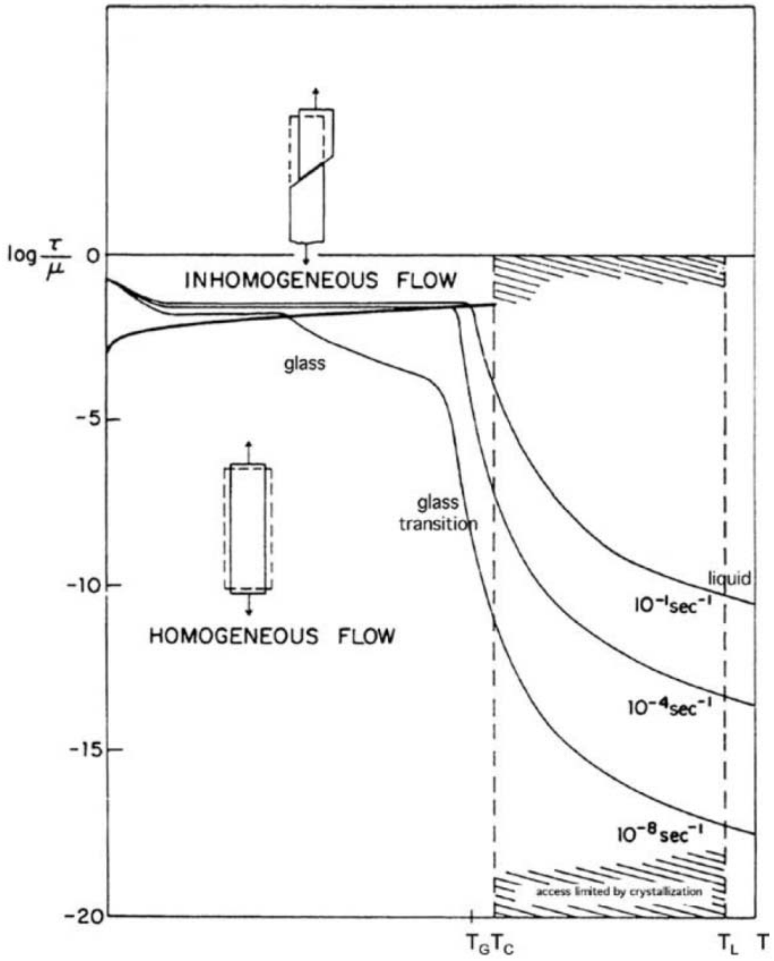

Fig. 1. Deformation mechanism map for a metallic glass.

Homogeneous deformation: Liquid Flow

❖ Liquid Region (above and near T_g)

- Homogeneous Flow
- Low stress in liquid region
- Strain rate is proportional to the stress
- Viscosity is not dependent on stress, but temperature.

$$\sinh\left[\frac{\varepsilon_0 v_0 \sigma}{2kT}\right] \approx \frac{\varepsilon_0 v_0 \sigma}{2kT} \quad \text{@ low stress}$$

- Newtonian Viscous Flow

$$\underbrace{\tau}_{\text{Shear stress}} = \underbrace{\boxed{\eta}}_{\text{Viscosity}} \cdot \underbrace{\dot{\gamma}}_{\text{Strain rate}}$$

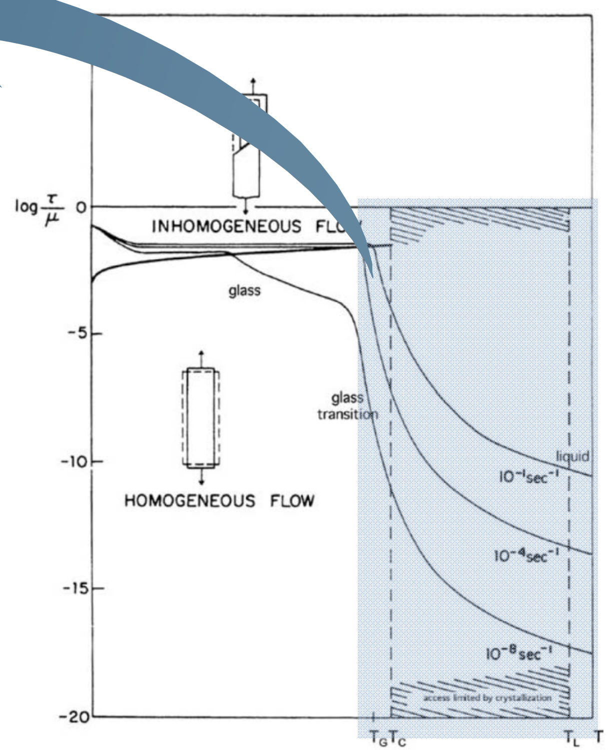

Fig. 1. Deformation mechanism map for a metallic glass.

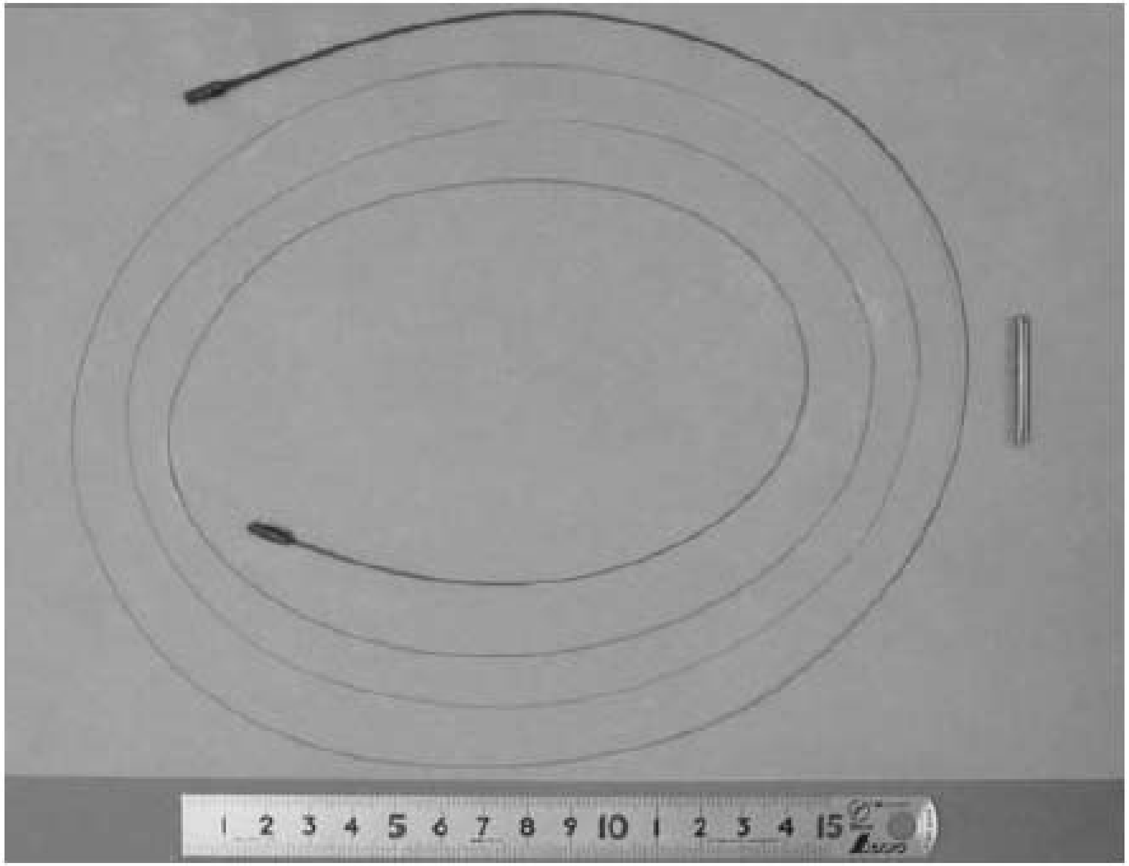

FIGURE 8.17
Extended elongation in a 3mm diameter BMG rod of $La_{55}Al_{25}Ni_{20}$ alloy superplastically deformed in the supercooled liquid region at 500K and a strain rate of $10^{-1} s^{-1}$.

Inhomogeneous deformation:
Deformation-induced Softening

- Softening : Lowering of viscosity in the shear bands

- Structural Change : Creation of free volume due to high stress level

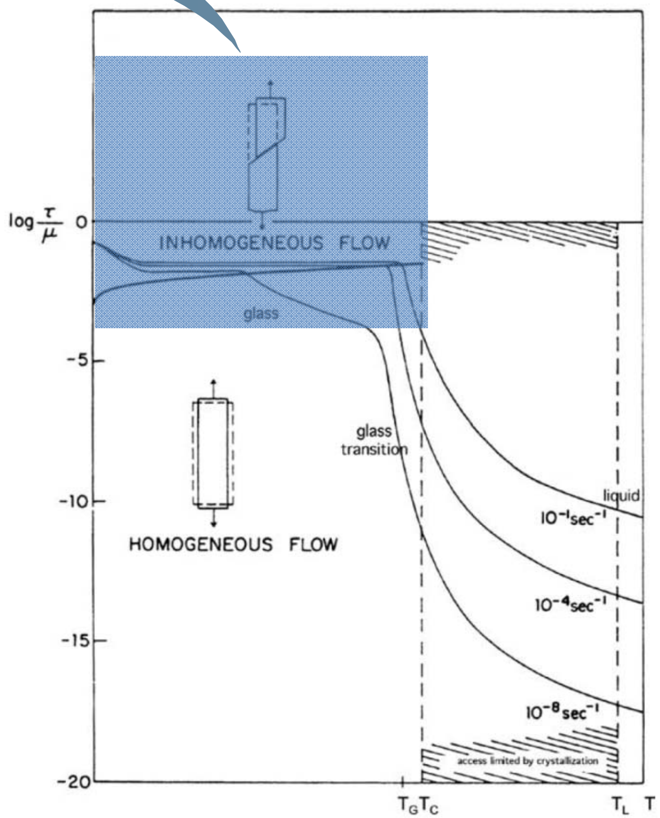

Fig. 1. Deformation mechanism map for a metallic glass.

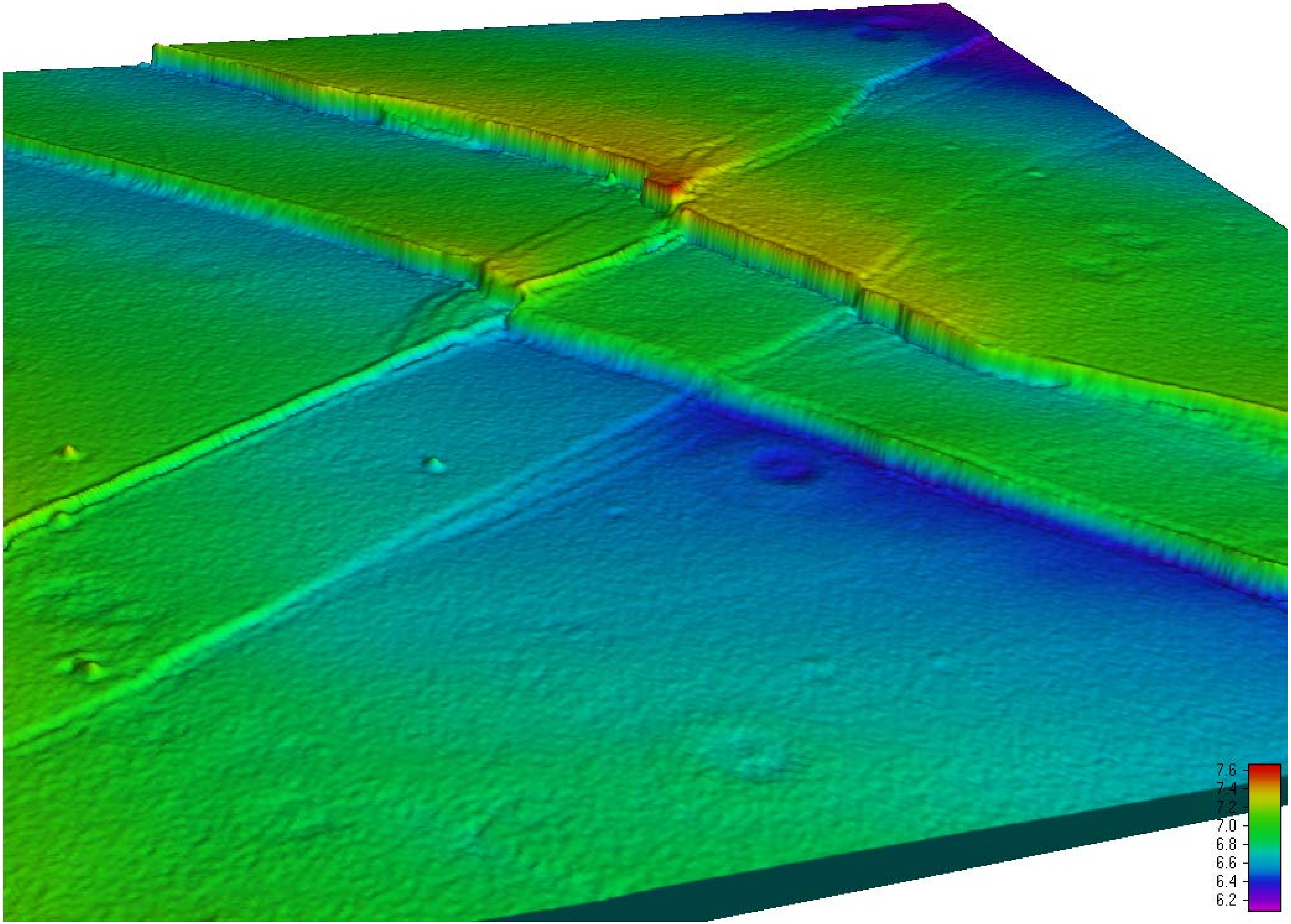
7.6
7.4
7.2
7.0
6.8
6.6
6.4
6.2

SB nucleation and propagation : Multiple serrations, observed only at slow strain rates

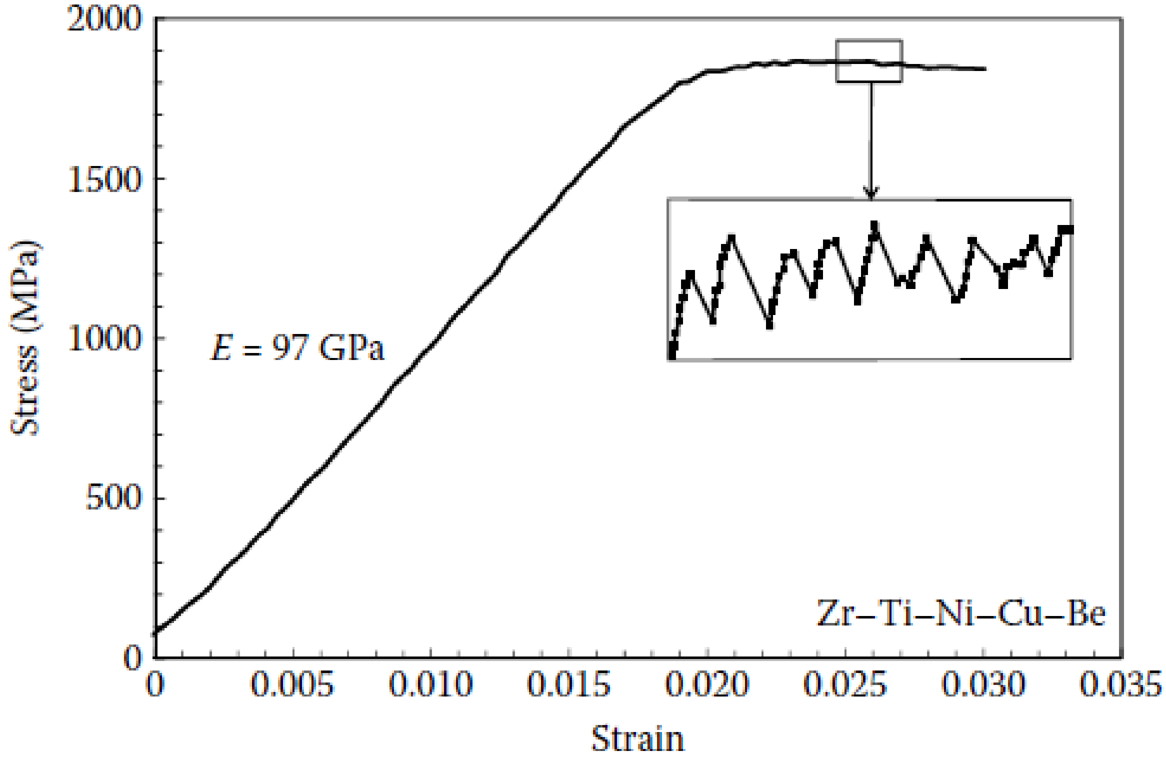

FIGURE 8.1
Compressive stress–strain curve for $Zr_{40}Ti_{14}Ni_{10}Cu_{12}Be_{24}$ BMG alloy tested at a strain rate of $1 \times 10^{-4} s^{-1}$. (Reprinted from Wright, W.J. et al., *Mater. Trans.*, 42, 642, 2001. With permission.)

8.4 Temperature rise at shear bands

Most of the plastic strain is localized in narrow shear bands, which form approximately on the planes of maximum resolved shear stress. The inhomogeneous flow in metallic glasses appears to be related to a local decrease in the viscosity in shear bands. One of the reasons suggested for this was the local adiabatic heating that could lead to a substantial increase in the temperature.

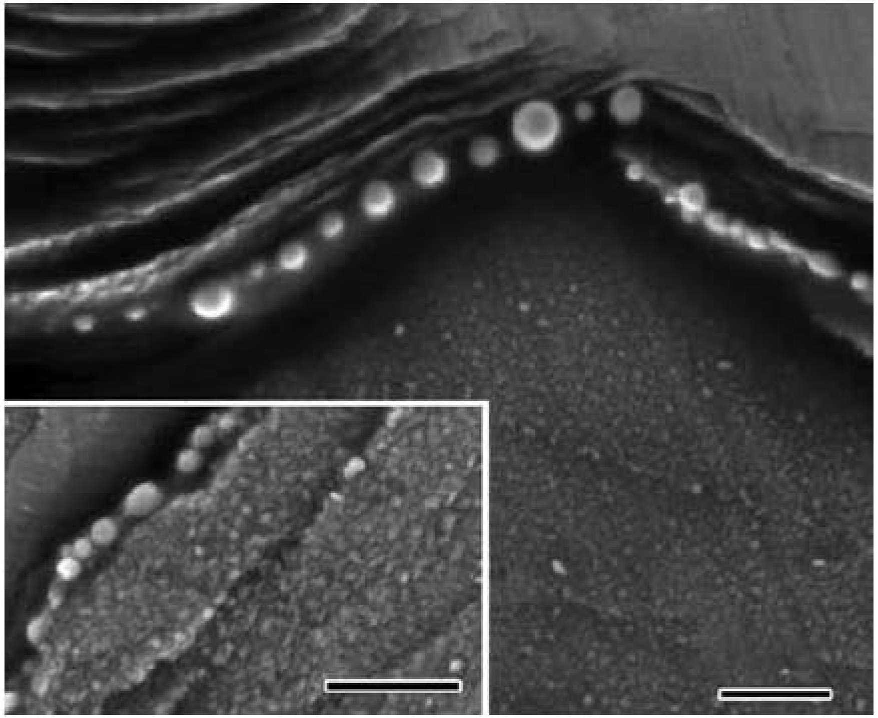

FIGURE 8.9
Scanning electron micrograph of the surface of $Zr_{41.2}Ti_{13.8}Cu_{12.5}Ni_{10}Be_{22.5}$ BMG, which was originally coated with a tin coating. During deformation, the "fusible coating" had melted near the shear bands. The round shape of the tin beads clearly suggests that the coating had melted due to the temperature rise as a result of deformation and had resolidified. The bar in the micrographs corresponds to 1 µm. (Reprinted from Lewandowski, J.J. and Greer, A.L., *Nat. Mater.*, 5, 15, 2006. With permission.)

8.4.1 Nanocrystallization near Shear Bands

TEM analysis after bend test in Al-based ribbon

* Compressive region of amorphous $Al_{90}Fe_5Gd_5$ (at - 40℃)

: A high density of nanocrystals is observed within shear bands.

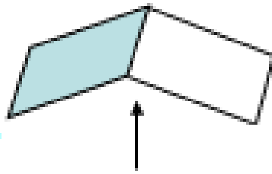

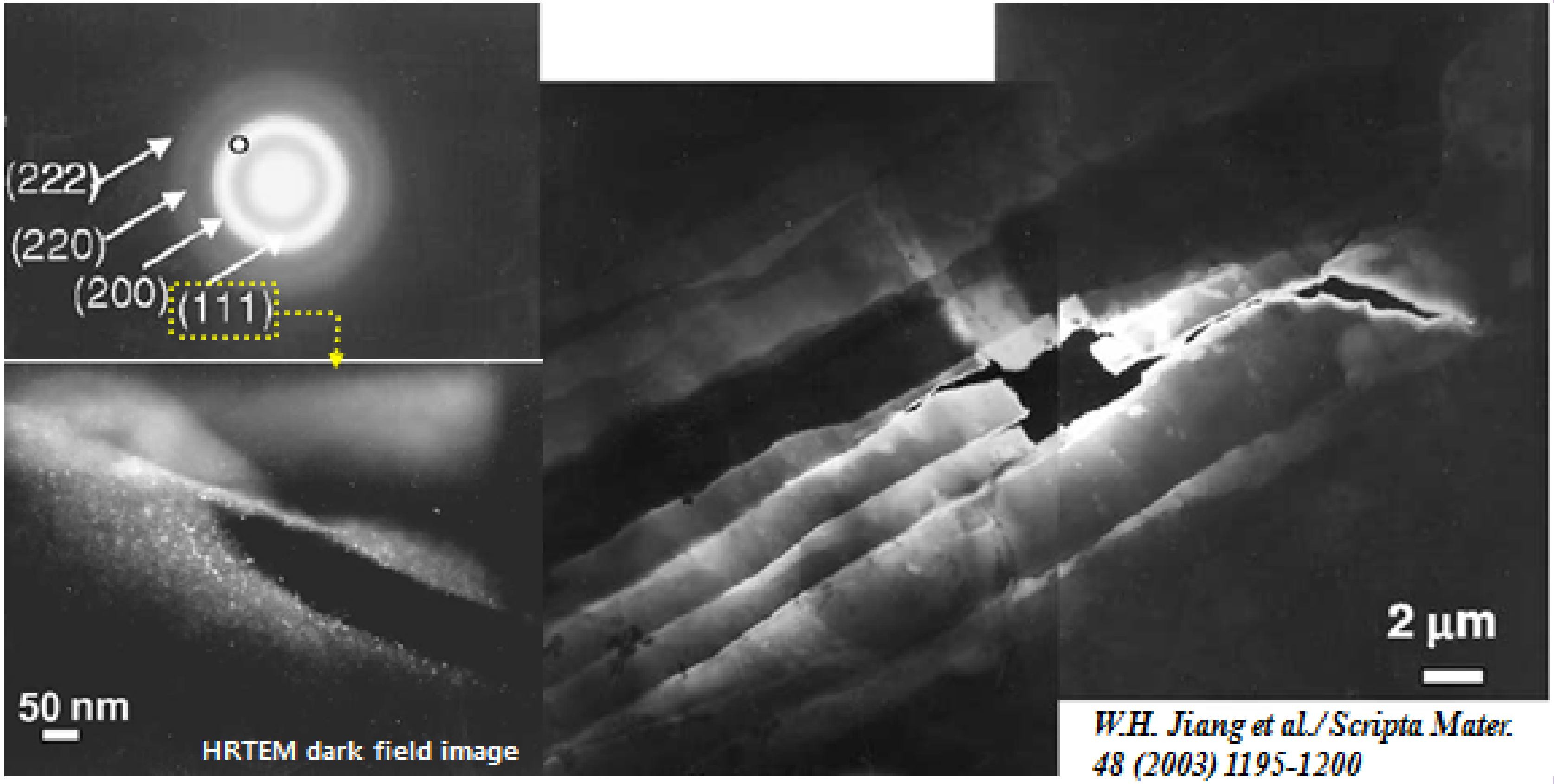

W.H. Jiang et al./Scripta Mater. 48 (2003) 1195-1200

Low GFA (unstable Amor. Matrix) ⇒ Severe plastic deformation ⇒ Precipitation of nanocrystals within shear bands

Atomic bond topology

Free volume theory ⟺ STZ model

F. Spaepen

Free volume theory

Homogeneous flow @ steady state

Inhomogeneous flow @ steady state

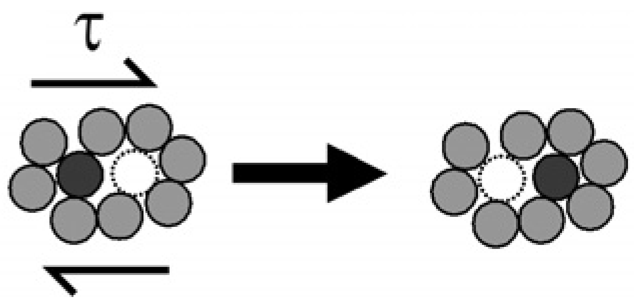

A. S. Argon

Shear transformation zone (STZ)

Homogeneous plastic flow | Steady / Non-steady

Inhomogeneous plastic flow

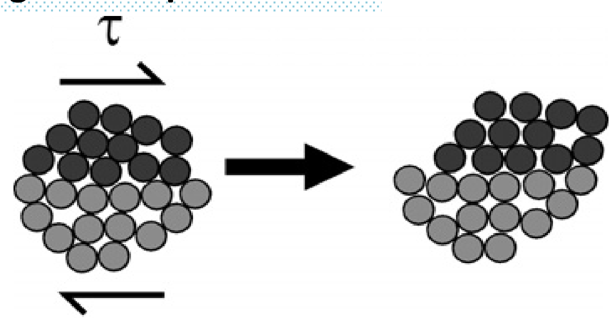

STZ: basic shear unit
(a few to perhaps up to 100 atoms)

T. Egami

Atomic bond topology

- **Network of atomic connectivity / topology of the atomic structure**
- **Bond-exchange mechanism of shear deformation**

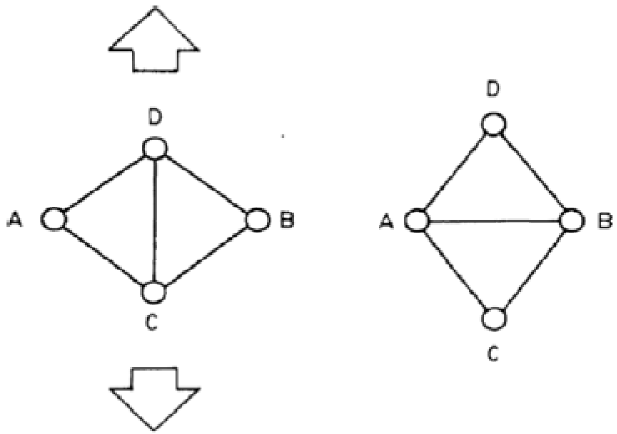

Deformation maps for metallic glasses

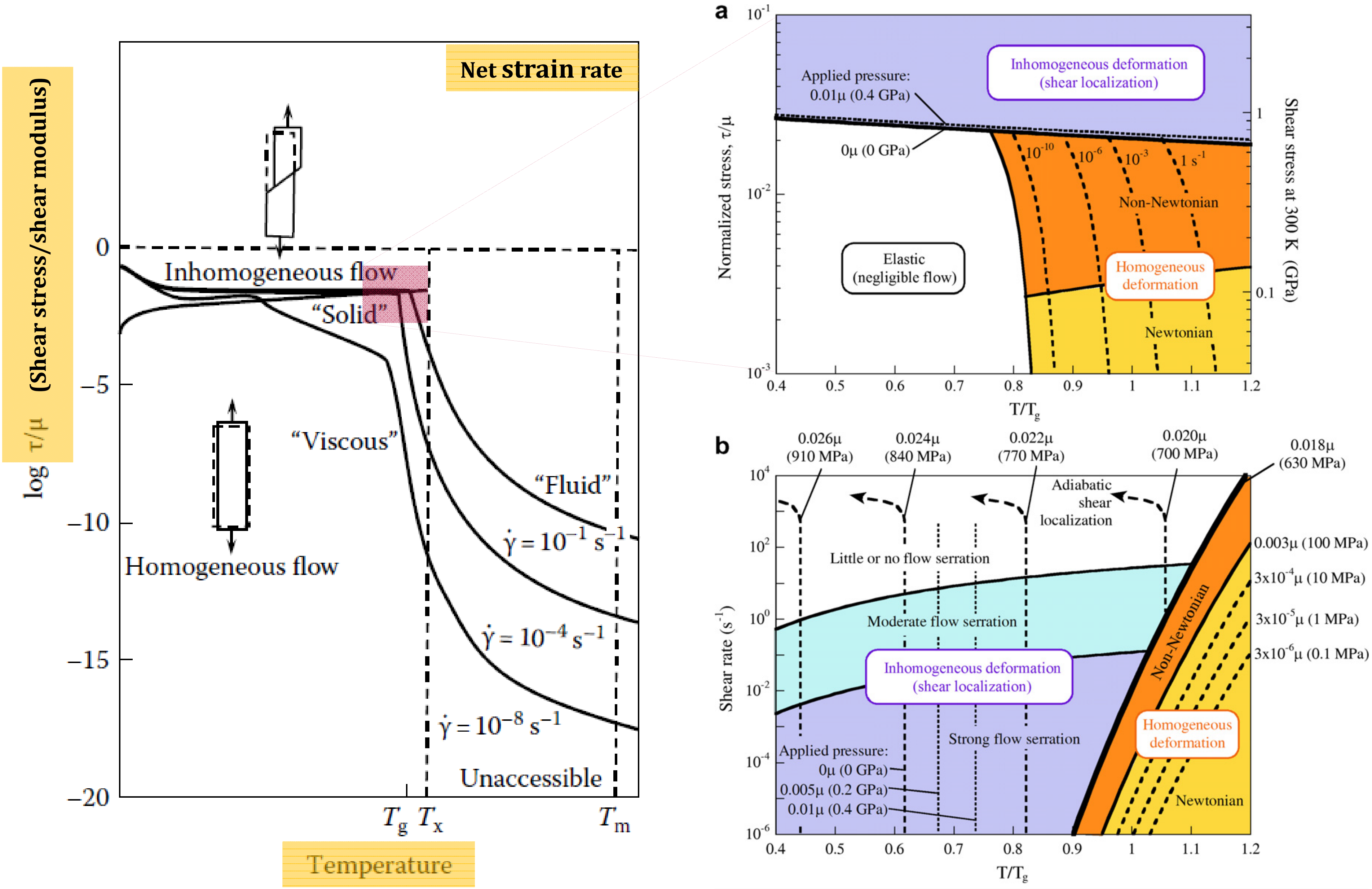

Thermal T_g vs Mechanical T_g for metallic glasses

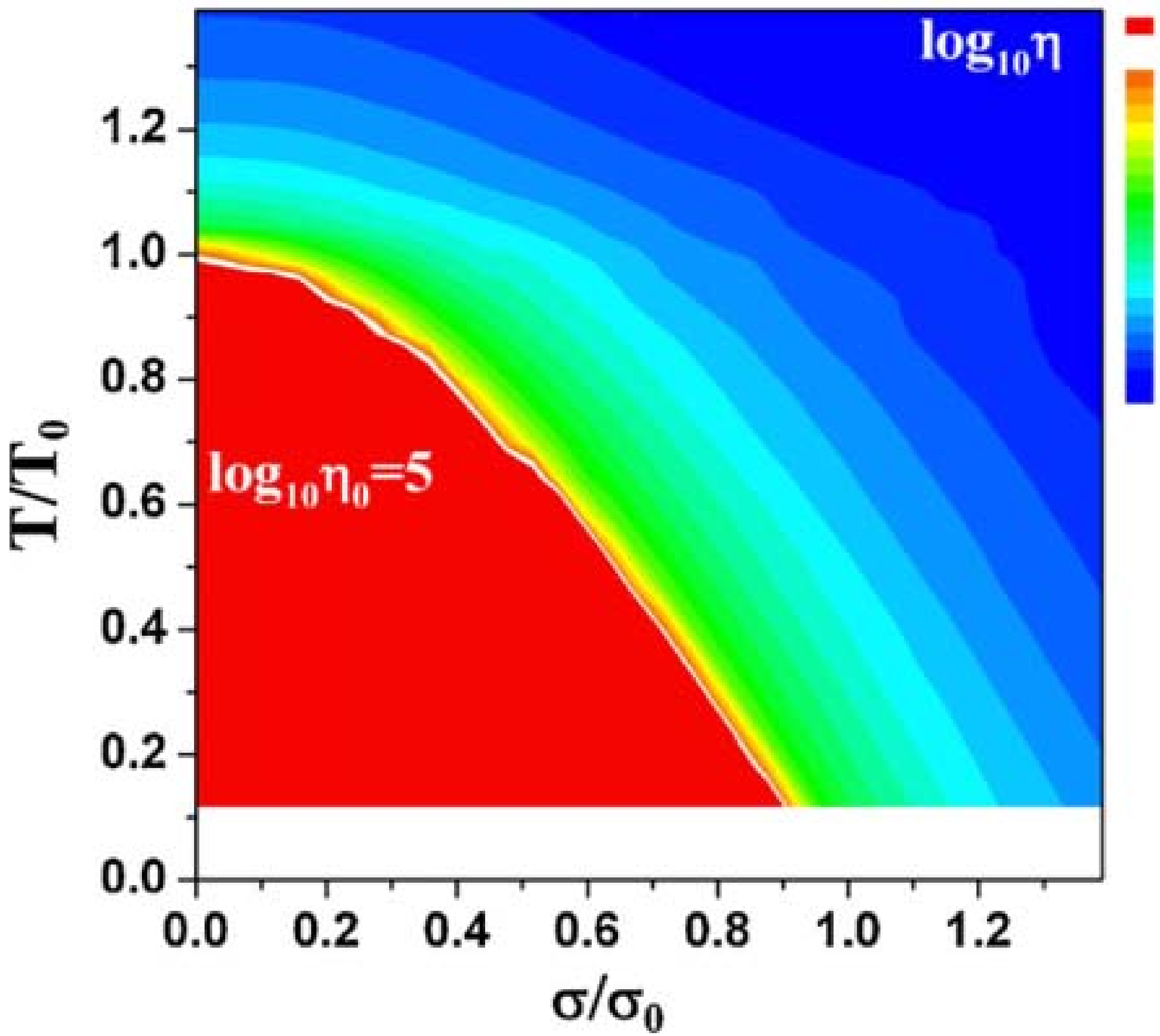

Limited Plasticity by shear softening and shear band

- Microscopically brittle fracture

  ➡ Death of a material for structural applications

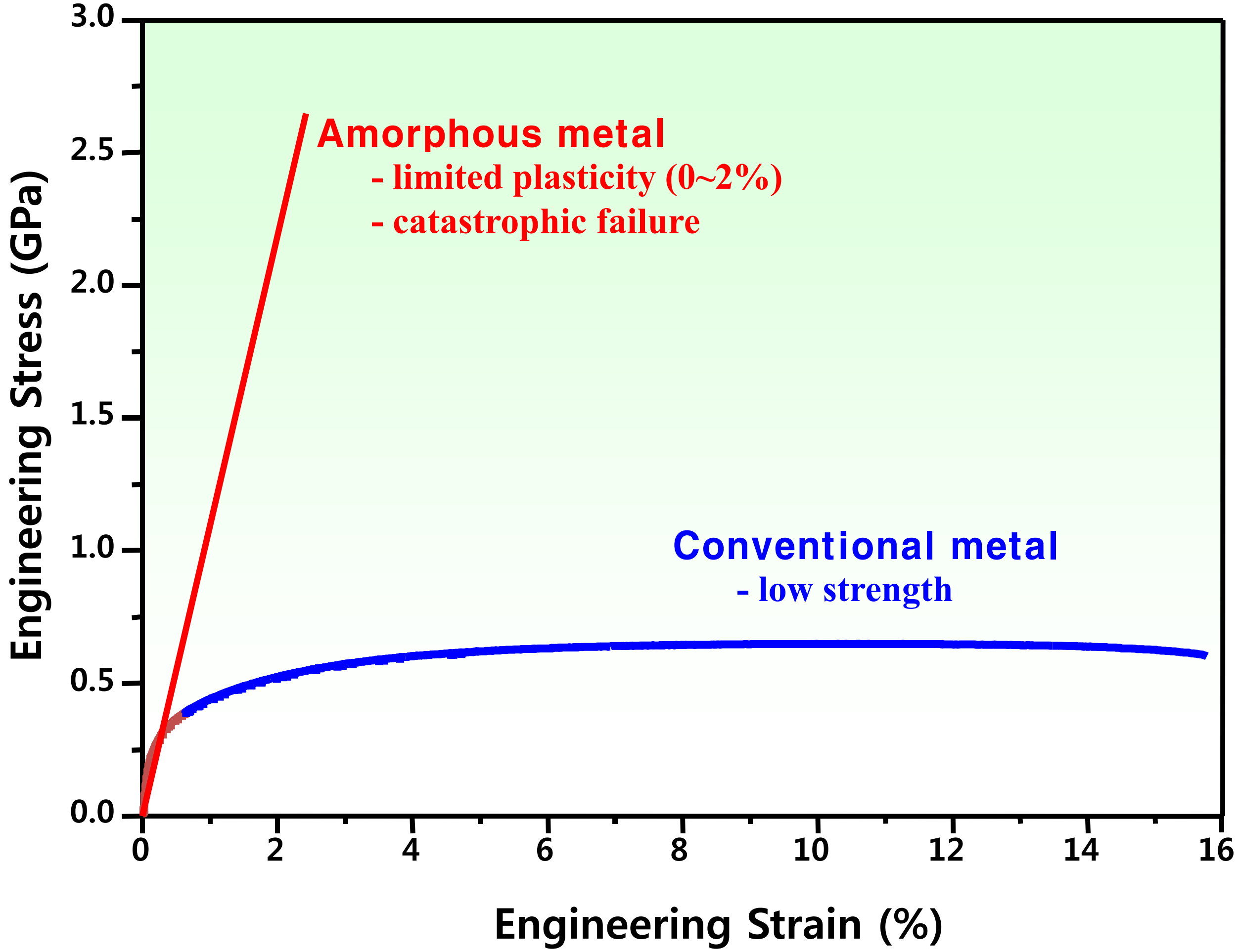

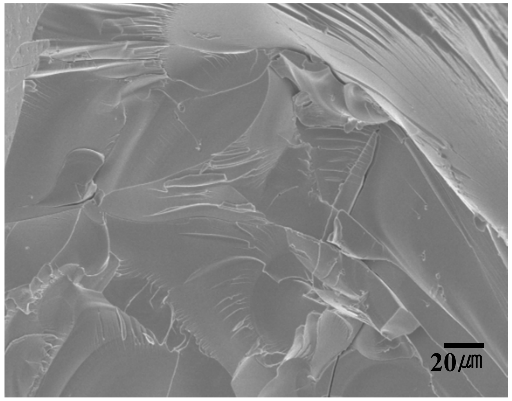

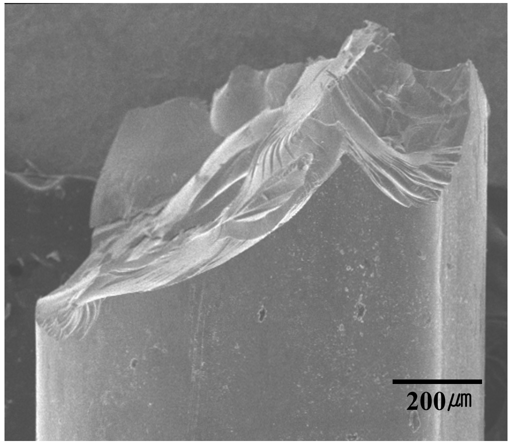

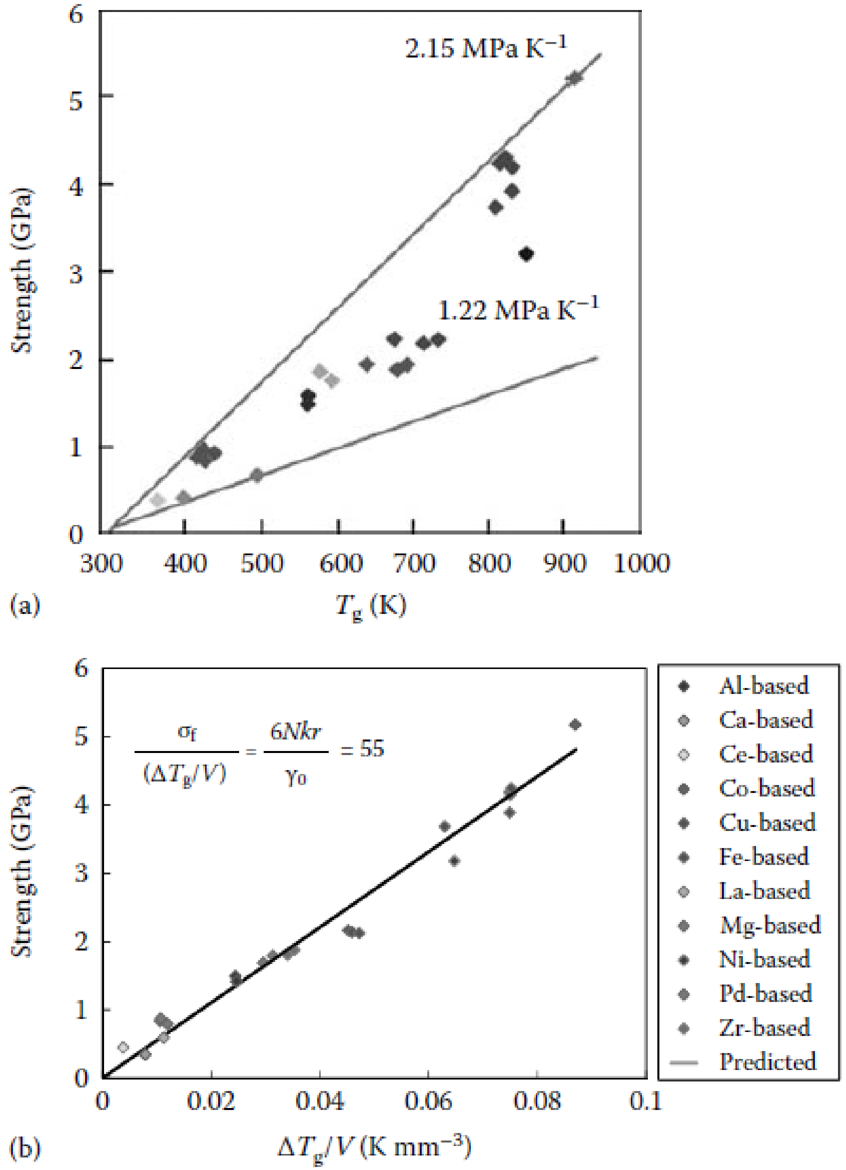

FIGURE 8.11
(a) Variation of strength with glass transition temperature, T_g for a number of BMGs. (b) Relationship between the calculated fracture strength from a free-volume model and the ratio of $\Delta T_g/V$ for a variety of BMGs. (Reprinted from Yang, B. et al., *Appl. Phys. Lett.*, 88, 221911-1, 2006. With permission.)

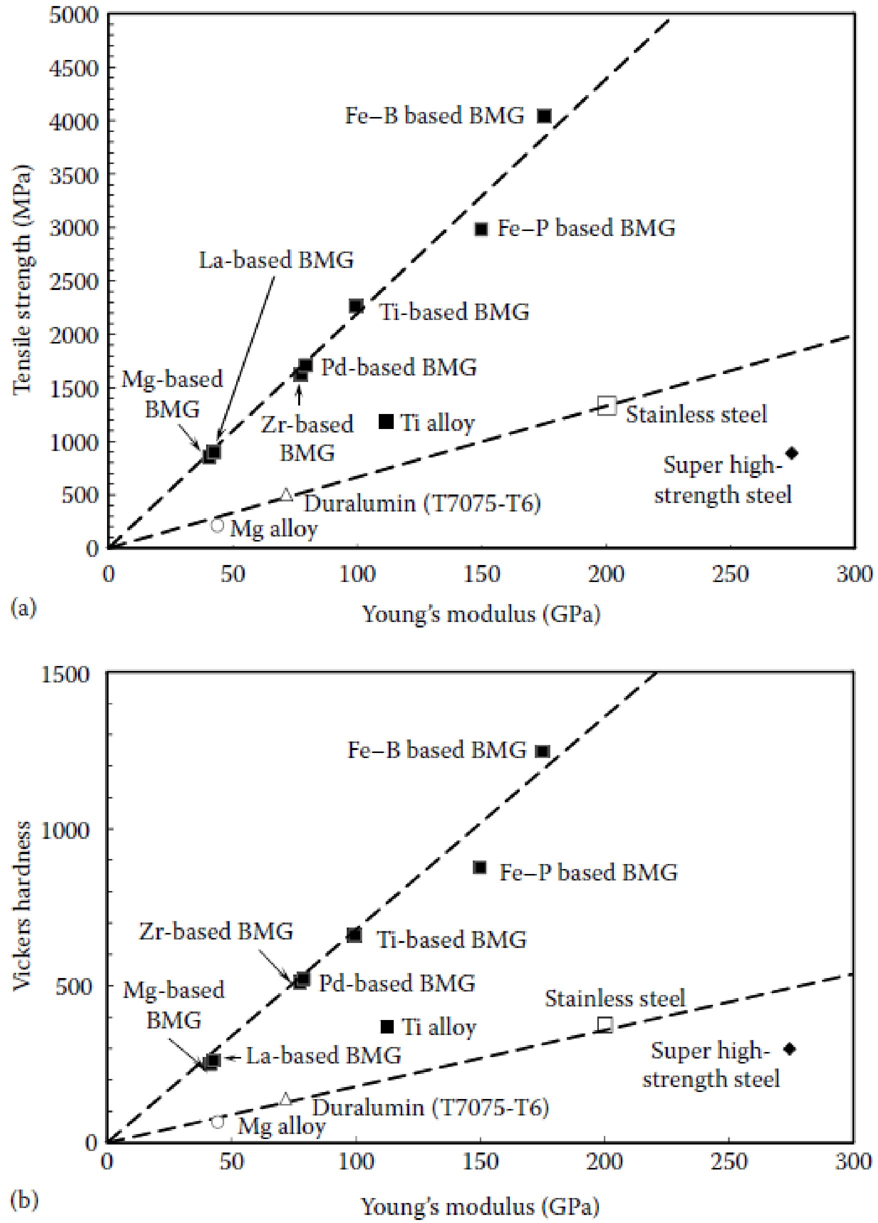

FIGURE 8.13
Relationship between (a) tensile strength and Young's modulus and (b) Vickers hardness and Young's modulus for some typical BMGs. The data for crystalline alloys are also shown for comparison. (Reprinted from Inoue, A., *Acta Mater.*, 48, 279, 2000. With permission.)

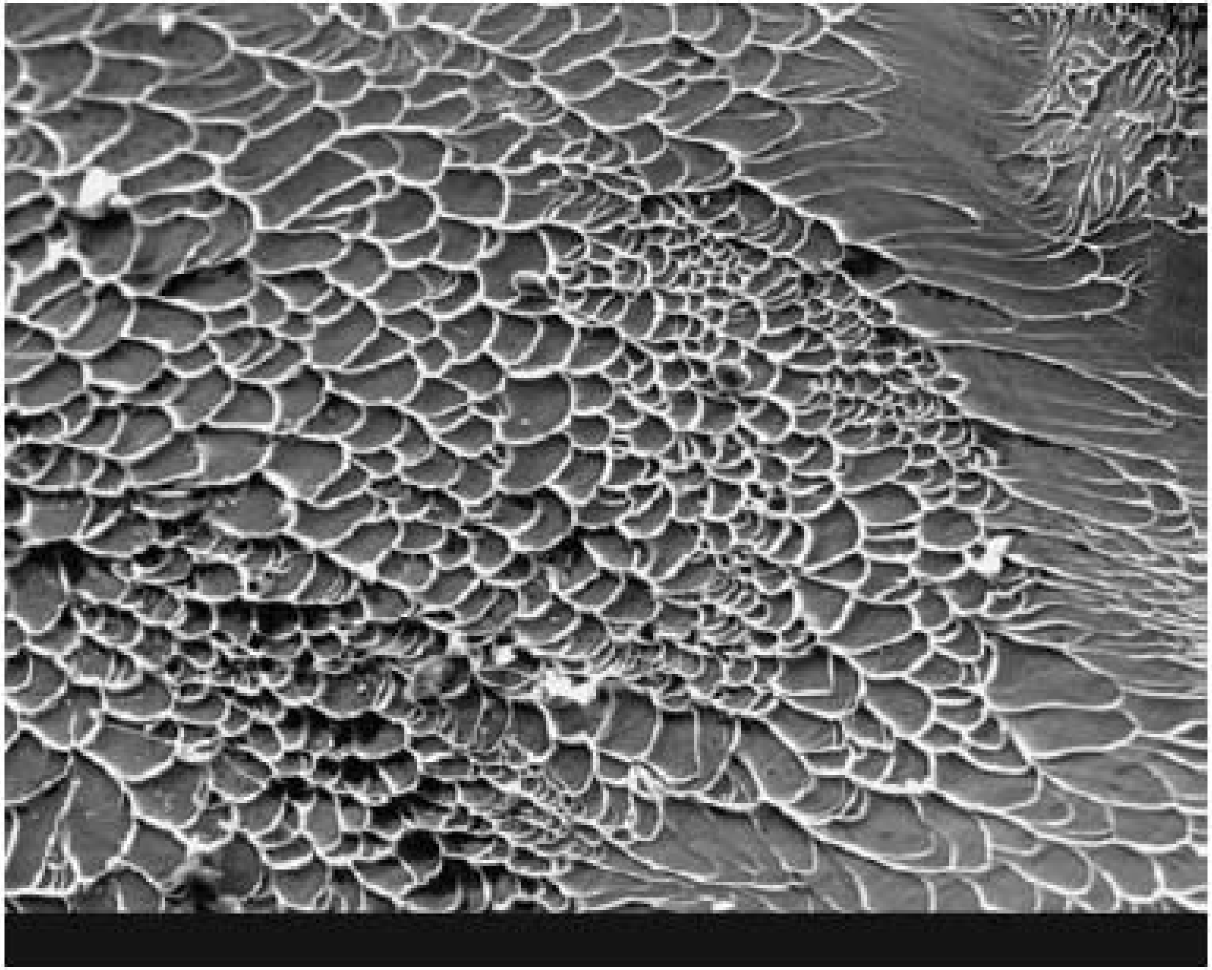

FIGURE 8.27
Scanning electron micrograph of the fractured surface of a bulk metallic glass alloy specimen. Note the vein pattern, which is typical of many metallic glasses that fracture along a shear band. Such microstructures are obtained both in tension and compression.

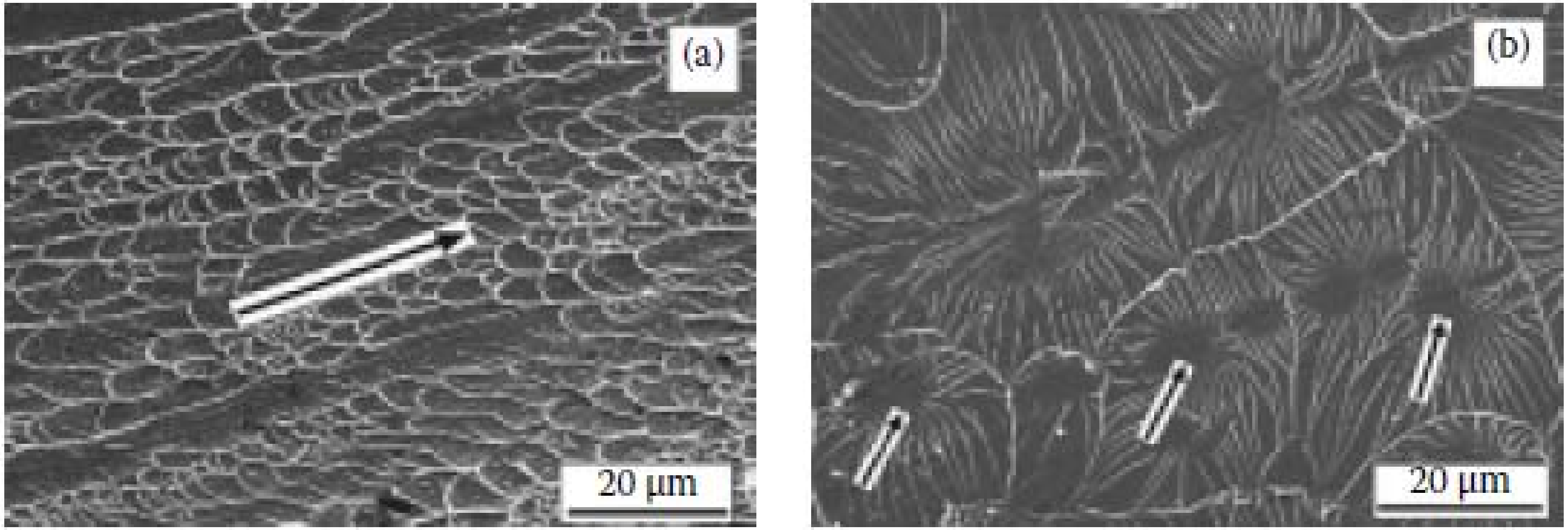

FIGURE 8.28
Comparison of the fracture surfaces of $Zr_{59}Cu_{20}Al_{10}Ni_8Ti_3$ BMG alloy that has failed under (a) compressive loading and (b) tensile loading. Notice that the specimen that has failed under compressive loading exhibits vein-like pattern while the specimen that had failed in tension shows round cores with vein-like features radiating outward from their centers. The arrow in (a) shows the shear direction, while the arrows in (b) indicate the location of the round cores. (Reprinted from Zhang, Z.F. et al., *Acta Mater.*, 51, 1167, 2003. With permission.)

What governs plasticity in metallic glasses?

Plastic deformation in metallic glasses

Plastic deformation in metallic glass

• *No* dislocation / *No* slip plane

• Inhomogeneously localized plastic flow in the shear band

interrupt the localization of stress and deformation

• Prevent propagation of single shear band ⇨ BMG matrix composites

• Multiple shear band formation

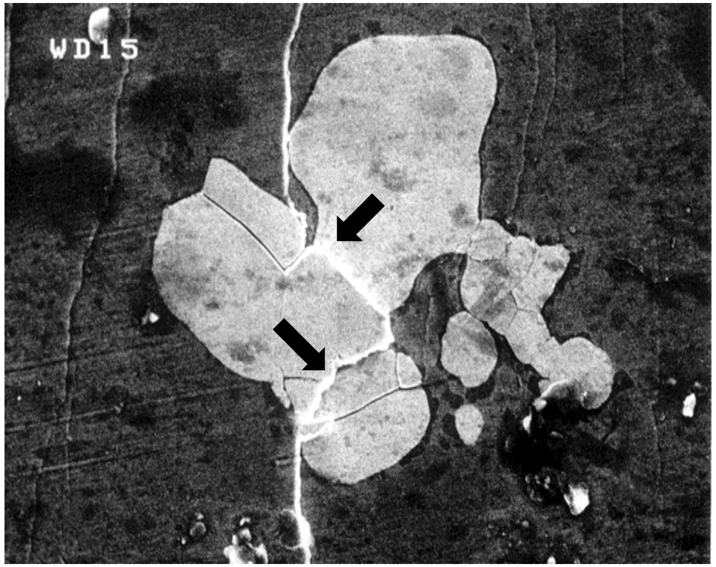

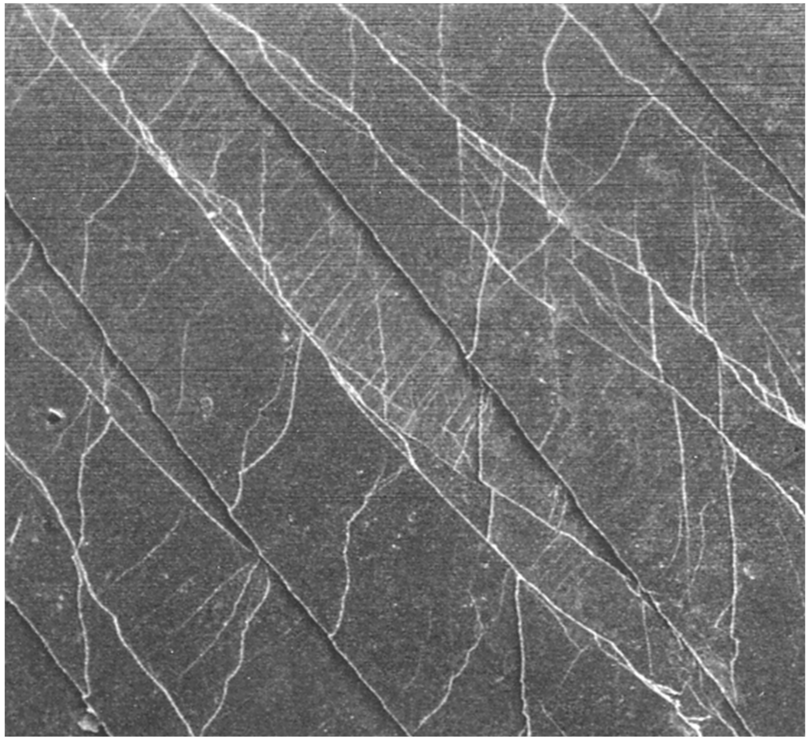

Ex-situ BMG matrix composites

1) Casting : hard/ductile particle

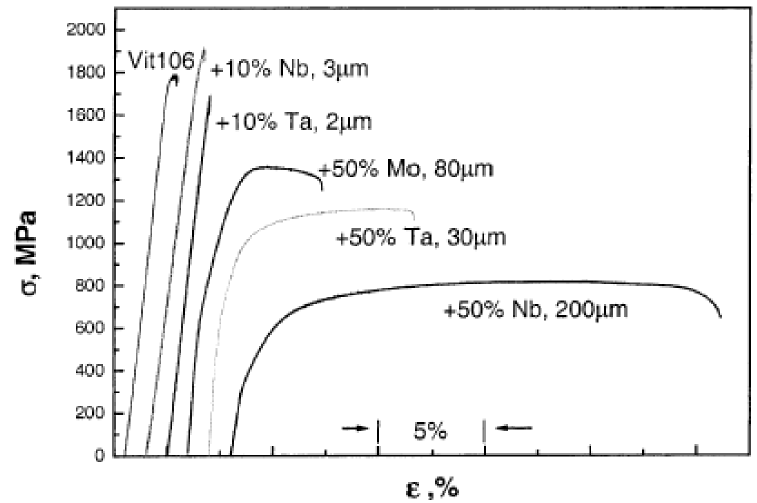

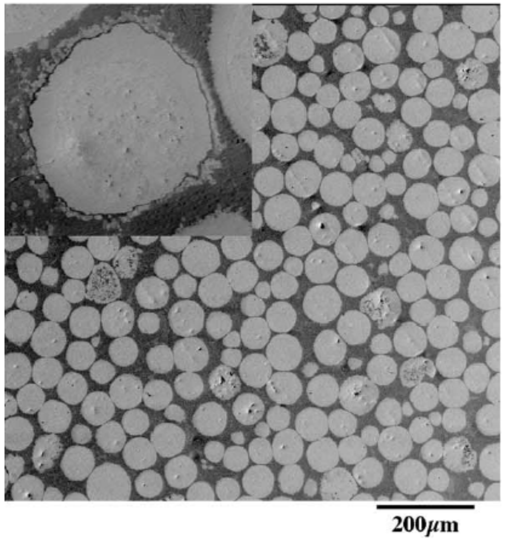

(Johnson et al., Acta Mater.,1999)

2) Extrusion : ductile powder

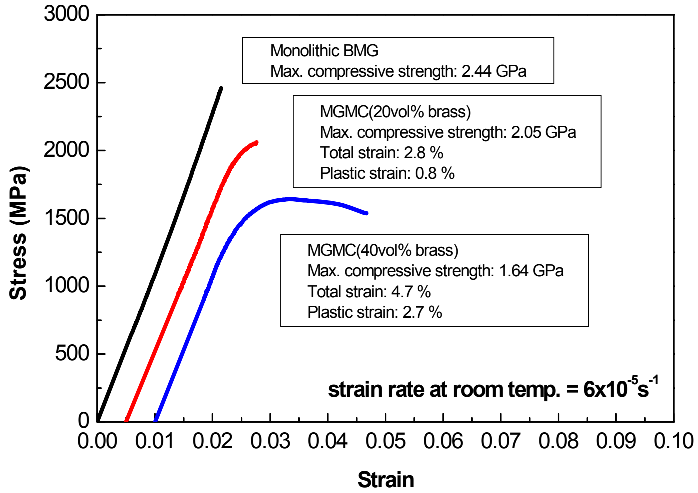

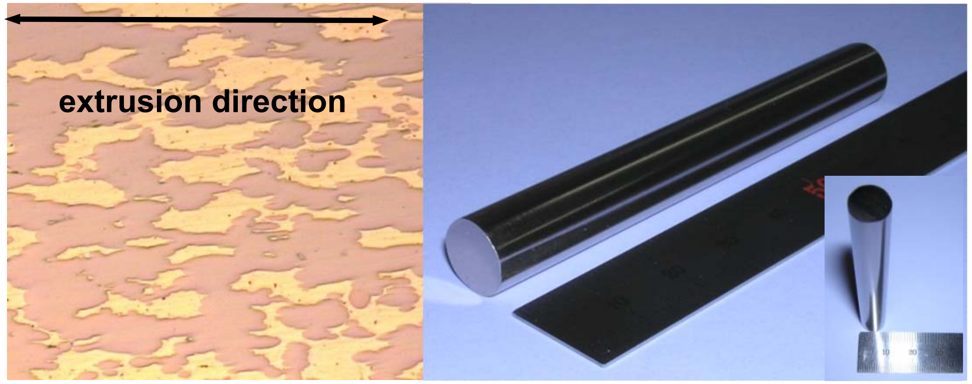

(Kim et al., J. Non-cryst. Solids, 2002)

In-situ BMG matrix composites

1) Solidification : formation of primary ductile phase

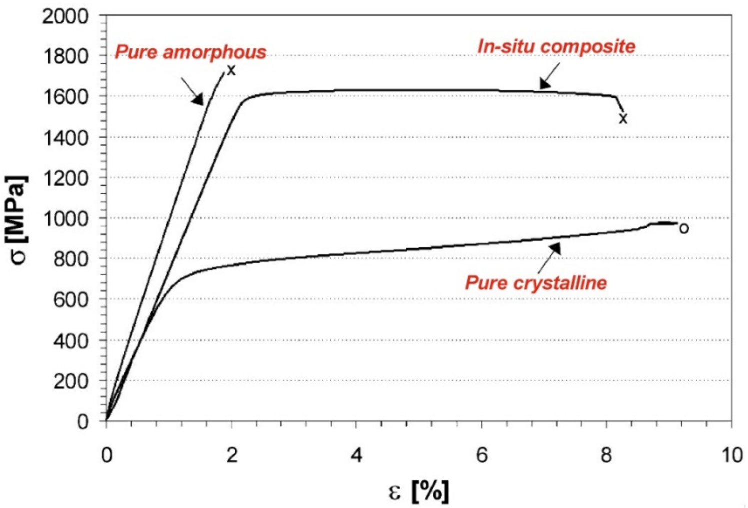

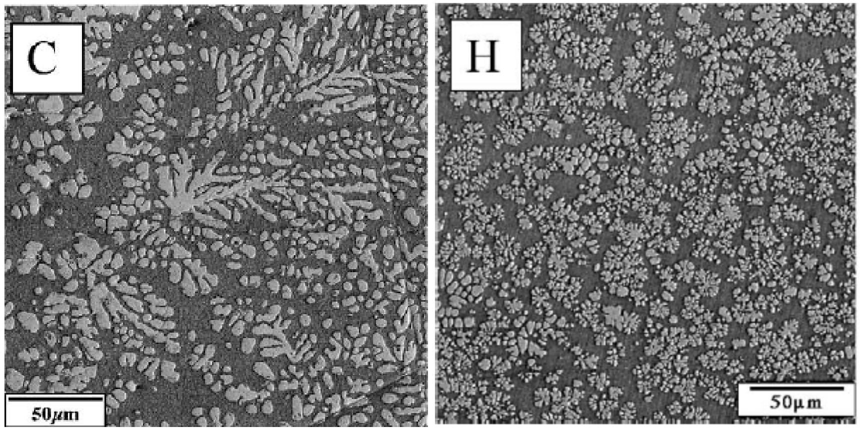

(Johnson et al., Acta Mater., 2001)

2) Solidification : precipitation of ductile phase

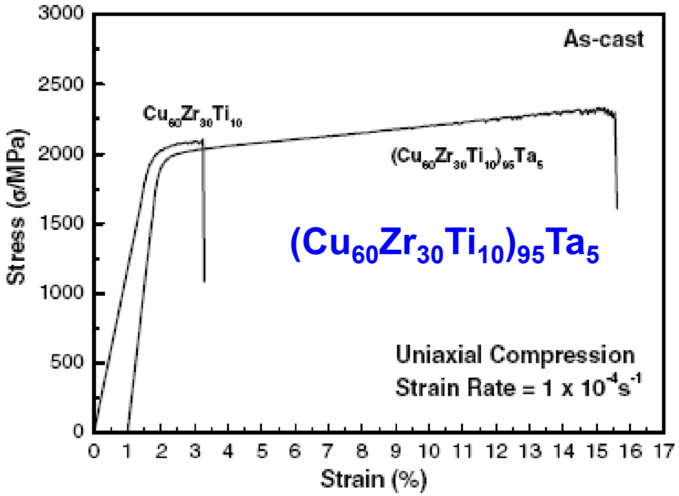

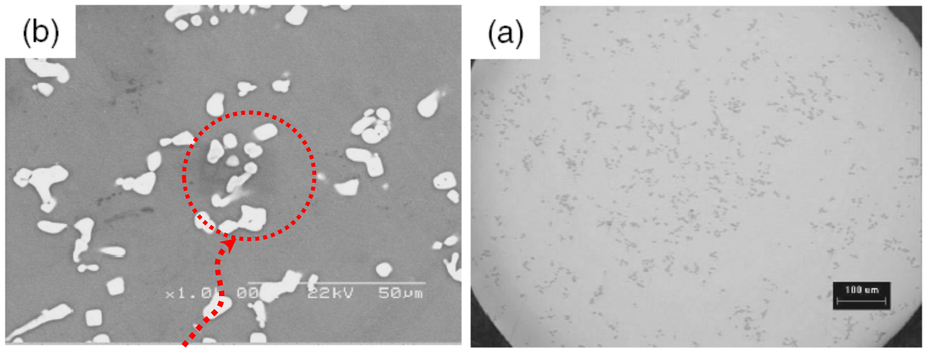

Ta rich particle

(Johnson et al., Acta Mater., 2001)

Size of heterogeneity

Shear bands are ~20 nm in width

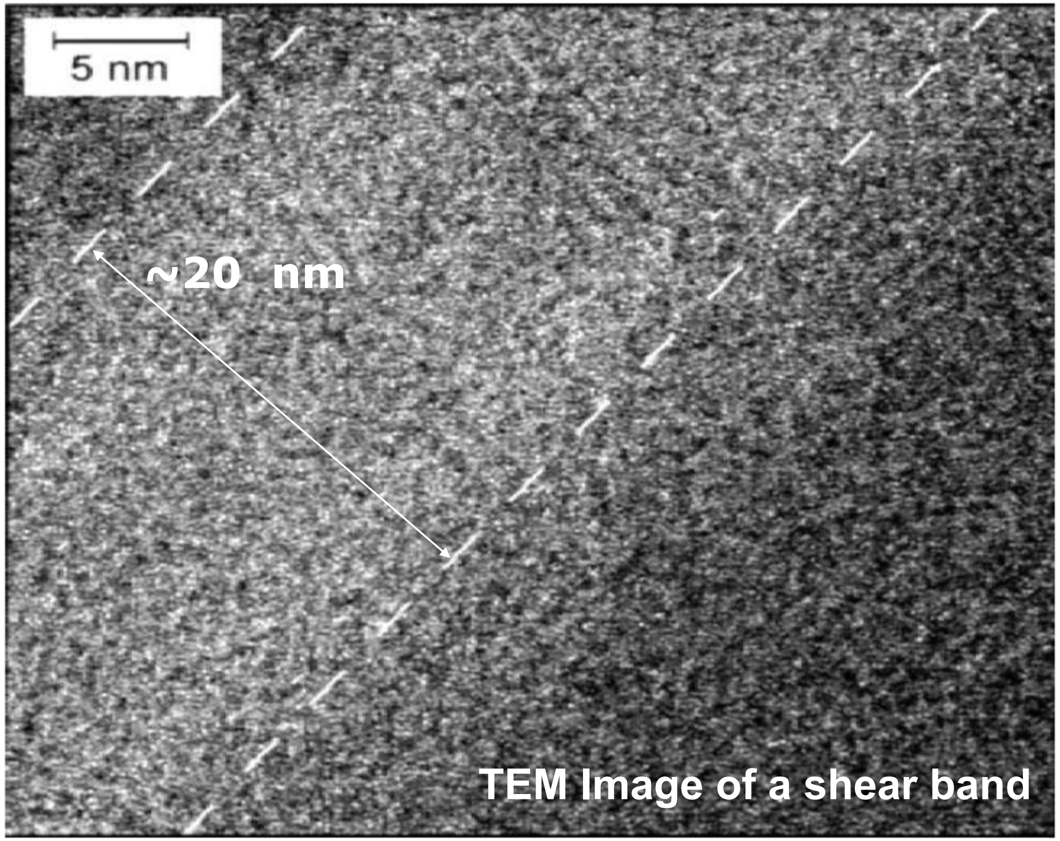

- **Prevent propagation of single shear band**

➡ **Micro- or nanometer scale heterogeneity**

Size of heterogeneity

- Elementary flow event in an metallic glasses

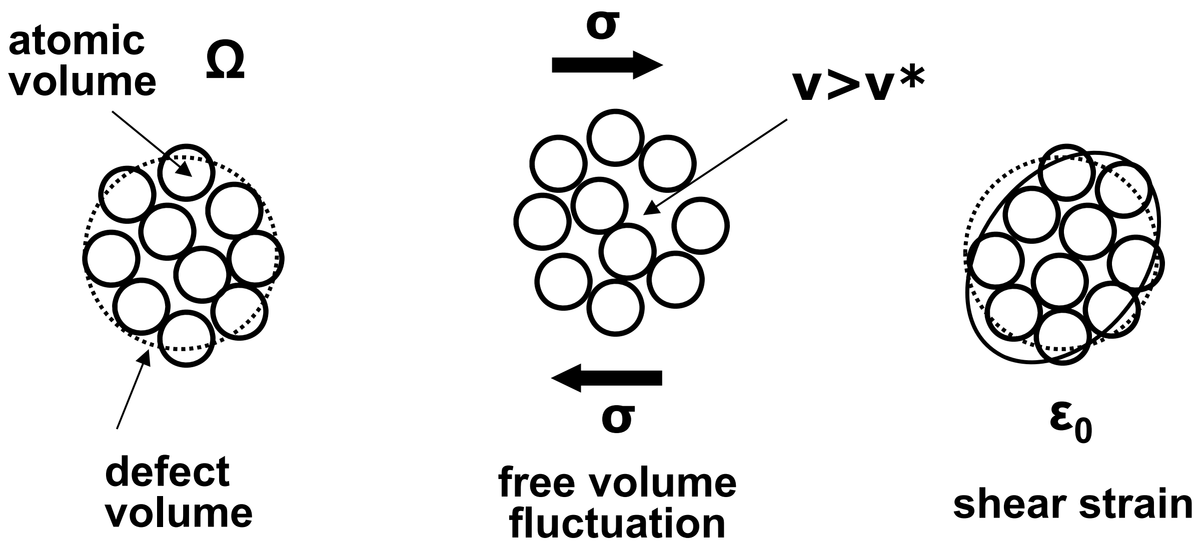

Probability $\exp(A\frac{v^*}{v_f})$

average free volume

Flow governed by localized defect (~10 atoms) and creates defects

atomic scale heterogeneity ⇒

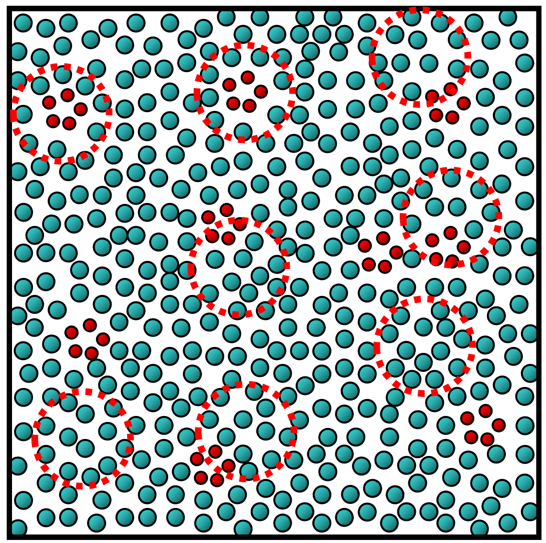

$$\eta = \eta_0 \exp\left\{ A\frac{V_0}{V_f} \right\}$$

Plastic deformation in metallic glasses

- Flow governed by localized defect (~10 atoms)

- Flow creates defects

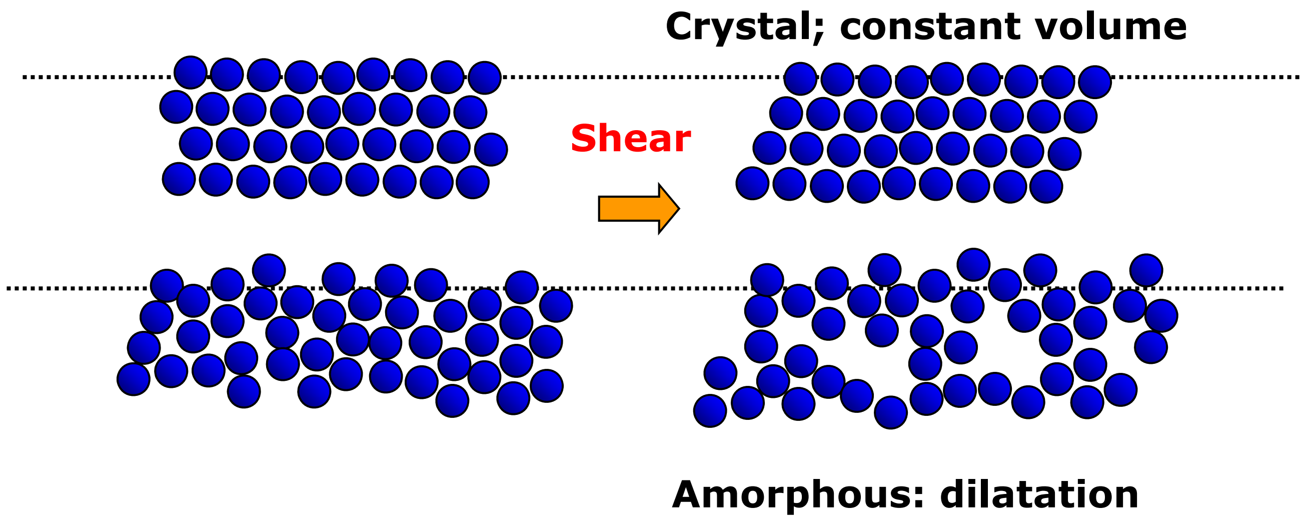

- Shear bands form by accumulation of defects

Understanding how shear bands form and propagate in metallic glasses

Fragility

- **Fragility ~ extensively use to figure out liquid dynamics and glass properties corresponding to "frozen" liquid state**

< Classification of glass >

Strong network glass **: Arrhenius behavior**

$$\eta = \eta_0 \exp[\frac{E_a}{RT}]$$

Fragile network glass **: Vogel-Fulcher relation**

$$\eta = \eta_0 \exp[\frac{B}{T - T_0}]$$

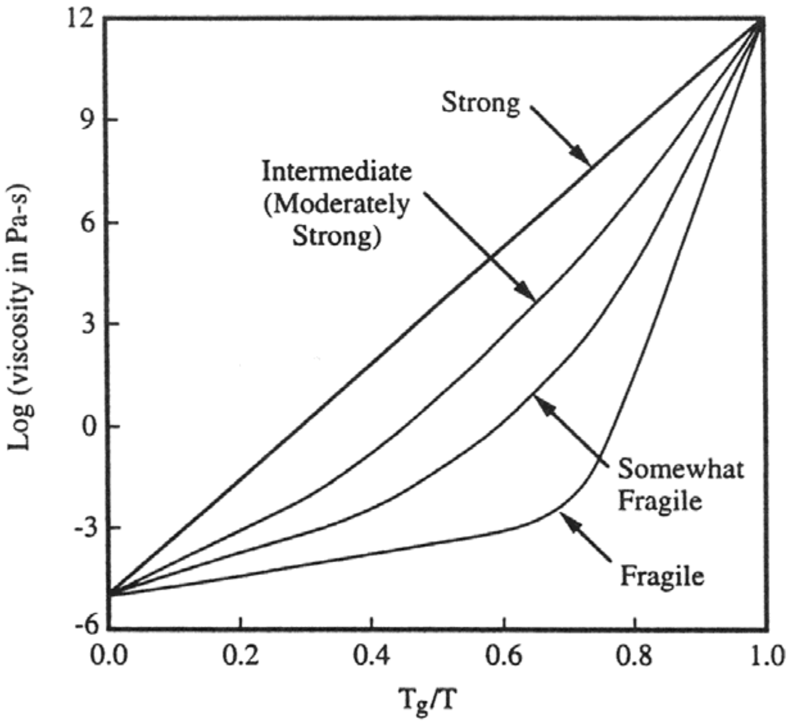

< Quantification of Fragility >

$$m = \left.\frac{d\log\eta(T)}{d(T_{g,n}/T)}\right|_{T=T_{g,n}} = \left.\frac{d\log\tau(T)}{d(T_g/T)}\right|_{T=T_g}$$

Slope of the logarithm of viscosity, η (or structural relaxation time, τ) at T_g

Correlation between fragility and plasticity

- Correlation between elastic constants and plasticity

Low G/B → ***High ν*** → **shear collapse**

(shear modulus / bulk modulus) *(poisson's ratio)* *(multiple shear band)*

Jan Schroers et al, , Phys. Rev. Lett. 93, 255506 (2004).

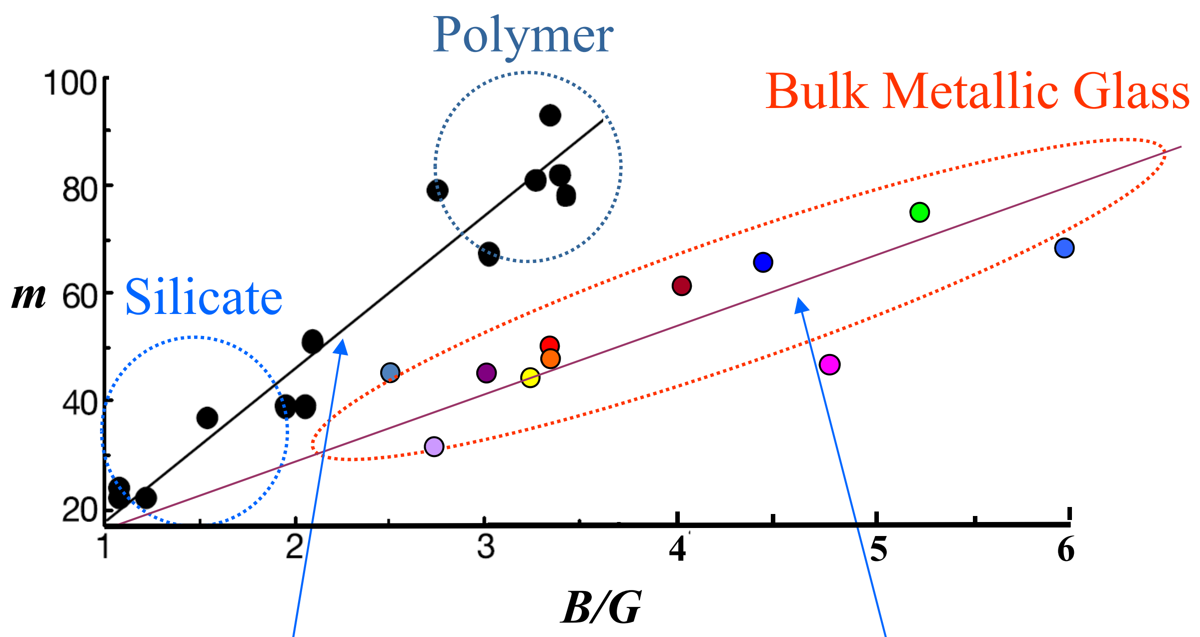

$$m-17=29(B/G-1)$$

$$m-17=14(B/G-1)$$

*** J. Mater. Res. 23, 523 (2008)**

Correlation between fragility and plasticity

Low G/B
High ν → *High m* (*fragility index*) → **Large Plasticity** (*multiple shear band*)

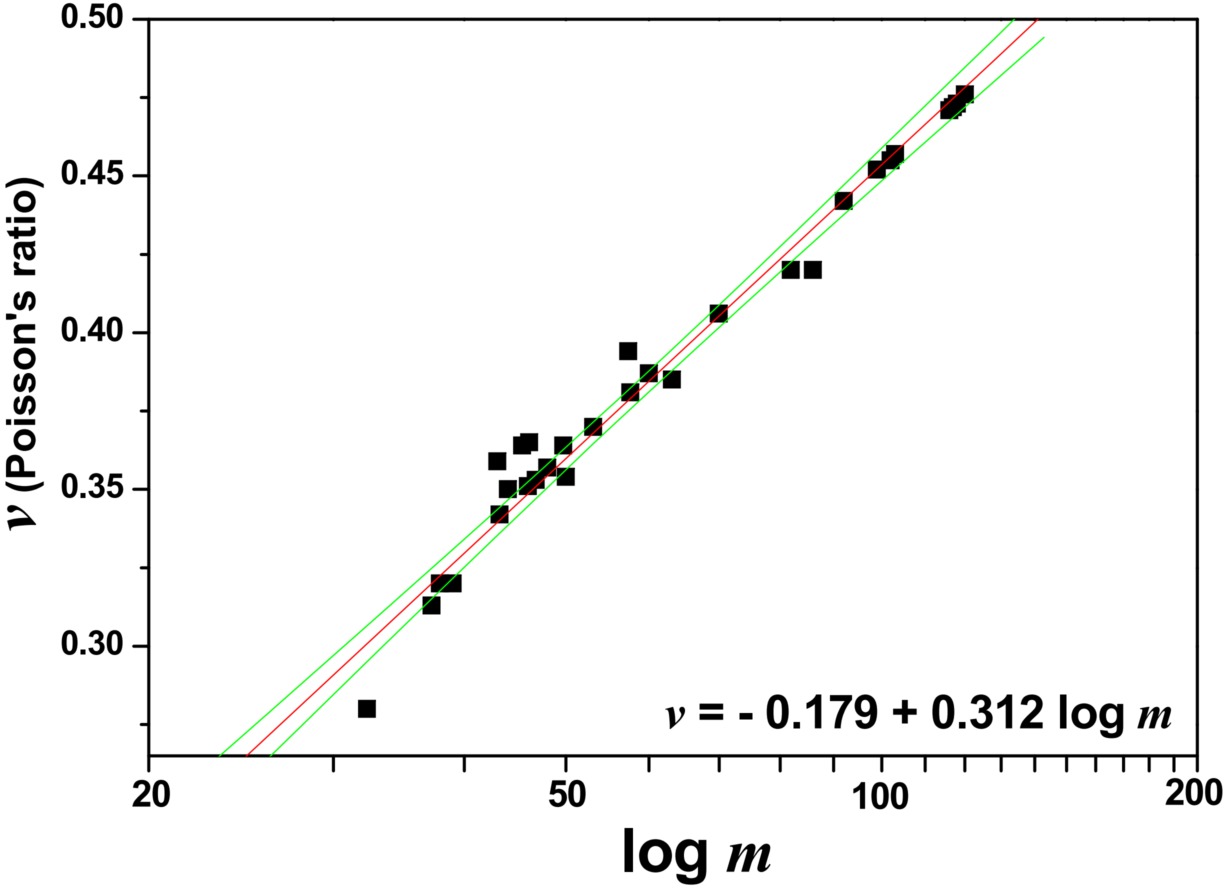

* Appl. Phys. Lett., 91, 031907.

Enhancement plasticity in BMGs with atomic scale heterogeneity

a) Effect of quenched-in quasicrystal nuclei

Effect of secondary phase in amorphous matrix

3 mm rod

(a) $Zr_{63}Ti_5Nb_2Cu_{15.8}Ni_{6.3}Al_{7.9}$

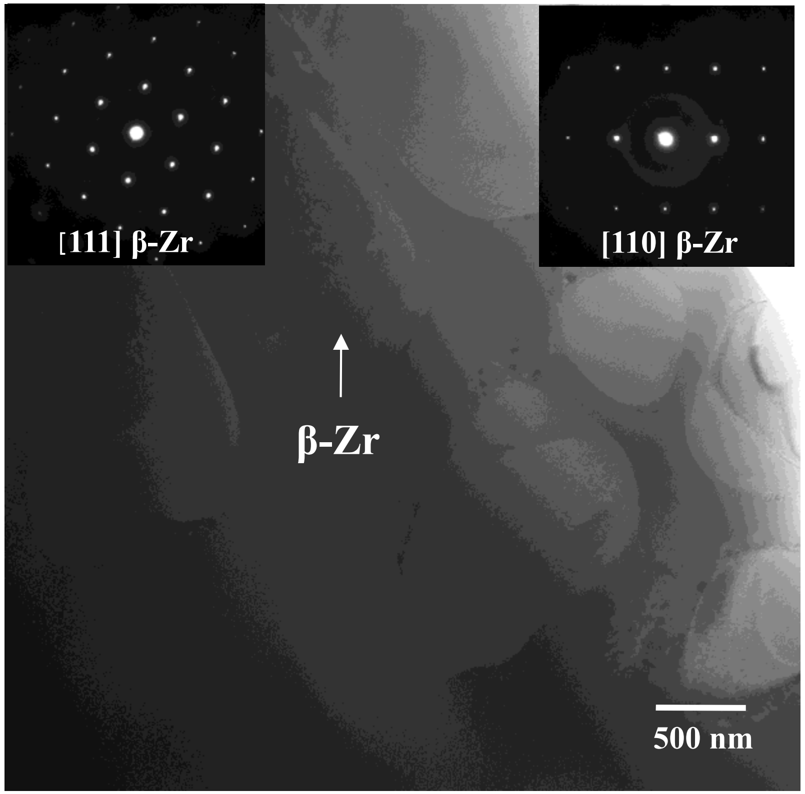

β-Zr dendrite in amorphous matrix

(b) $Zr_{57}Ti_8Nb_{2.5}Cu_{13.9}Ni_{11.1}Al_{7.5}$

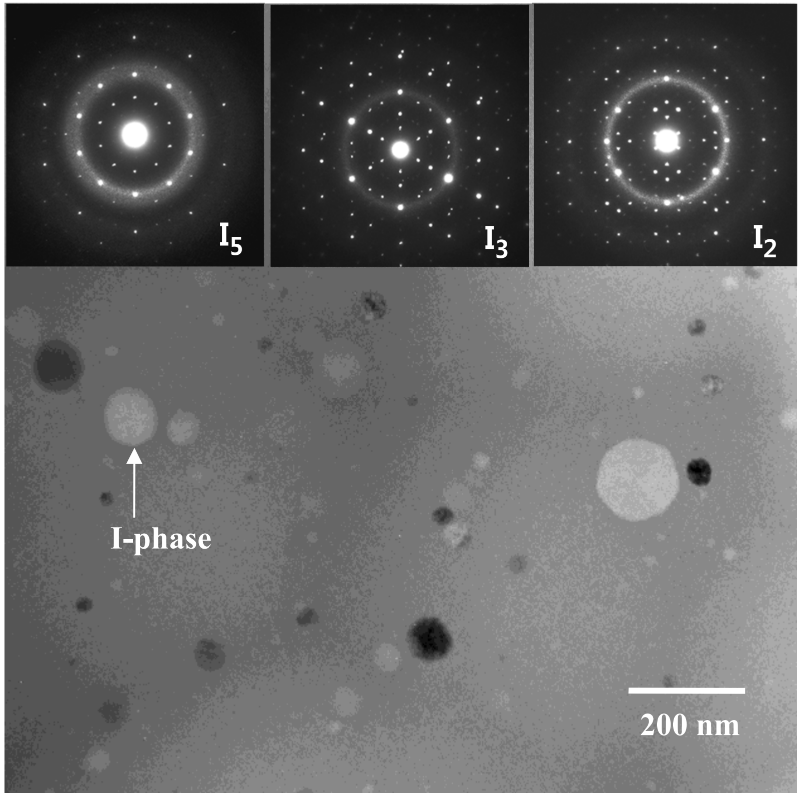

I-phase particle in amorphous matrix

Effect of secondary phase in amorphous matrix

*** unpublished (2008)**

- Compression test

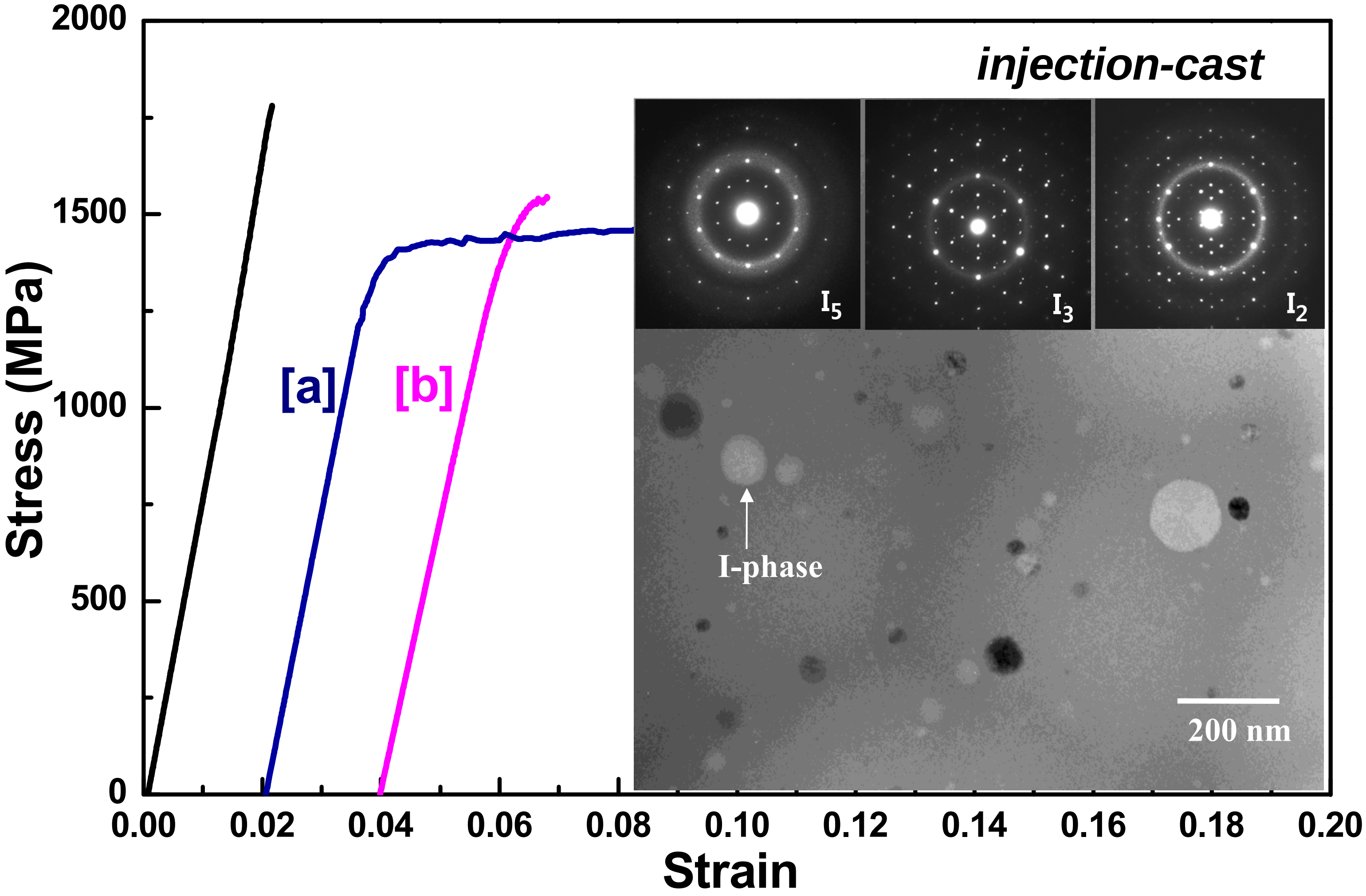

Continuous interface between amorphous and I-phase

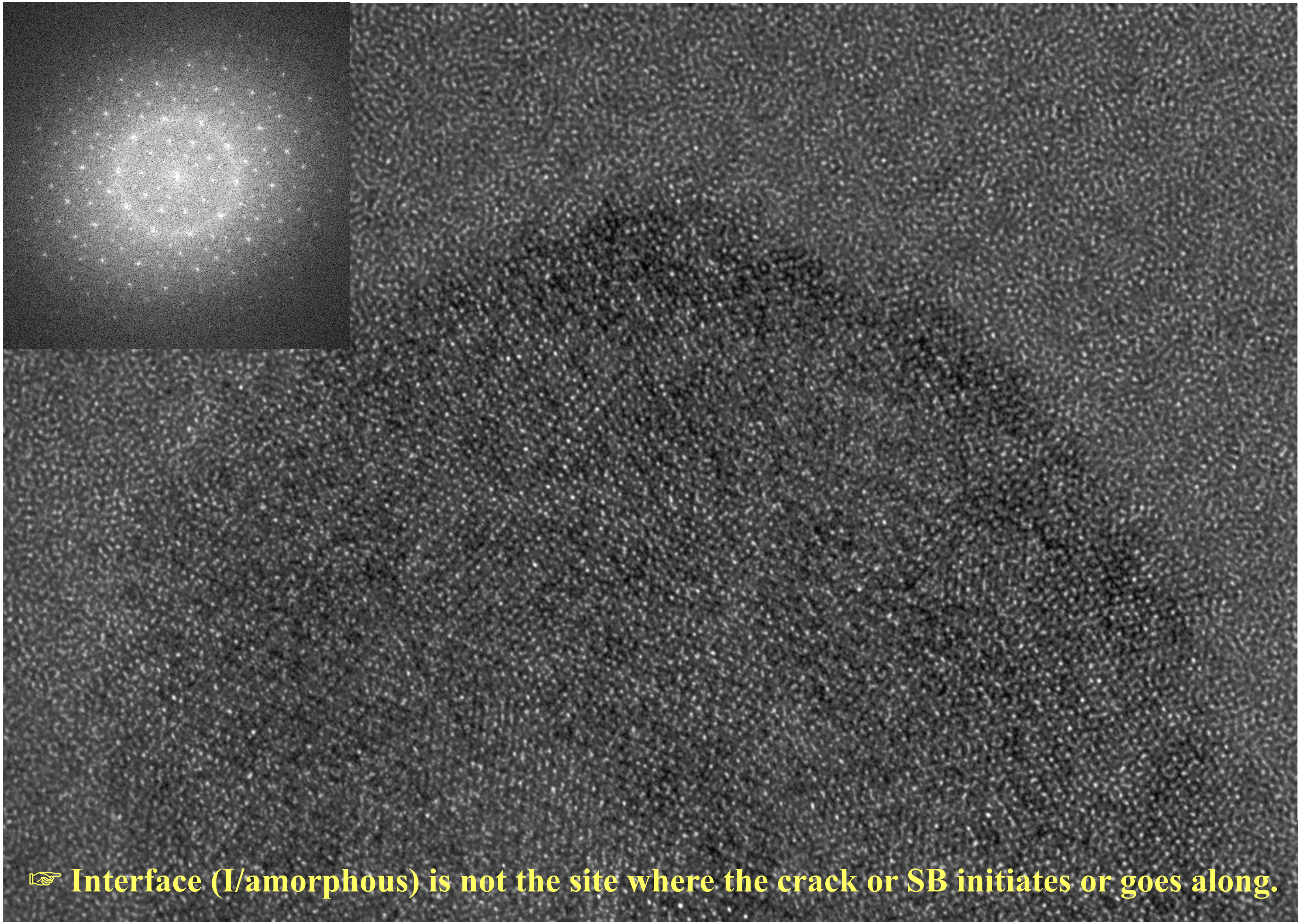

Role of icosahedral particle on the propagation of SB

Before deformation

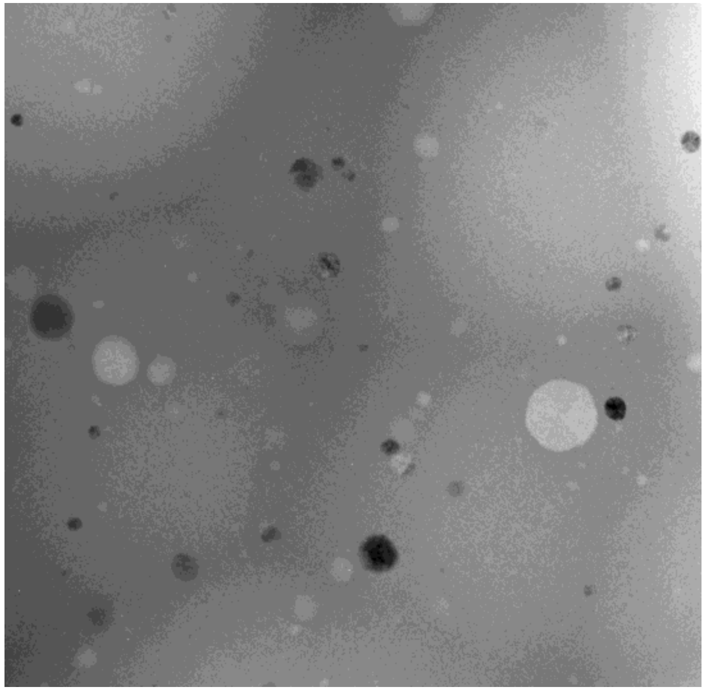

After deformation

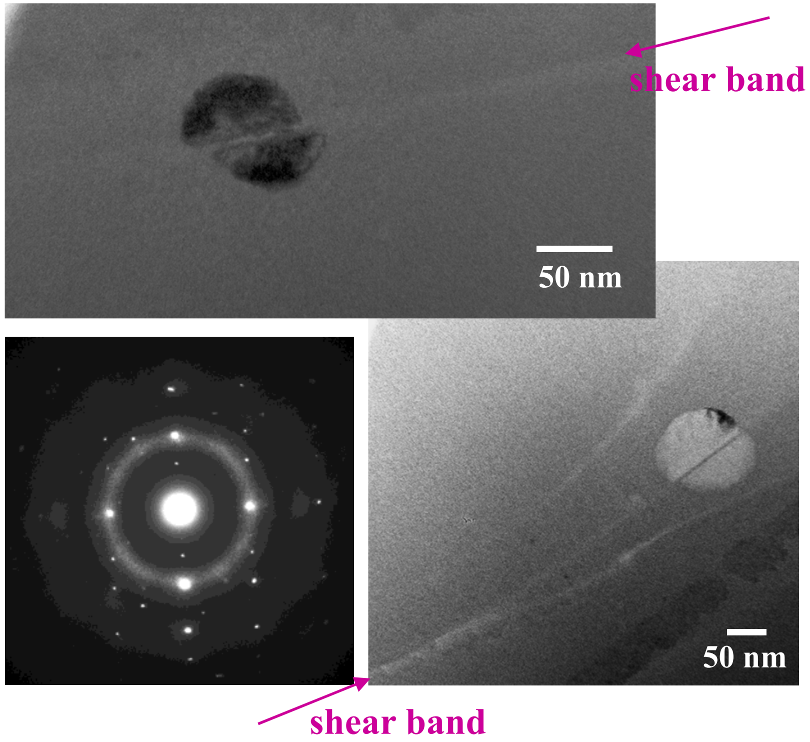

- **Shear band passes through icosahedral particle.**
- **Icosahedral particle splits across with the plastic deformation of metallic glass matrix**

☞ **No distribution of icosahedral particle to blocking the propagation of shear band.**

☞ **No enhancement of plasticity in MGMC with icosahedral particle**

Effect of quenched-in quasicrystal nuclei

2 mm rod

(a) $Zr_{63}Ti_5Nb_2Cu_{15.8}Ni_{6.3}Al_{7.9}$

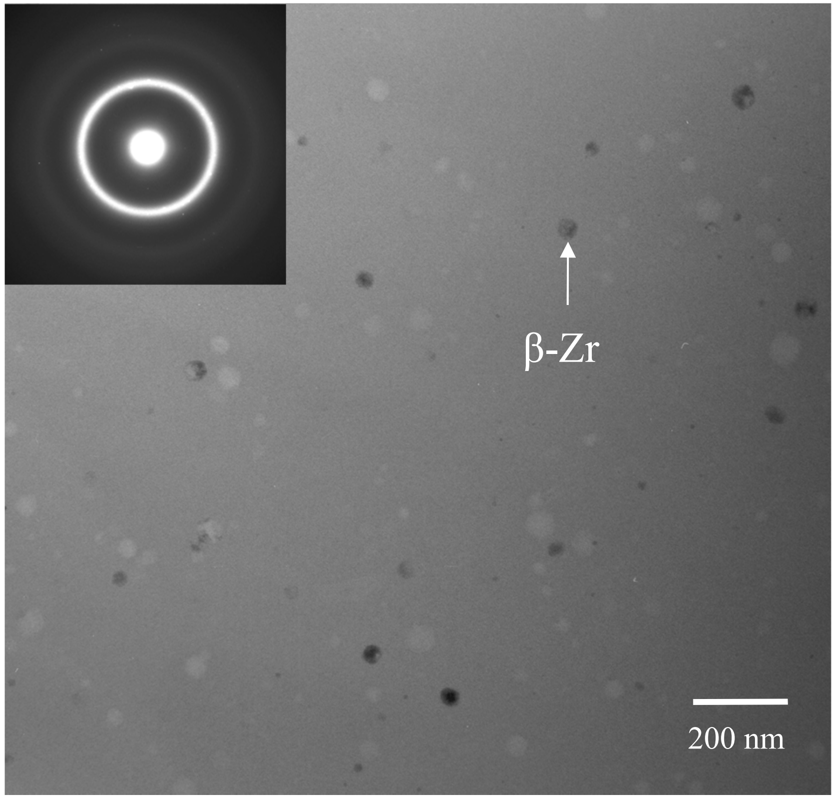

β-Zr particle (~70 nm) in amorphous matrix

(b) $Zr_{57}Ti_8Nb_{2.5}Cu_{13.9}Ni_{11.1}Al_{7.5}$

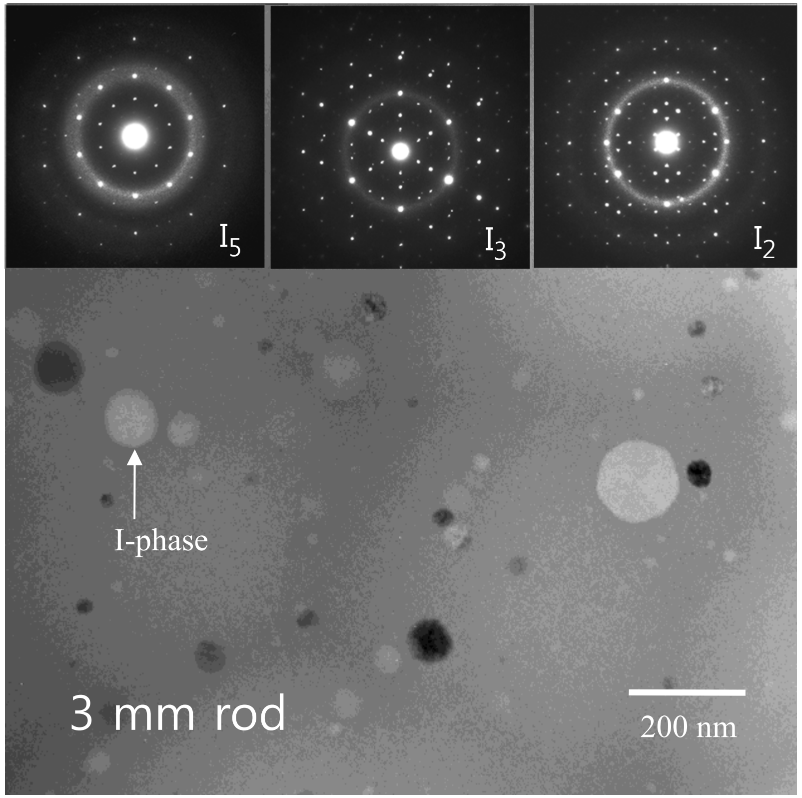

I-phase particle in amorphous matrix

Effect of quenched-in quasicrystal nuclei

- Compression test

* unpublished (2008)

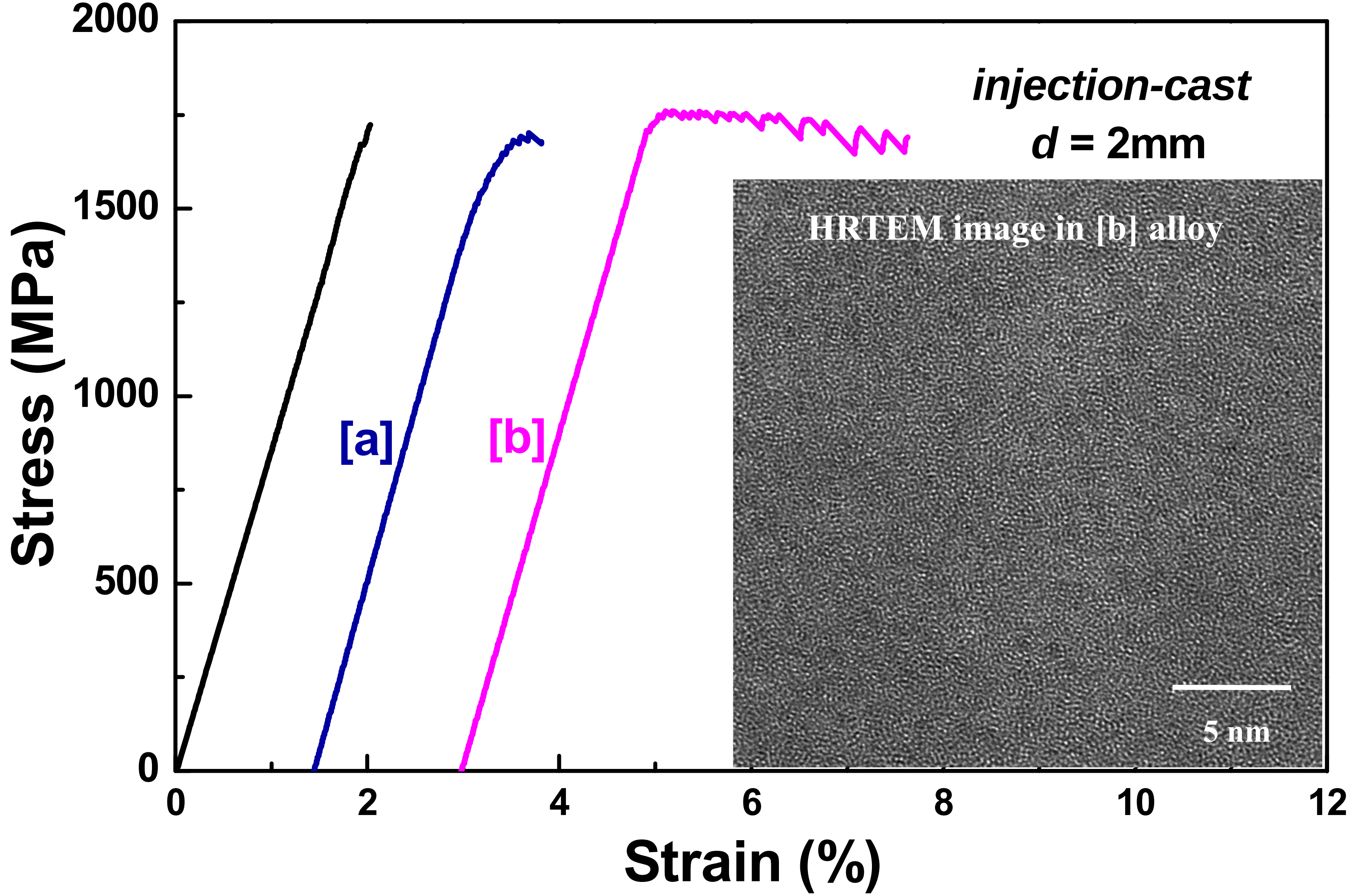

Effect of quenched-in quasicrystal nuclei

- *Activation E : driving force for nucleation*

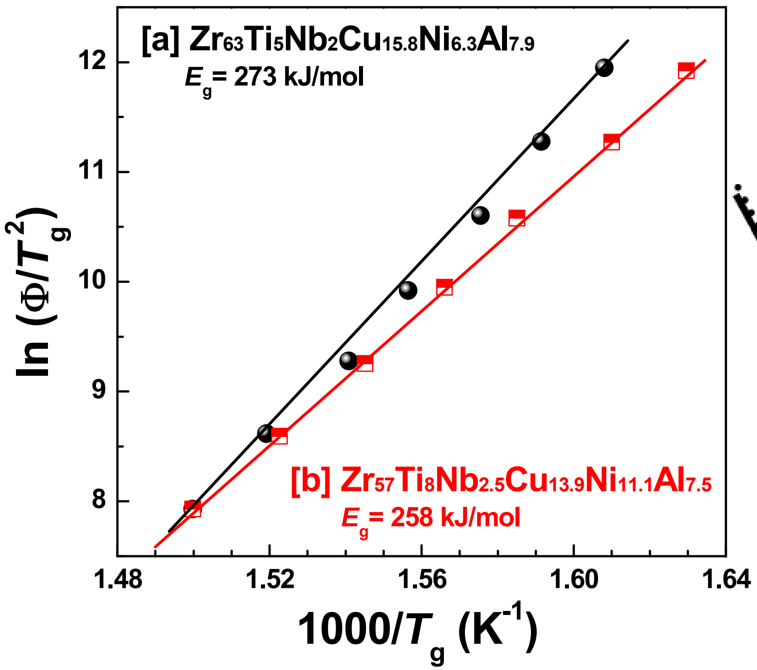

Kissinger's equation

$$\ln(\Phi / T_g^2) = -Q / RT_g + const.$$

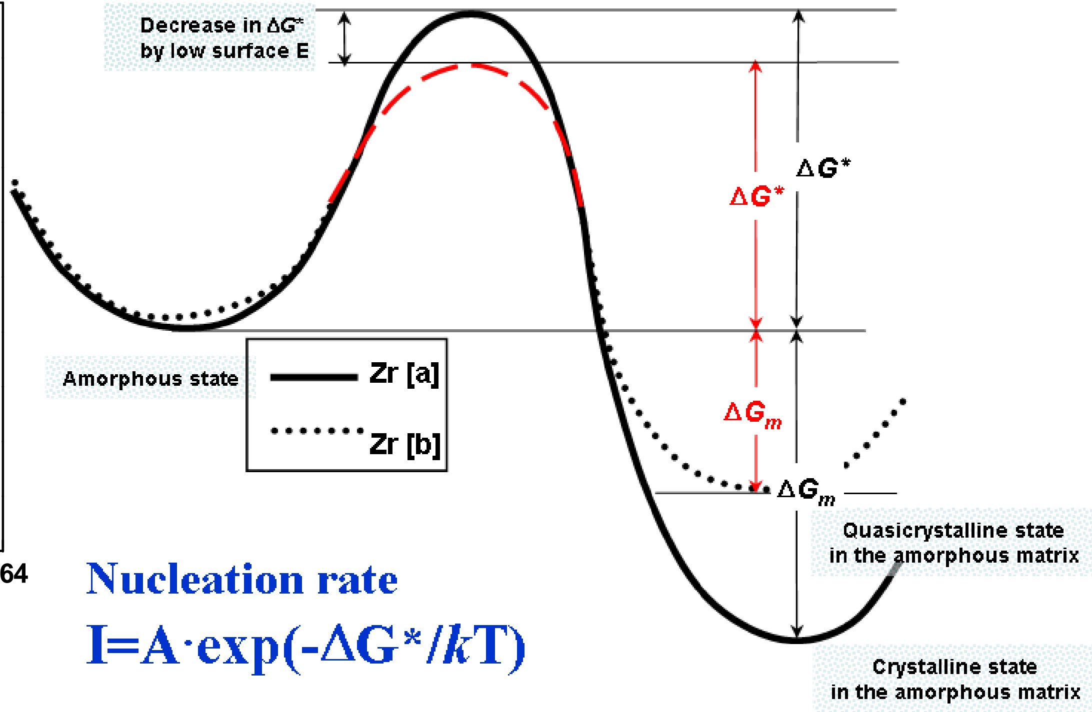

Nucleation rate

$$I = A \cdot \exp(-\Delta G^* / kT)$$

Effect of quenched-in quasicrystal nuclei

- Isotherm in DSC

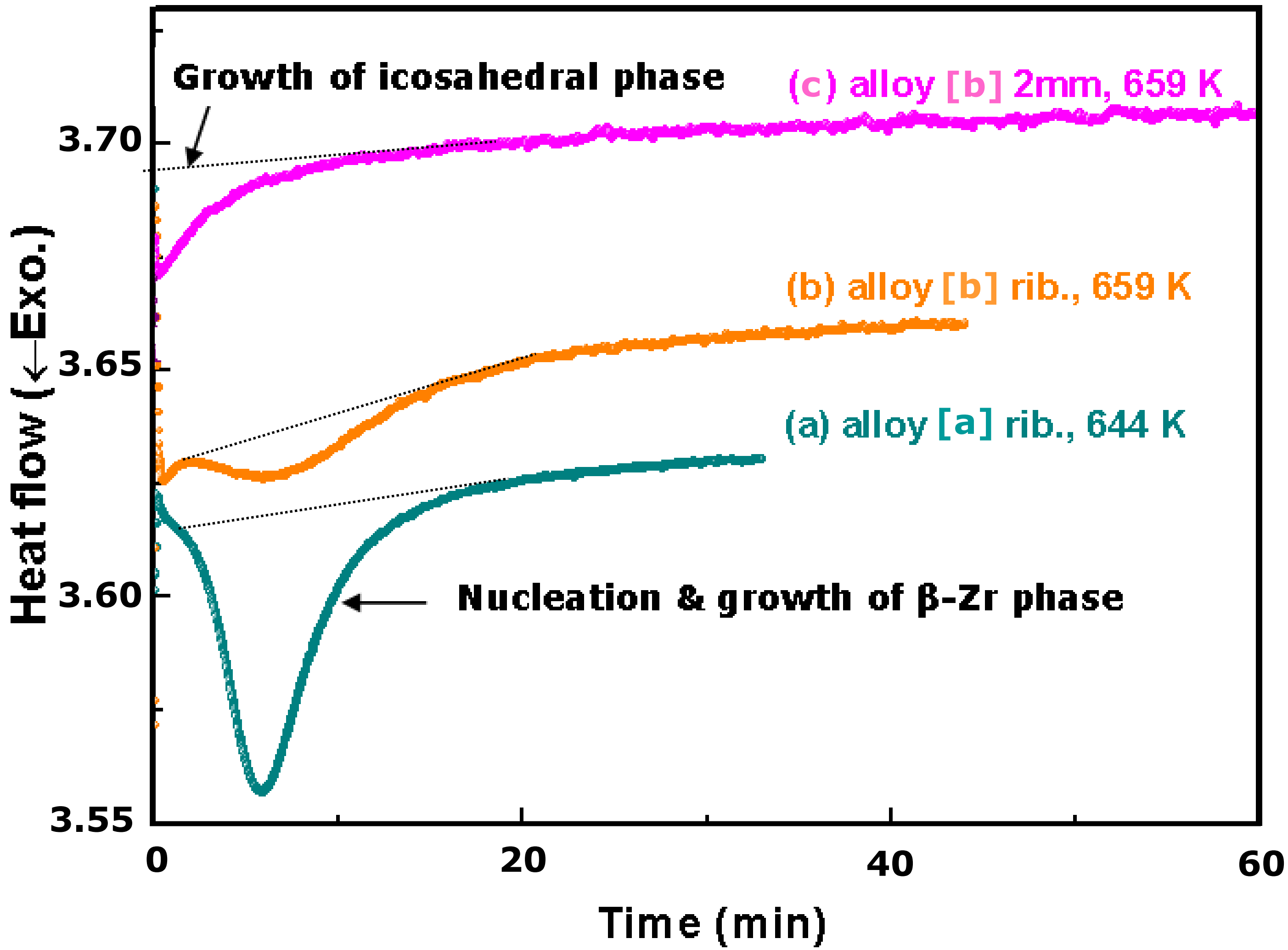

Effect of quenched-in quasicrystal nuclei

- EXAFS analysis

(b) $Zr_{57}Ti_8Nb_{2.5}Cu_{13.9}Ni_{11.1}Al_{7.5}$

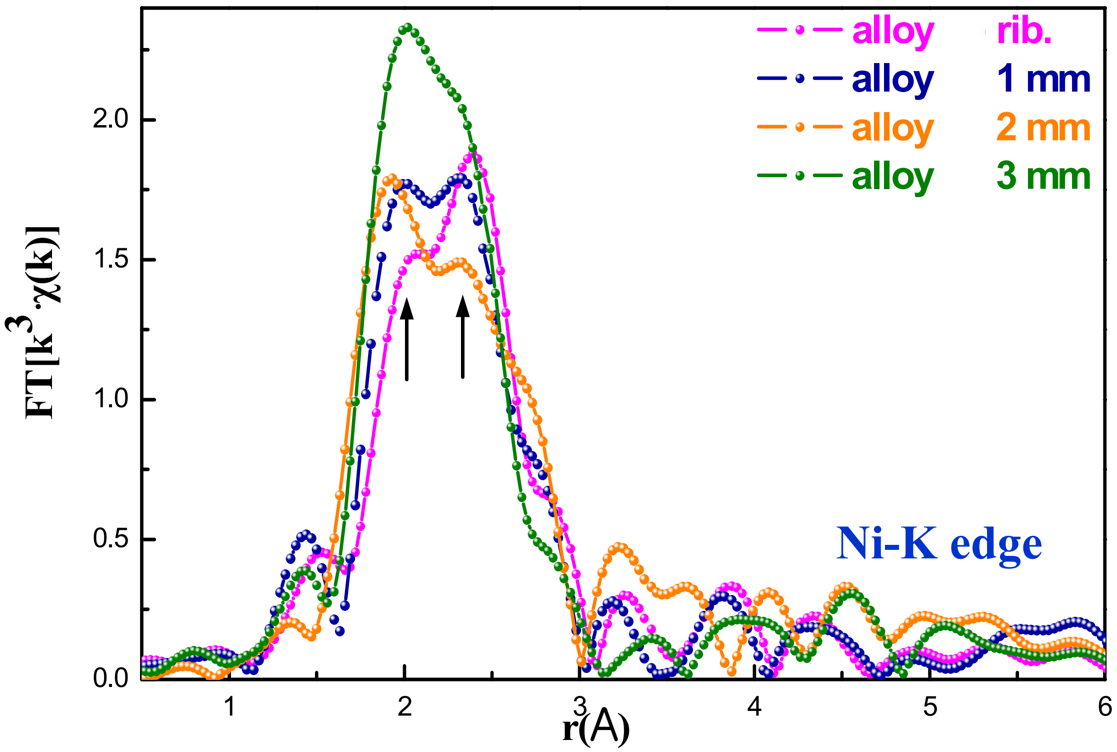

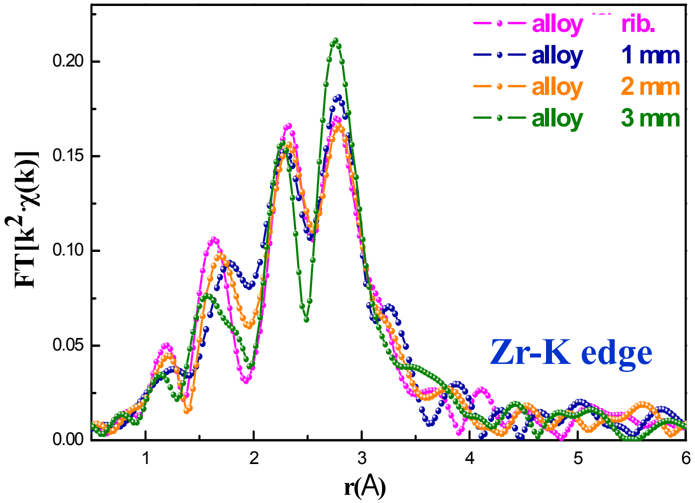

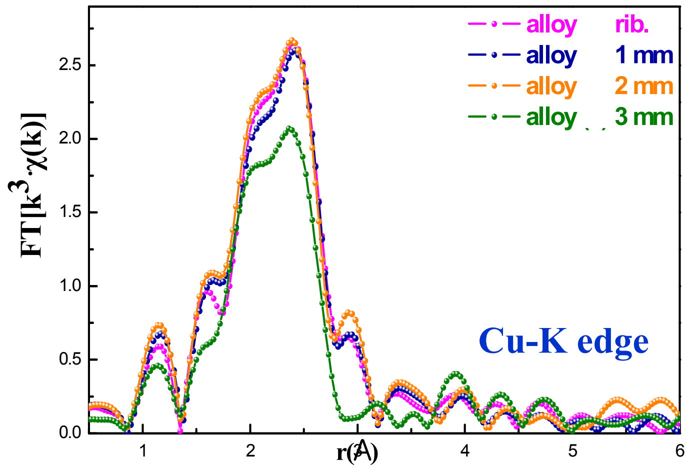

Distinctive structural change around Ni atom

Intensity change due to microstructural change

* unpublished (2008)

Enhancement plasticity in BMGs with atomic scale heterogeneity

b) Effect of element having positive enthalpy of mixing among constituent elements

Improvement of plasticity in monolithic BMGs

* **Enhancement of plasticity in monolithic BMGs**

→ No clear explanations so far.

* **Reports for enhancement of plasticity in monolithic BMGs**

	Compressive plastic strain, ε_p (%)
$Zr_{59}Ta_5Cu_{18}Ni_8Al_{10}$ [1]	~ 6.1
$Zr_{57}Ti_5Cu_{20}Ni_8Al_{10}$	~ 1.1
$Ni_{59}Zr_{16}Nb_7Ti_{13}Si_3Sn_2$ [2]	~ 6.2
$Ni_{59}Zr_{20}Ti_{16}Si_2Sn_3$	~ 2.1
$Cu_{47}Ti_{33}Zr_7Nb_4Ni_8Si_1$ [3]	~ 4.1
$Cu_{47}Ti_{33}Zr_{11}Ni_8Si_1$	~ 1.5
$Cu_{43}Ag_7Zr_{43}Al_7$ [4]	~ 4.1
$Cu_{50}Zr_{43}Al_7$	~ 1.5

1 *Xing et al., Phys. Rev. B (2001)*

2 *Lee et al., Intermetalics (2004), BMG III*

3 *Park et al., J. Non-cryst. Sol. (2005)*

4 *Sung et al., Met. Mater. –Int (2004) and Oh et al., Scripta Mater. (2005)*

(Ta-Zr: +13KJ/mol, Nb-Zr: +17KJ/mol, Nb-Ti: +9KJ/mol,Cu-Ag: +5 KJ/mol)

- Previous results on the effect of micro-alloying on plasticity

: **Effect of elements having positive heat of mixing**

Alloy design

* Substitution of Zr with Y in Cu-Zr-Al system

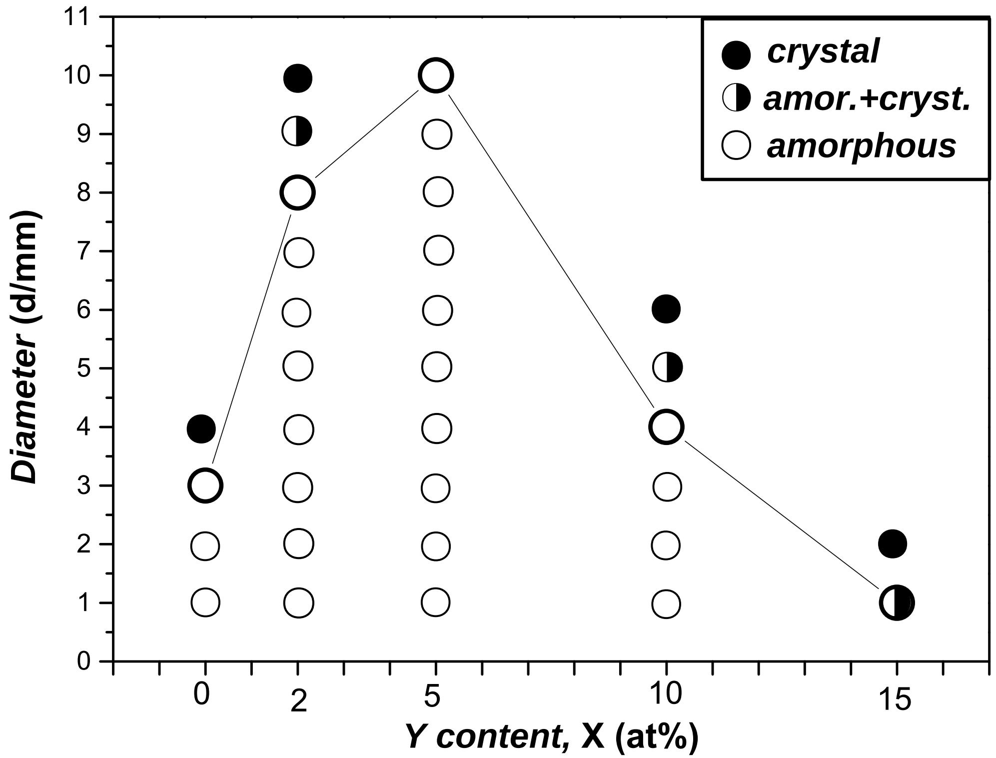

D. Xu, G. Duan and W.L. Johnson, Phys. Rev. Lett. 92, 245504 (2004)

$Cu_{46}Zr_{47-x}Al_7Y_x$

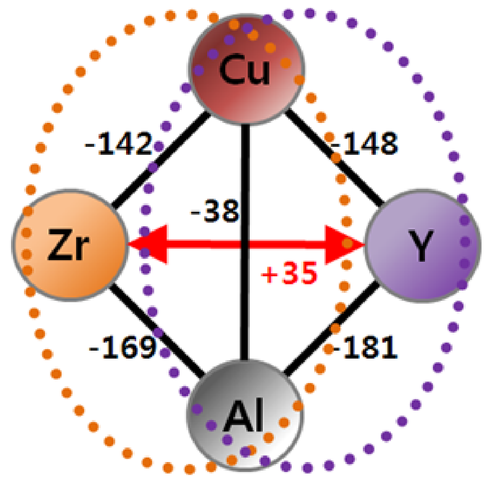

Possibility of two phase !!!

→ **Cu-Zr-Al , Cu-Y-Al**

Indirect evidence of inhomogeneity
= Phase separation

*** Acta Materialia, 54, 2597 (2006)**

Thermal analysis : DSC results

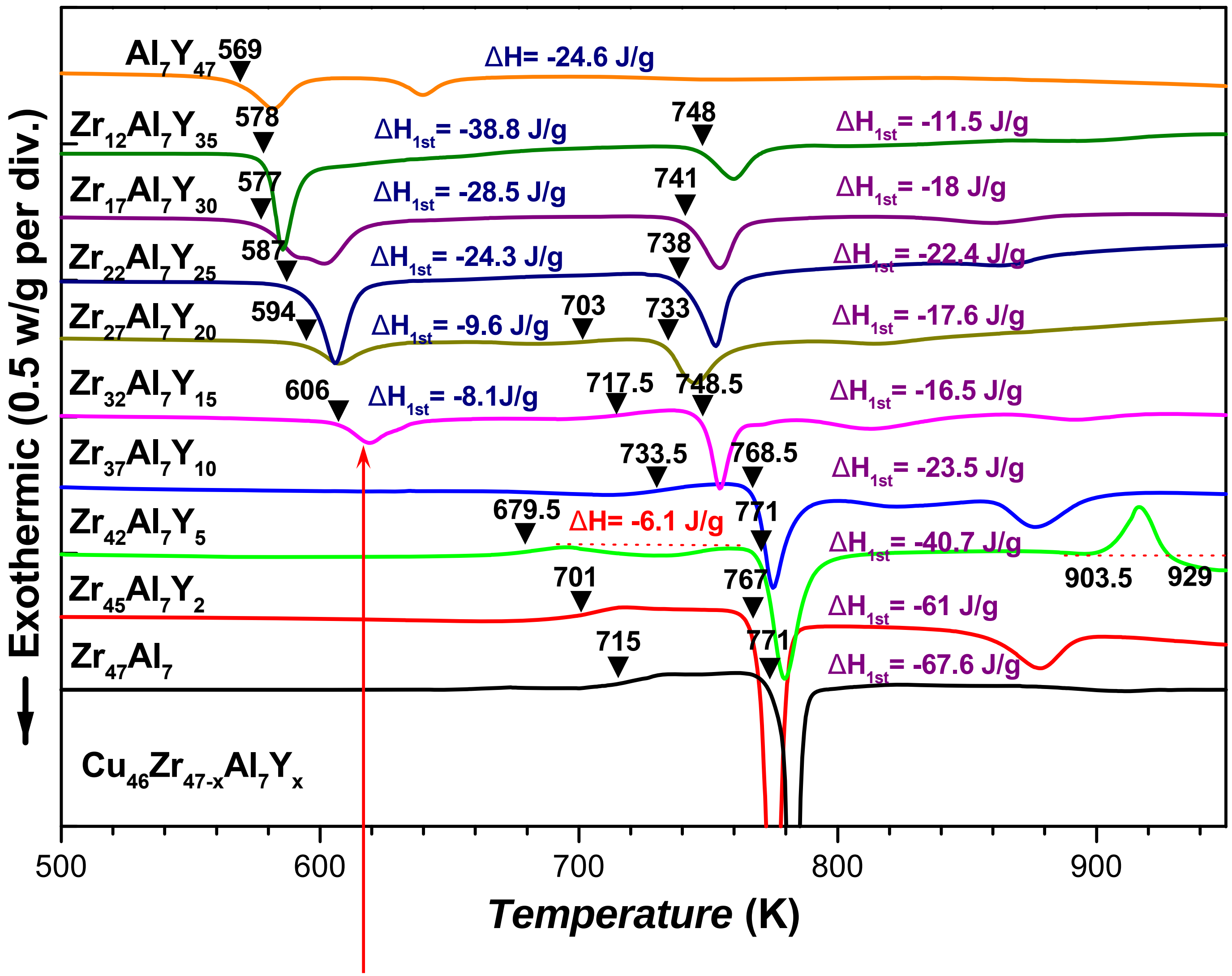

Exothermic peak which exhibit that Y rich amorphous phase crystallize

Structural analyses : TEM results

As-melt-spun

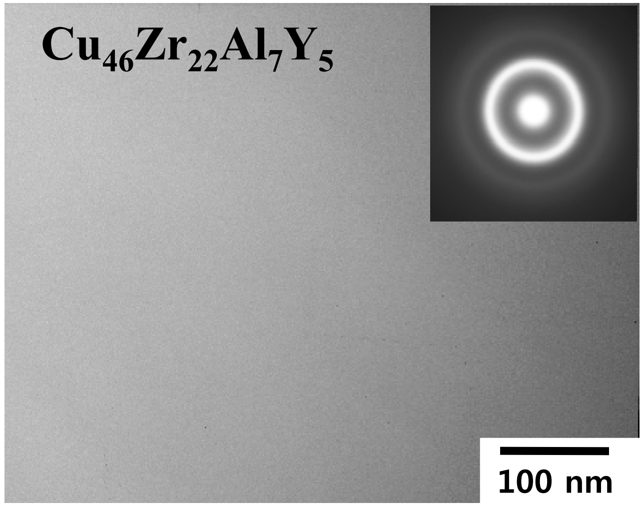

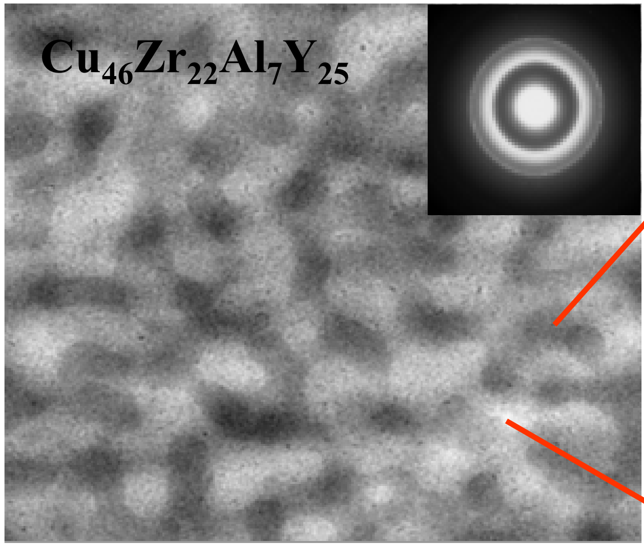

- With increasing Y content,

Compositional inhomogeniety → Phase separation

$Cu_{53.4}Zr_{31.8}Y_{8.3}Al_{6.5}$ (CuZr-rich)

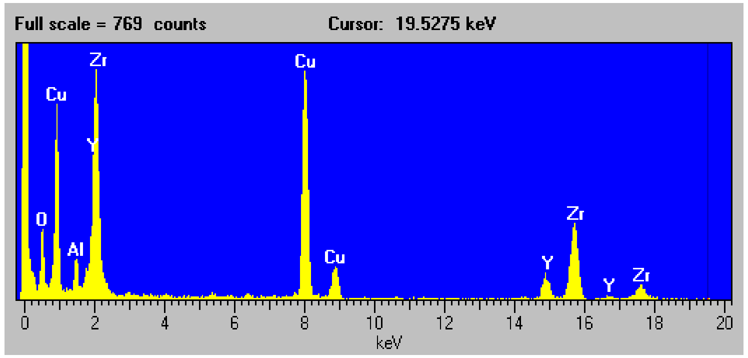

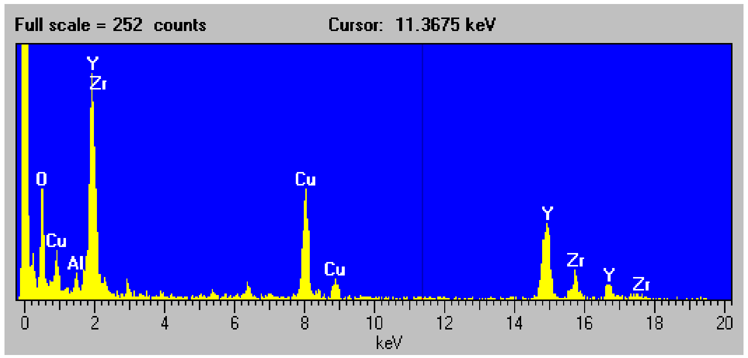

$Cu_{35.7}Zr_{12.8}Y_{44.3}Al_{7.2}$ (CuY-rich)

Compression test in Cu-Zr-Al-Y alloy system

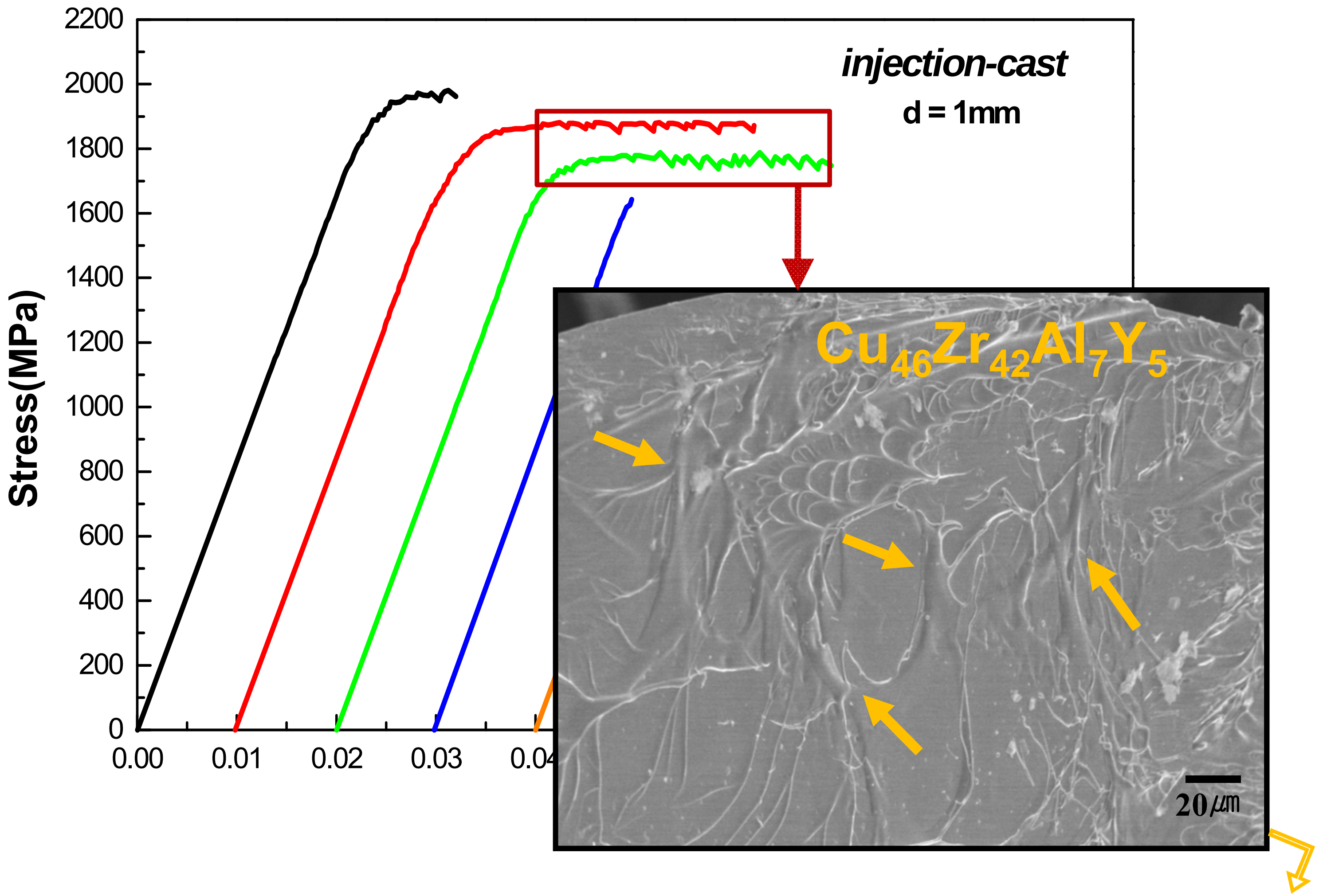

▶ A larger amount of strain along the shear band led to localized melting before fracture

Measurement of viscosity using TMA

<Supercooled liquid region>

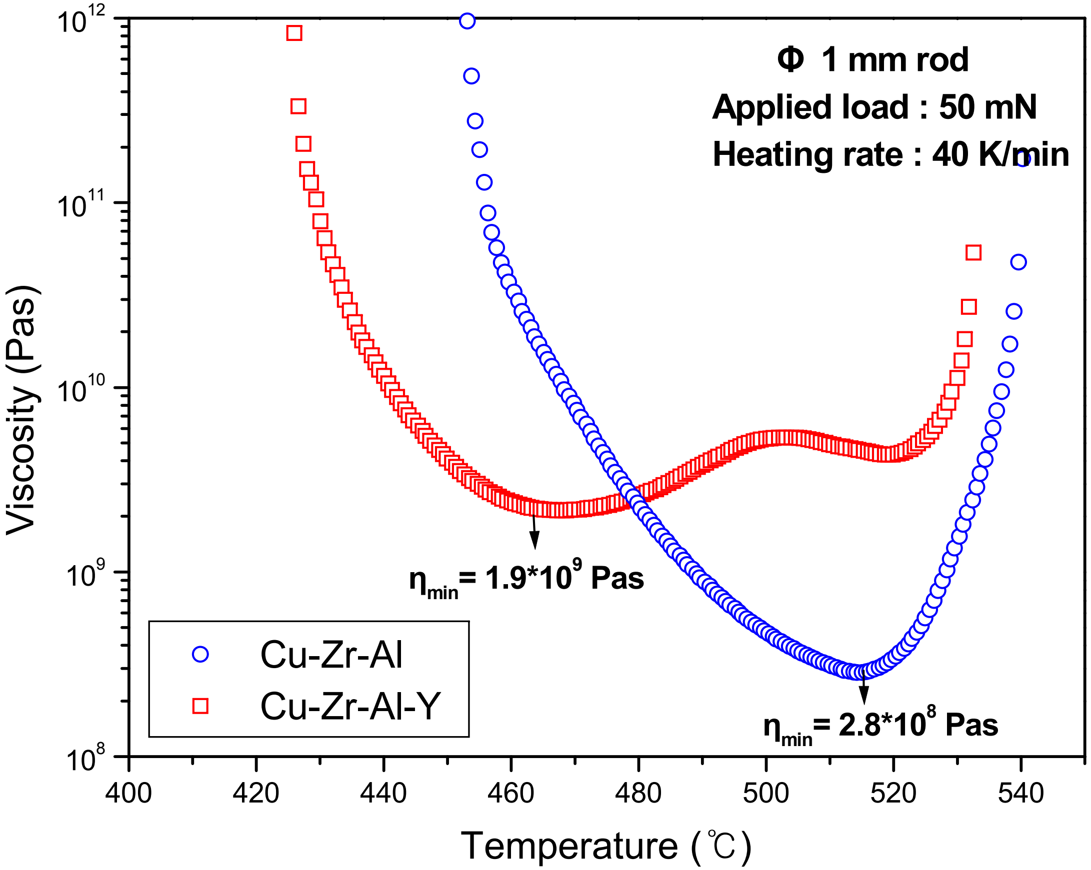

<1st Crystallization behavior>

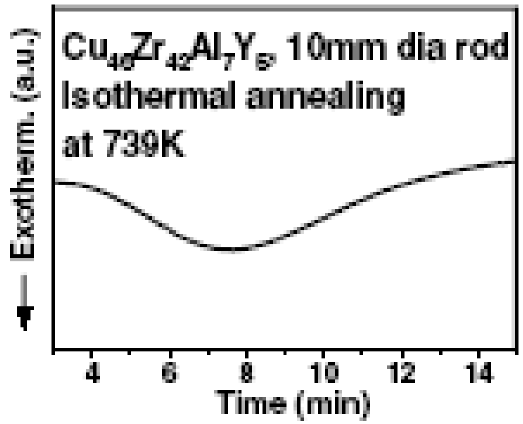

: nucleation and growth

$Cu_{46}Zr_{47}Al_7$ < $Cu_{46}Zr_{42}Al_7Y_5$

η_{min} = 2.8*10^8 pas

η_{min} = 1.9*10^9 pas

Relatively easy crystallization

Structural analyses: HRTEM

$Cu_{46}Zr_{42}Al_7Y_5$

As-melt-spun

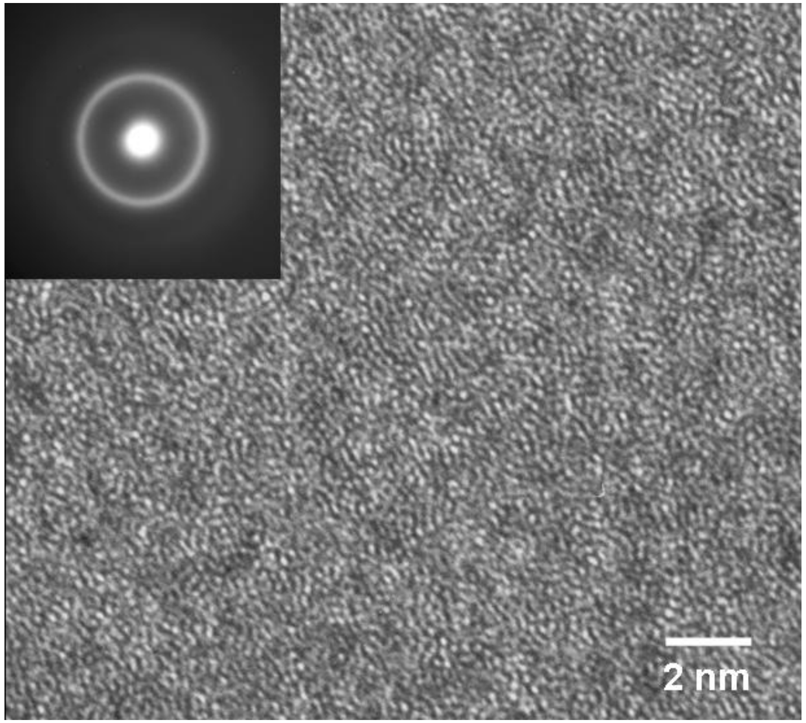

Heated up to 480℃

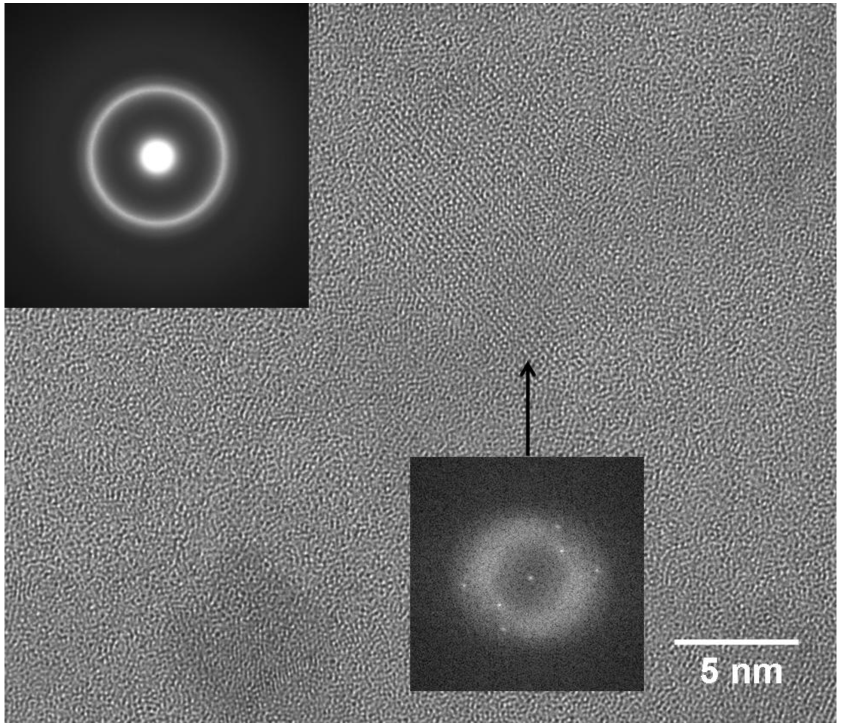

: nanocrystallization of Y rich amorphous phase due to relatively lower GFA

* Acta Materialia, 54, 2597 (2006)

In-situ WAXS analysis of $Cu_{46}Zr_{42}Al_7Y_5$ during heating

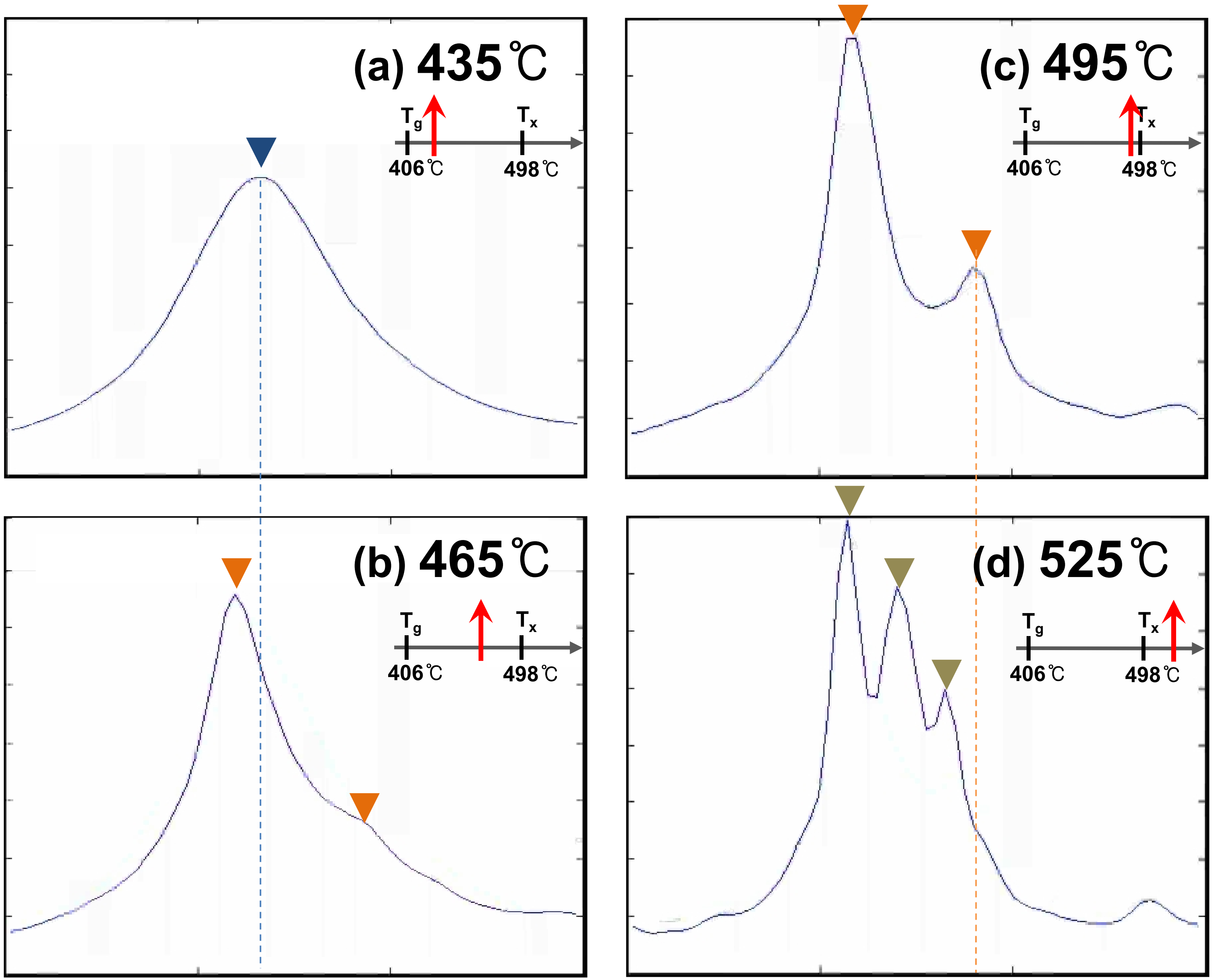

Obtained from Argon National Lab.

Effect of element having positive enthalpy of mixing

- **Abnormal behavior of supercooled liquid region**

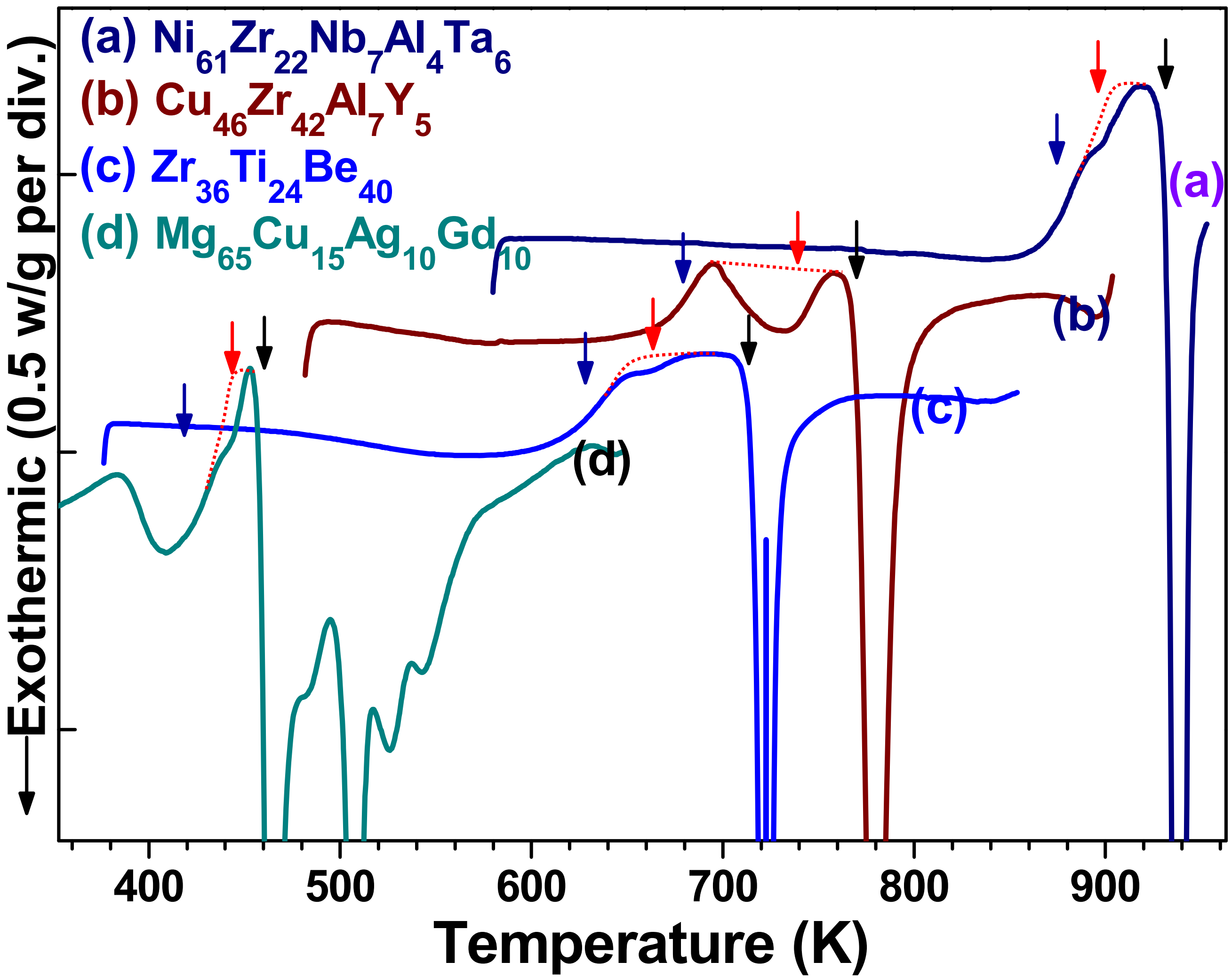

Effect of element having positive enthalpy of mixing

- **Atom probe concentration depth profiles in $Ni_{61}Zr_{22}Nb_7Al_4Ta_6$**

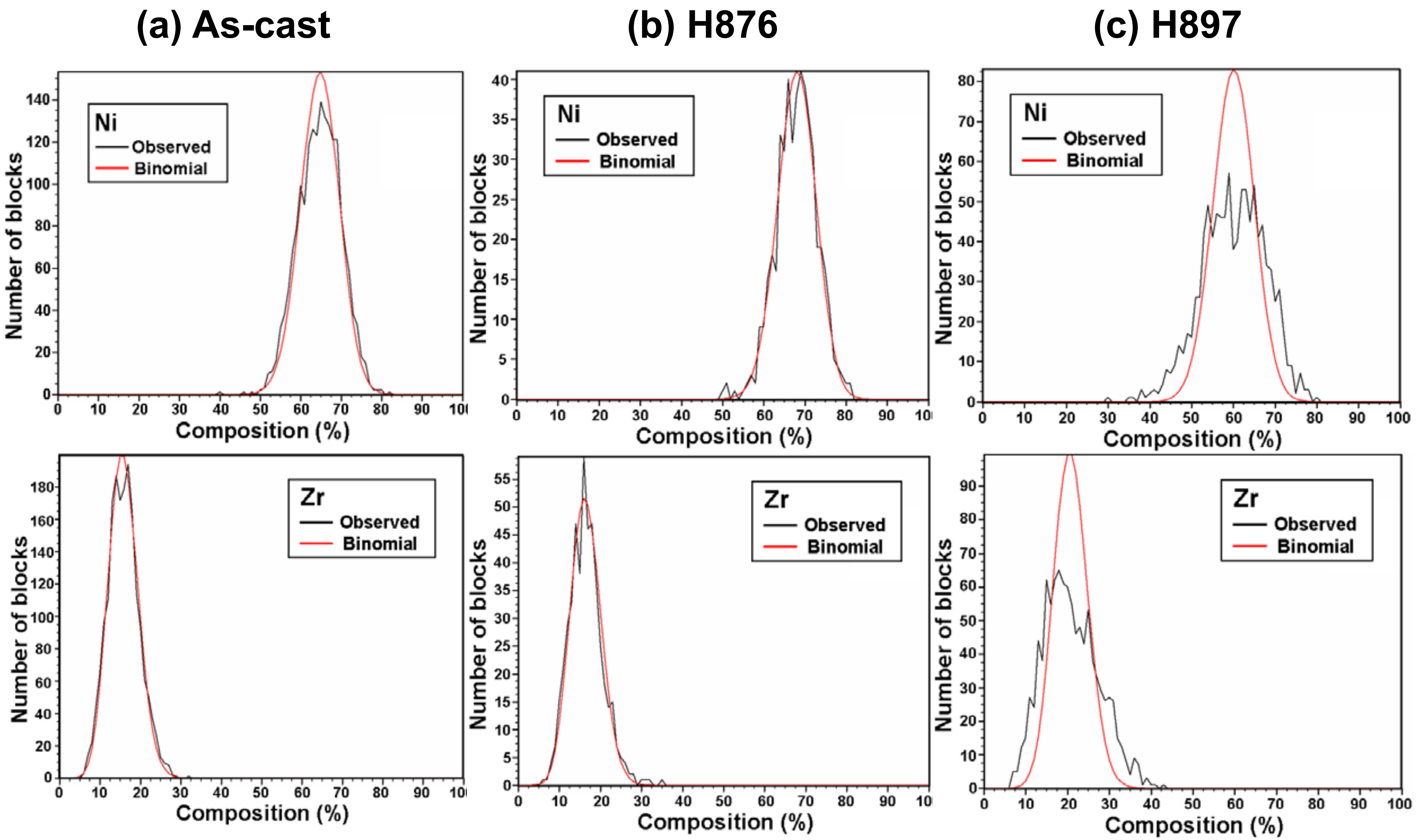

easy crystallization

Effect of element having positive enthalpy of mixing

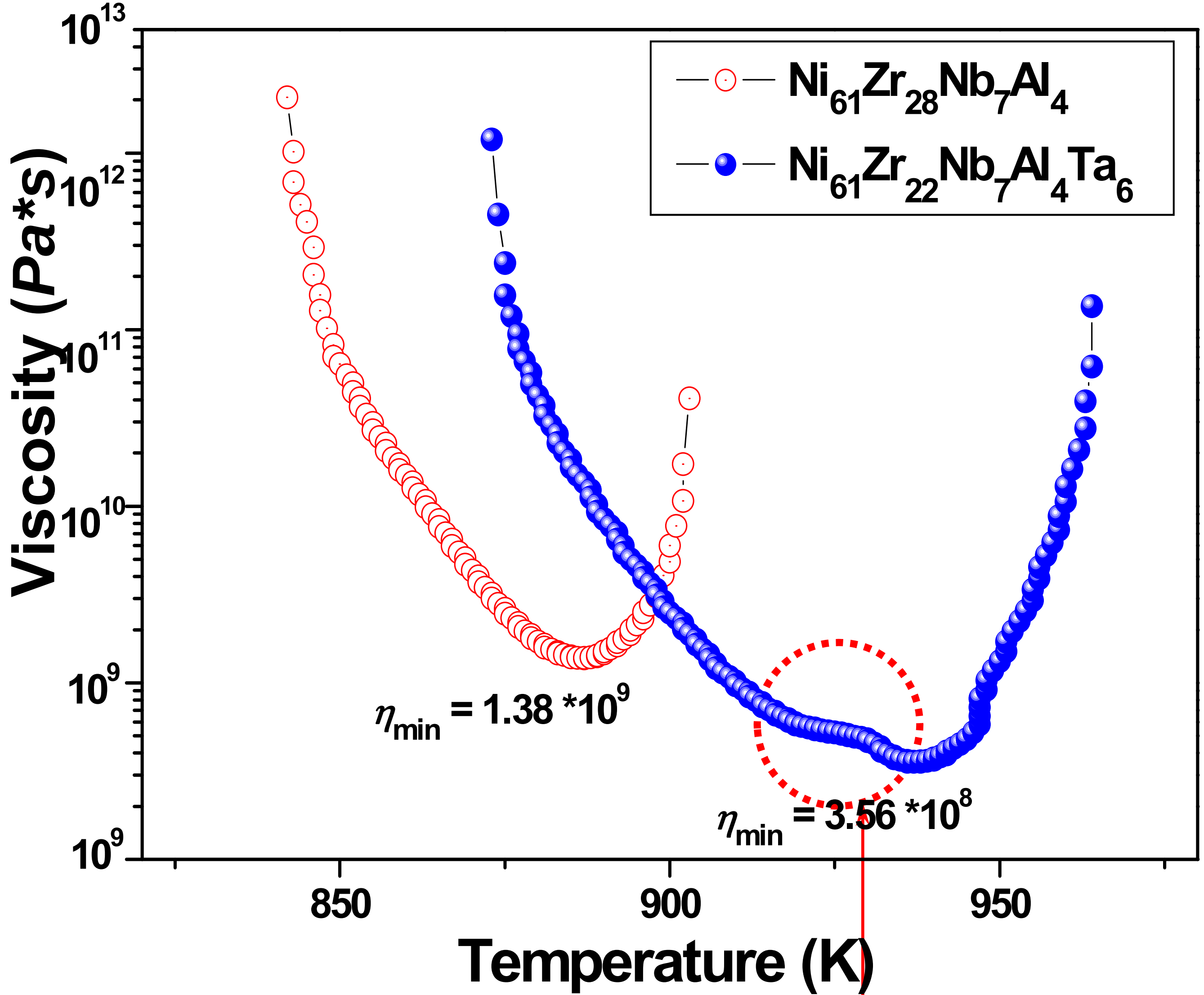

Ordering in supercooled liquid region

Enhancement plasticity in BMGs with atomic scale heterogeneity

c) Effect of element having significantly different enthalpy of mixing among constituent elements

Effect of element having large different enthalpy of mixing

- **Cu-Zr-Be ternary alloy system**

* Acta Materialia, 56 3120 (2008)

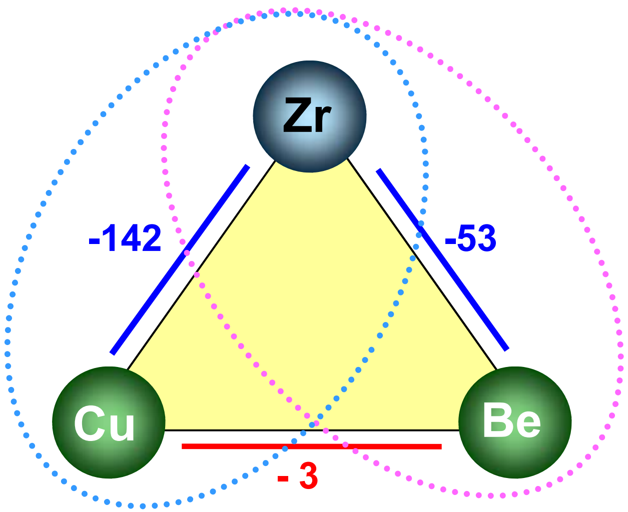

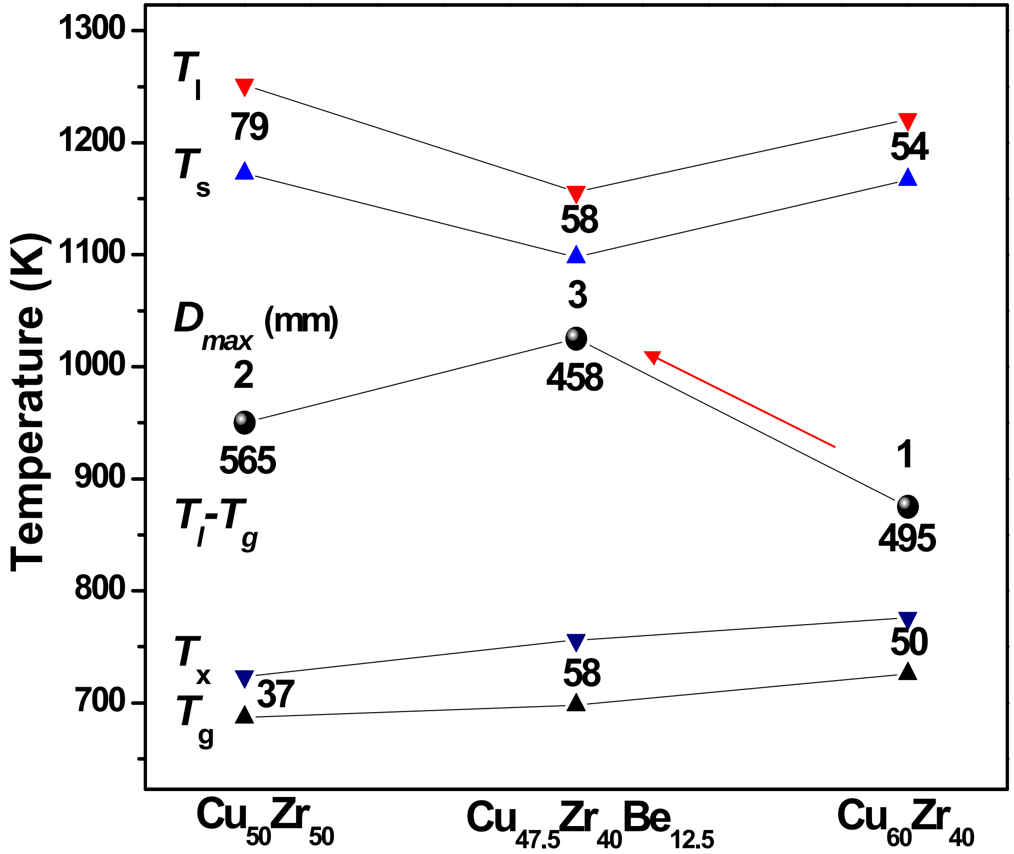

Effect of element having large different enthalpy of mixing

- Compression test

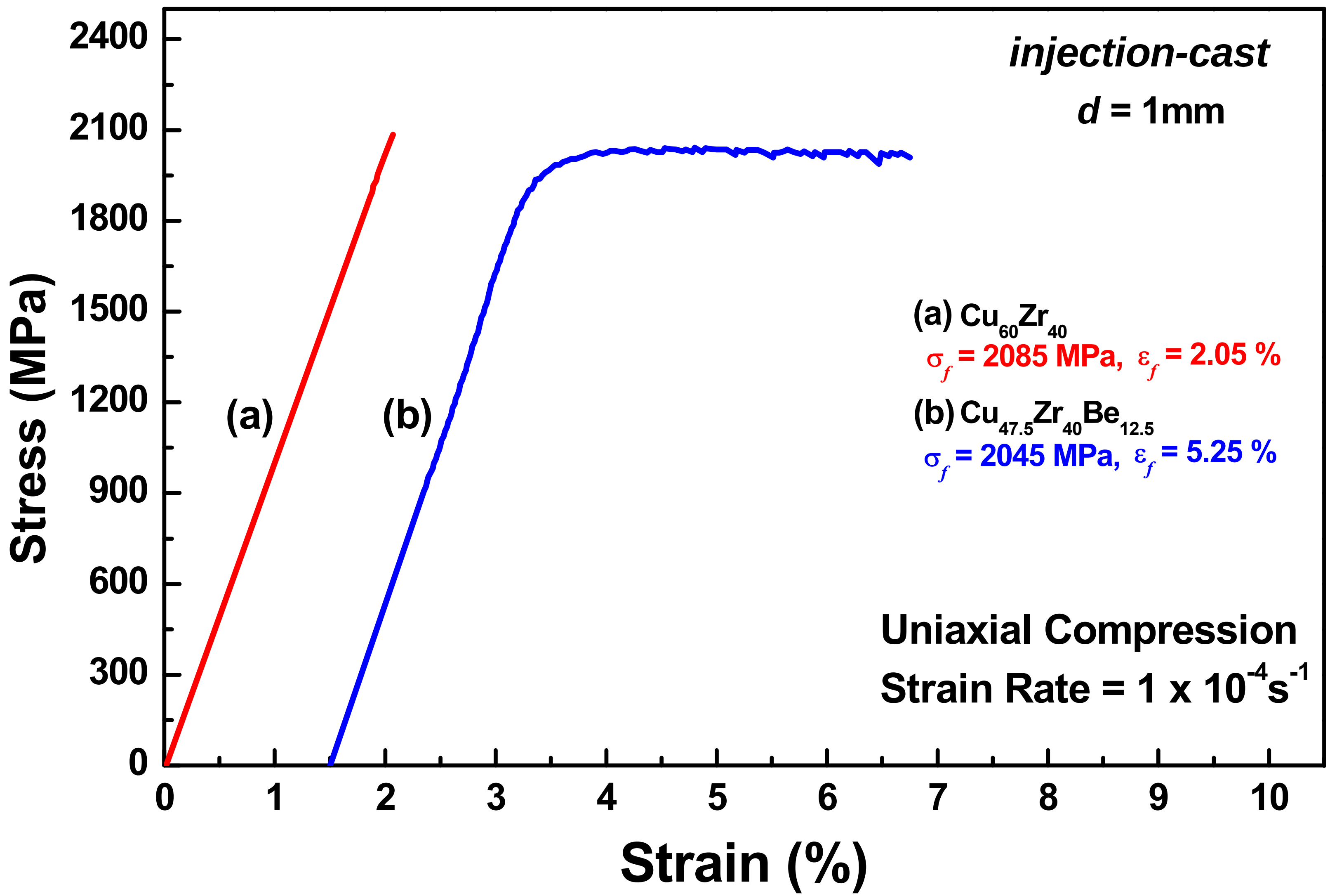

Effect of element having large different enthalpy of mixing

- **3DAP-FIM results**

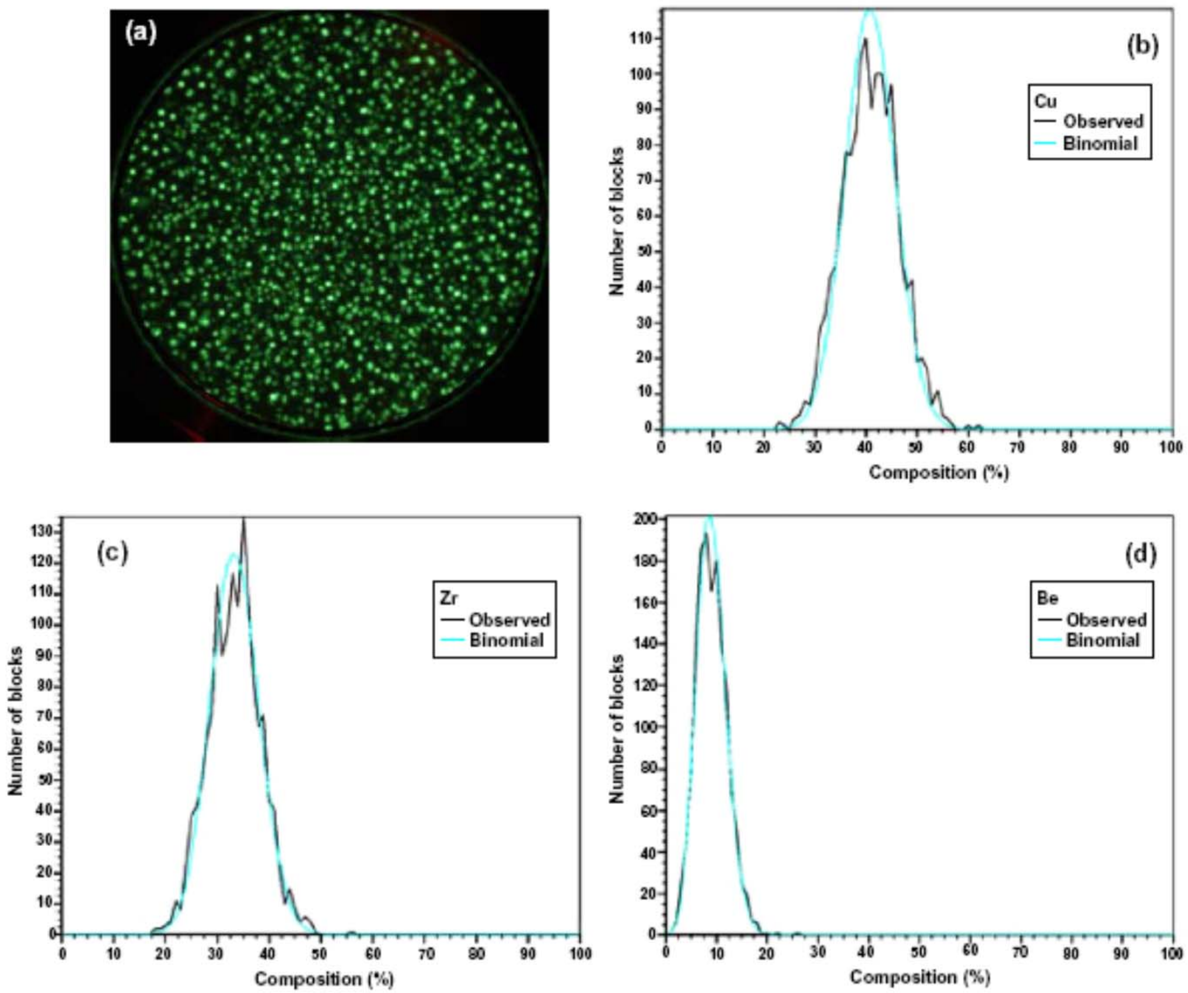

(a) FIM image and (b)-(d) composition depth profile of the as-spun $Cu_{47.5}Zr_{40}Be_{12.5}$ ribbon sample

Visualization of Atoms by FIM

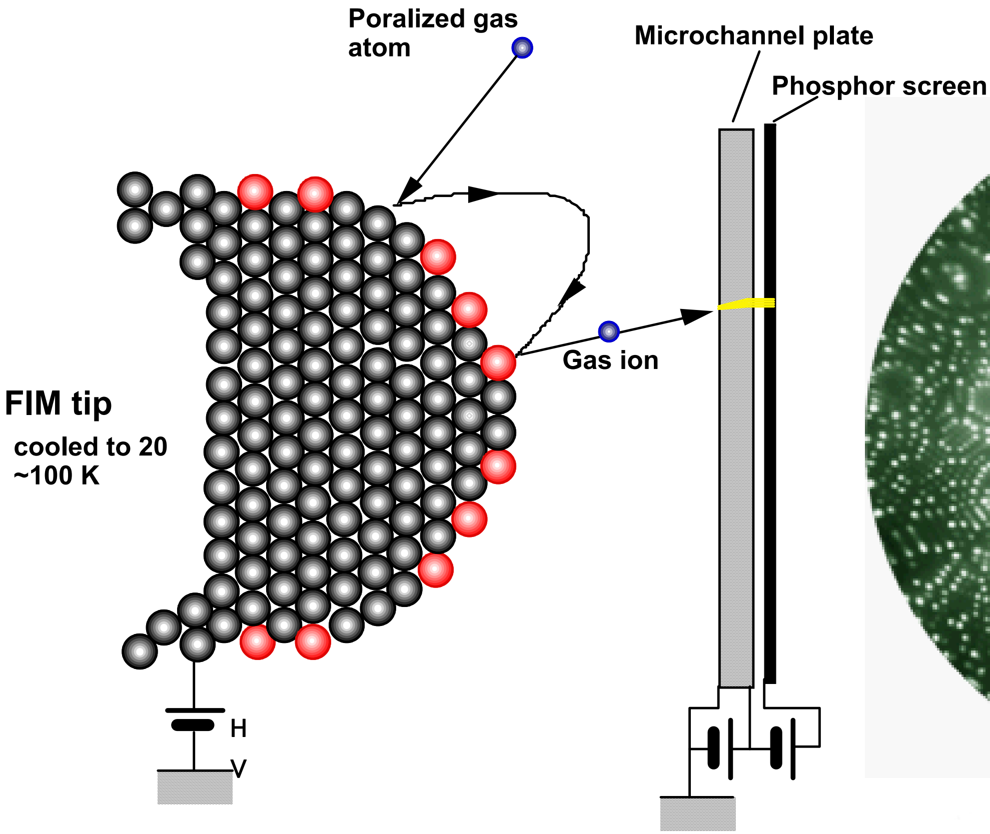

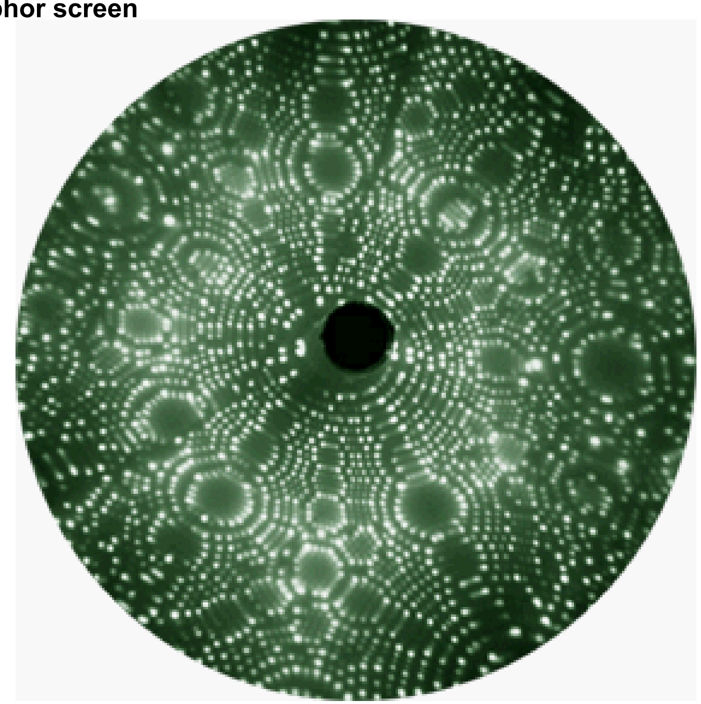

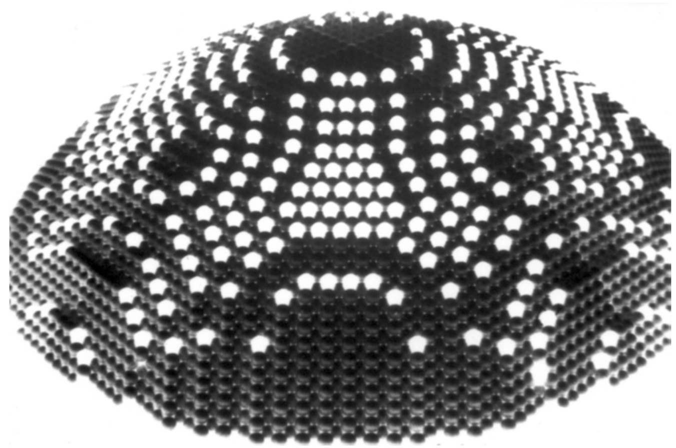

Analysis of atoms by 3DAP

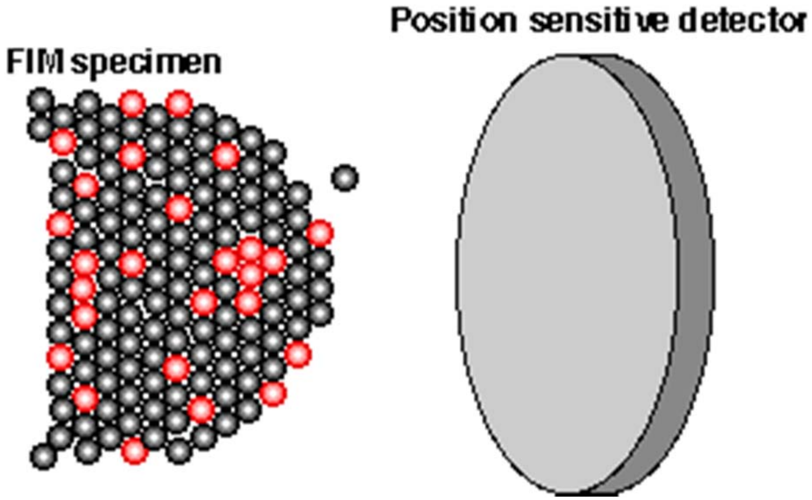

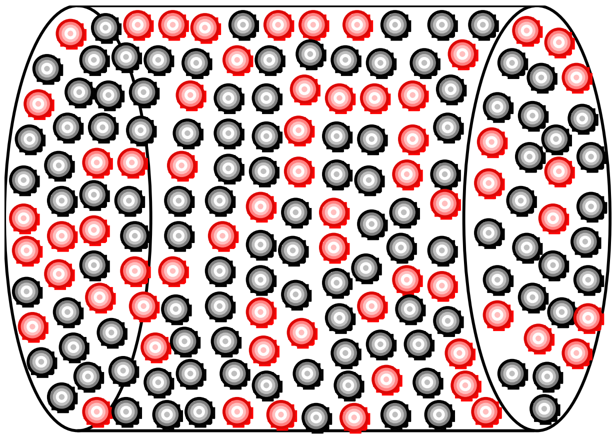

η’ precipitates in Al-Zn-Mg alloy

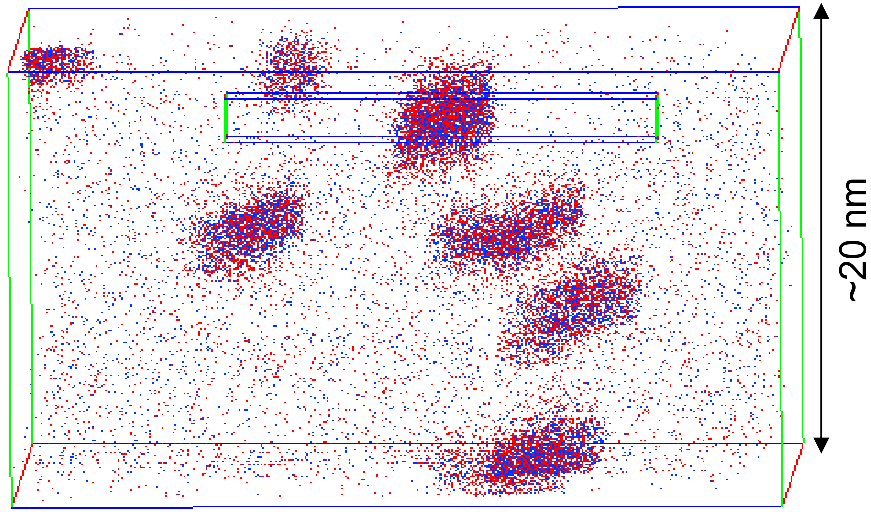

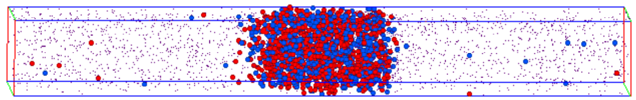

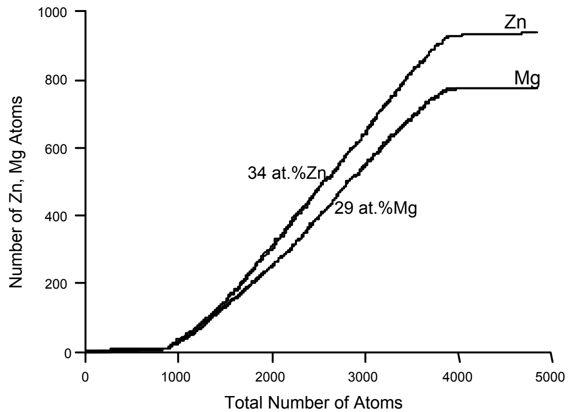

Energy-compensating reflectron lens

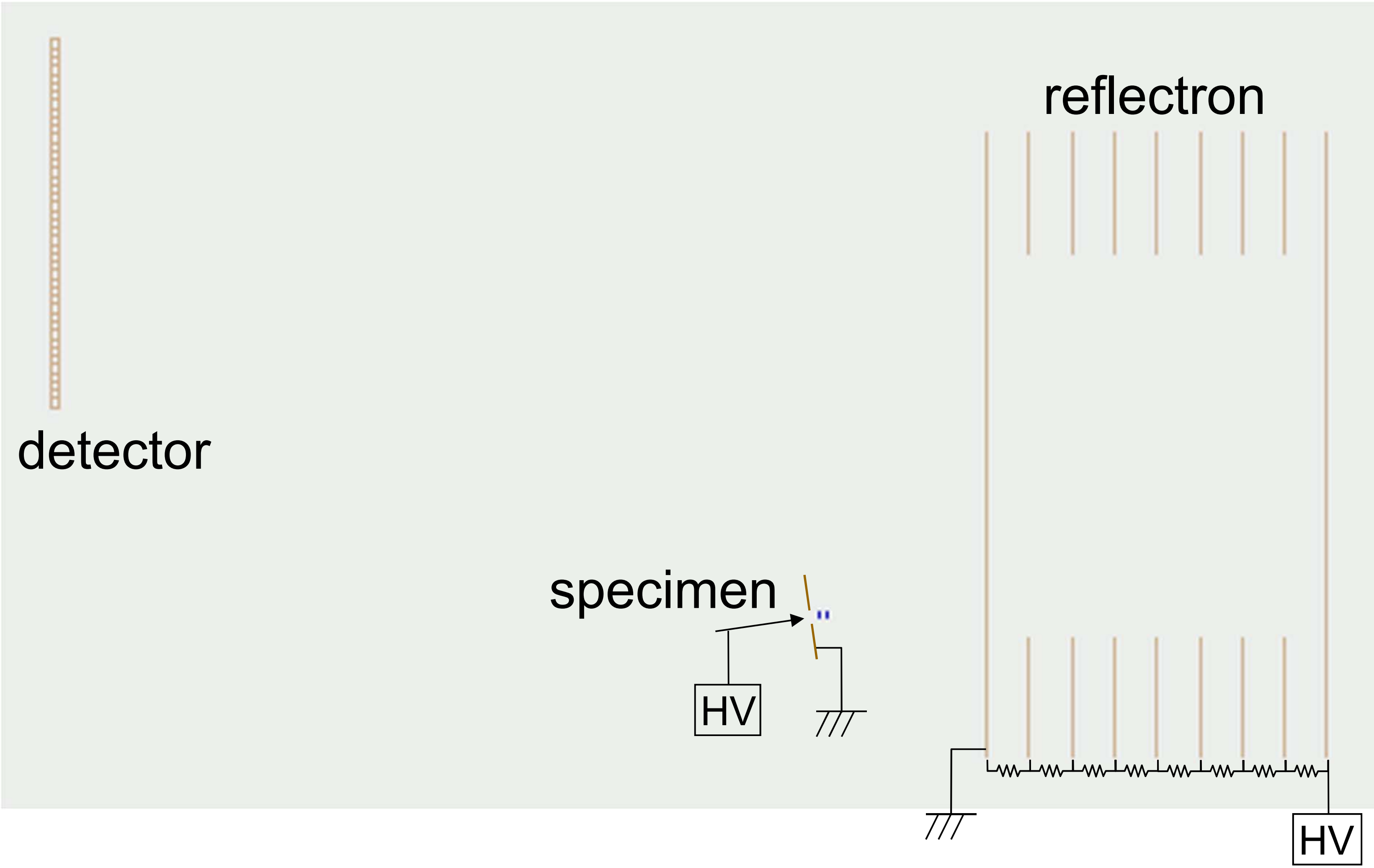

NIMS 3DAP

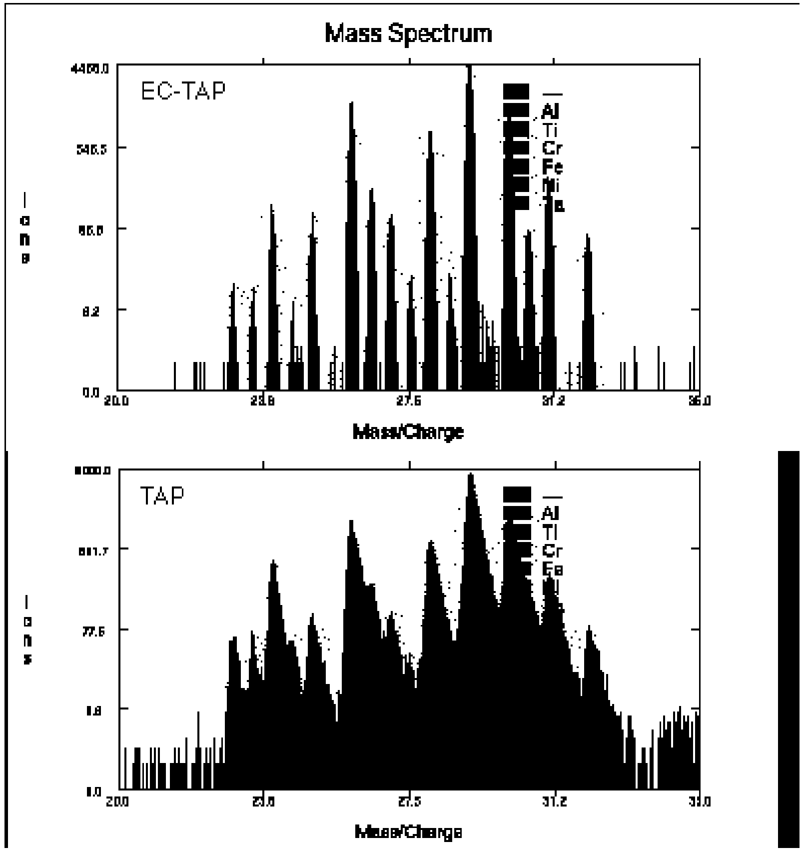
Mass Spectrum
EC-TAP
Al
Ti
Cr
Fe
Ni
Ta
Mass/Charge
TAP
Al
Ti
Cr
Fe
Mass/Charge

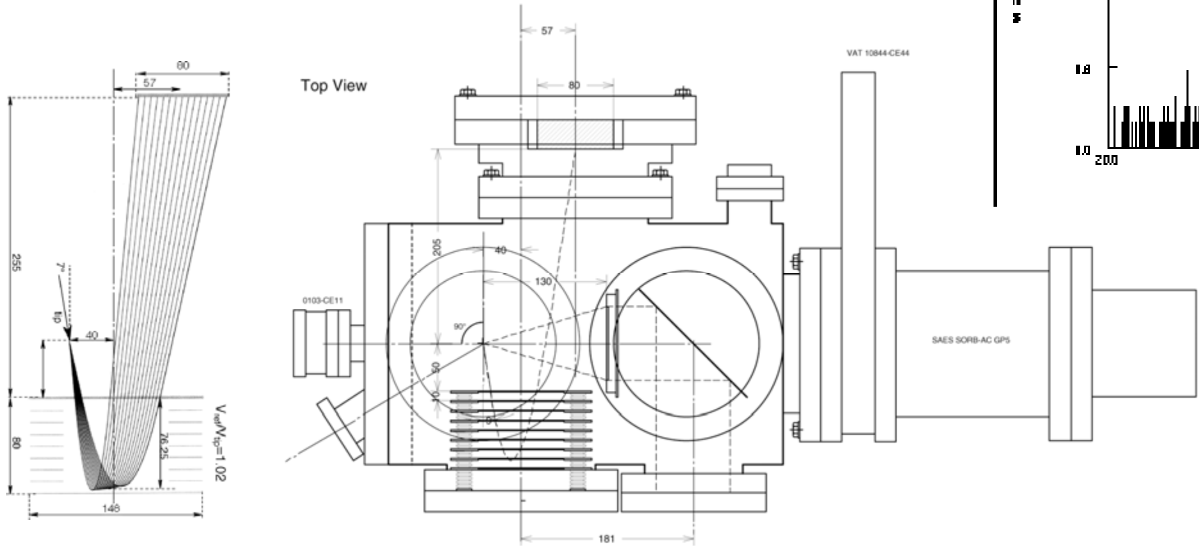
80
57
255
80
146
40
26.25
Top View
57
80
130
40
181
0103-CE11
VAT 10844-CE44
SAES SORB-AC GP5

Complementary structural analysis

Local Chemical Composition

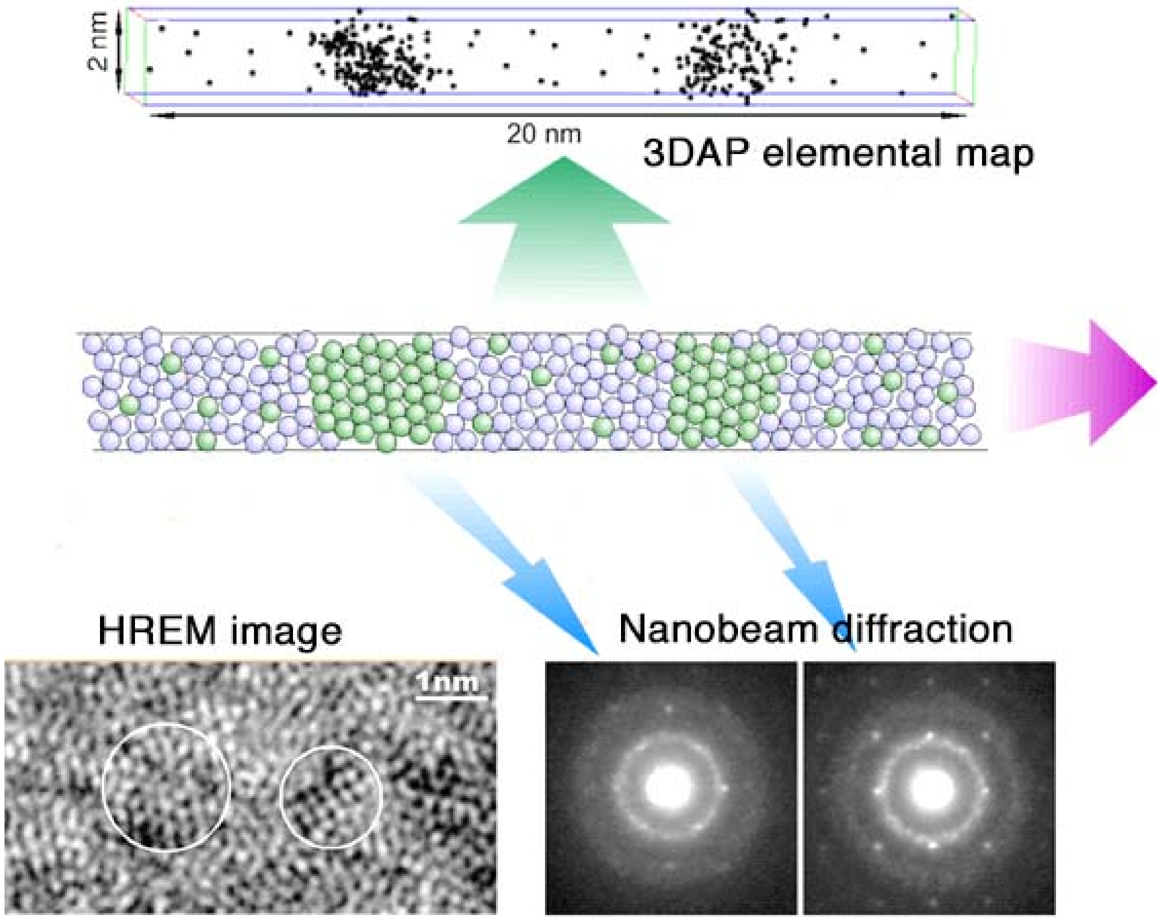

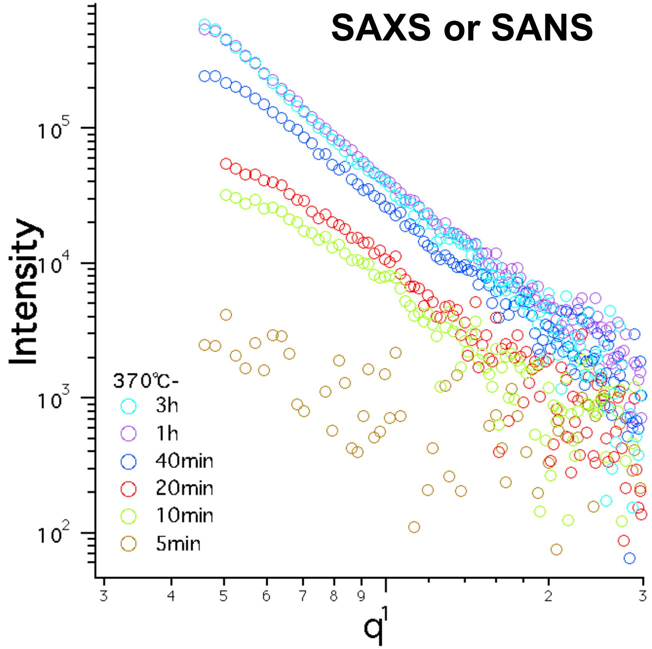

Average Scale

Local Structure

Effect of element having large different enthalpy of mixing

* Acta Materialia, 56 3120 (2008)

EXAFS analysis

	r (Å)		*N*		Total *N*	σ^2	
	Cu-Cu	Cu-Zr	Cu-Cu	Cu-Zr		Cu-Cu	Cu-Zr
$Cu_{60}Zr_{40}$	2.49	2.69	3.0	3.7	6.7	0.0116	0.0233
$Cu_{47.5}Zr_{40}Be_{12.5}$	2.51	2.70	2.5	4.8	7.3	0.0107	0.0227
	Zr-Zr	Zr-Cu	Zr-Zr	Zr-Cu		Zr-Zr	Zr-Cu
$Cu_{60}Zr_{40}$	3.10	2.68	6.9	4.4	11.3	0.0263	0.0124
$Cu_{47.5}Zr_{40}Be_{12.5}$	3.12	2.69	6.2	3.5	9.7	0.0257	0.0130

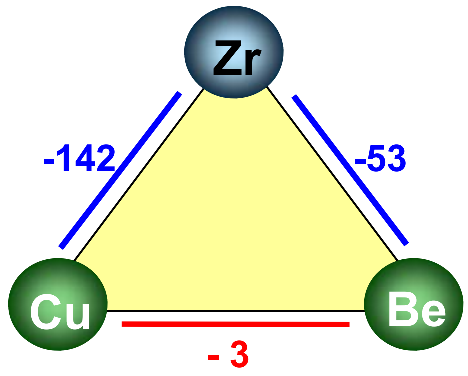

Atoimic diameter in Å: Cu-Cu = 2.56, Cu-Zr = 2.88, Zr-Zr = 3.20.

Cargill-Spaepen short-range order parameters, η

	Z_{AB}	$<Z>$	Z^*_{AB}	Z^{**}_{AB}	η
$Cu_{60}Zr_{40}$	3.7	8.540	3.416	3.546	0.043
$Cu_{47.5}Zr_{40}Be_{12.5}$	4.8	7.348	2.939	3.855	0.245

Cargill-Spaepen SRO parameter

$$\eta = Z_{AB} / Z^{**}_{AB} - 1$$

$$Z^{**}_{AB} = x_B Z_B Z_A / < Z >$$

η > 0

chemical ordering between AB nearest-neighbor pairs

d) Effect of atomic scale heterogeneity on SB nucleation

Effect of alloy composition on SB nucleation

***Ni-Nb-Zr ternary alloy system**

$Ni_{60}Nb_{40}$ and $Ni_{60}Nb_{20}Zr_{20}$ alloys

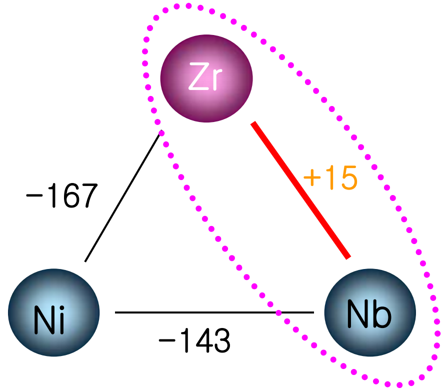

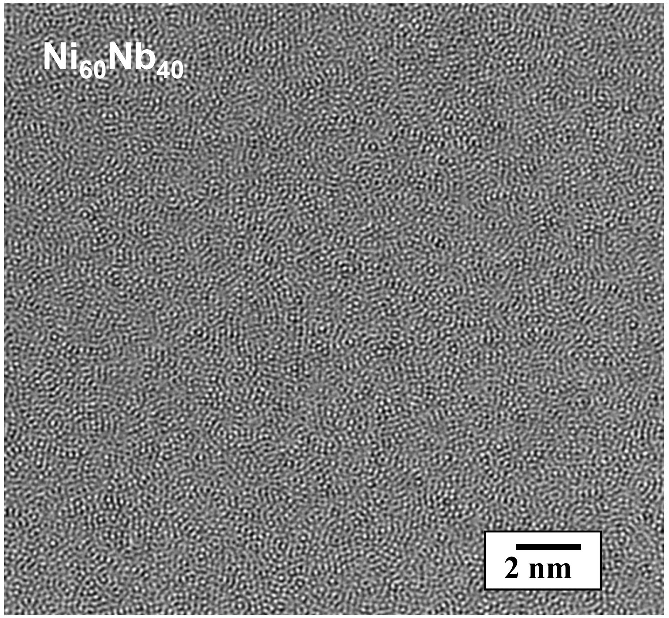

Zr addition

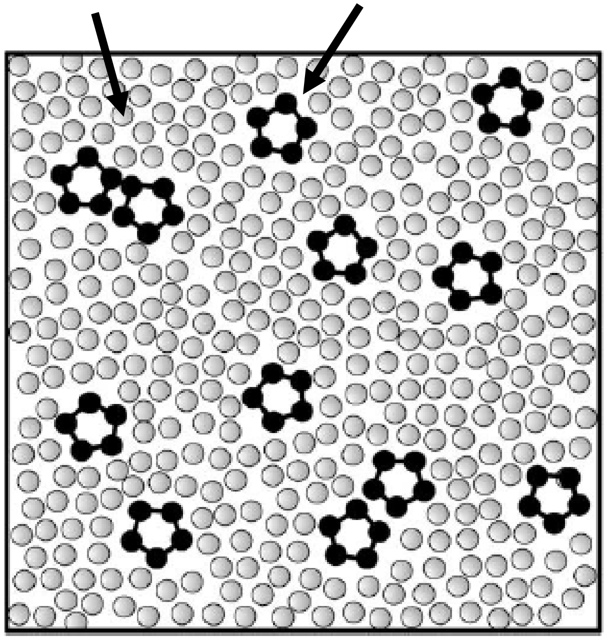

Compositional inhomogeniety

(conformed by EXAFS)

Experimental equipment

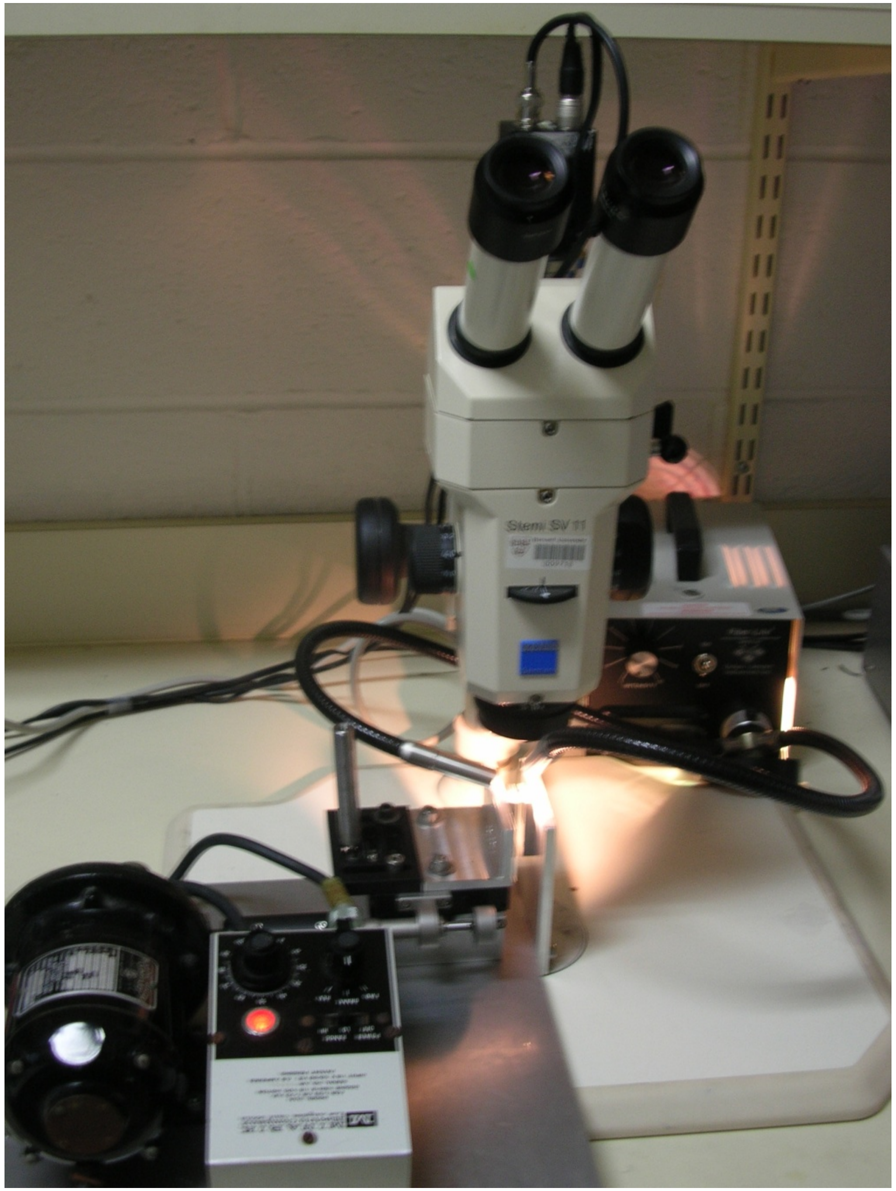

Normal camera
25 frames per sec
Interval : 0.04 sec

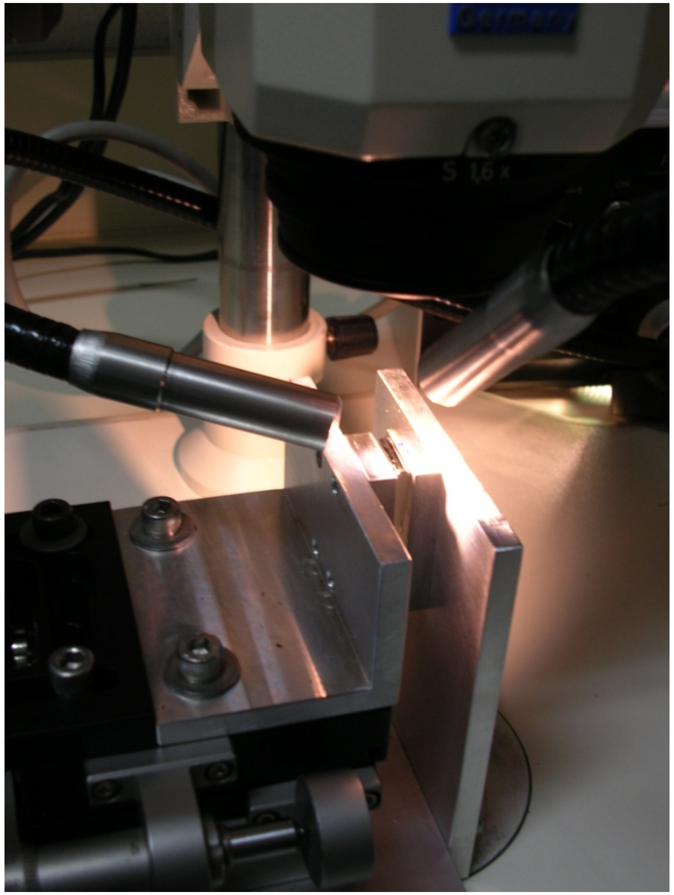

Effect of local favored structure on SB nucleation

- $Ni_{60}Nb_{40}$: fully amorphous phase

S=0.016 mm/sec

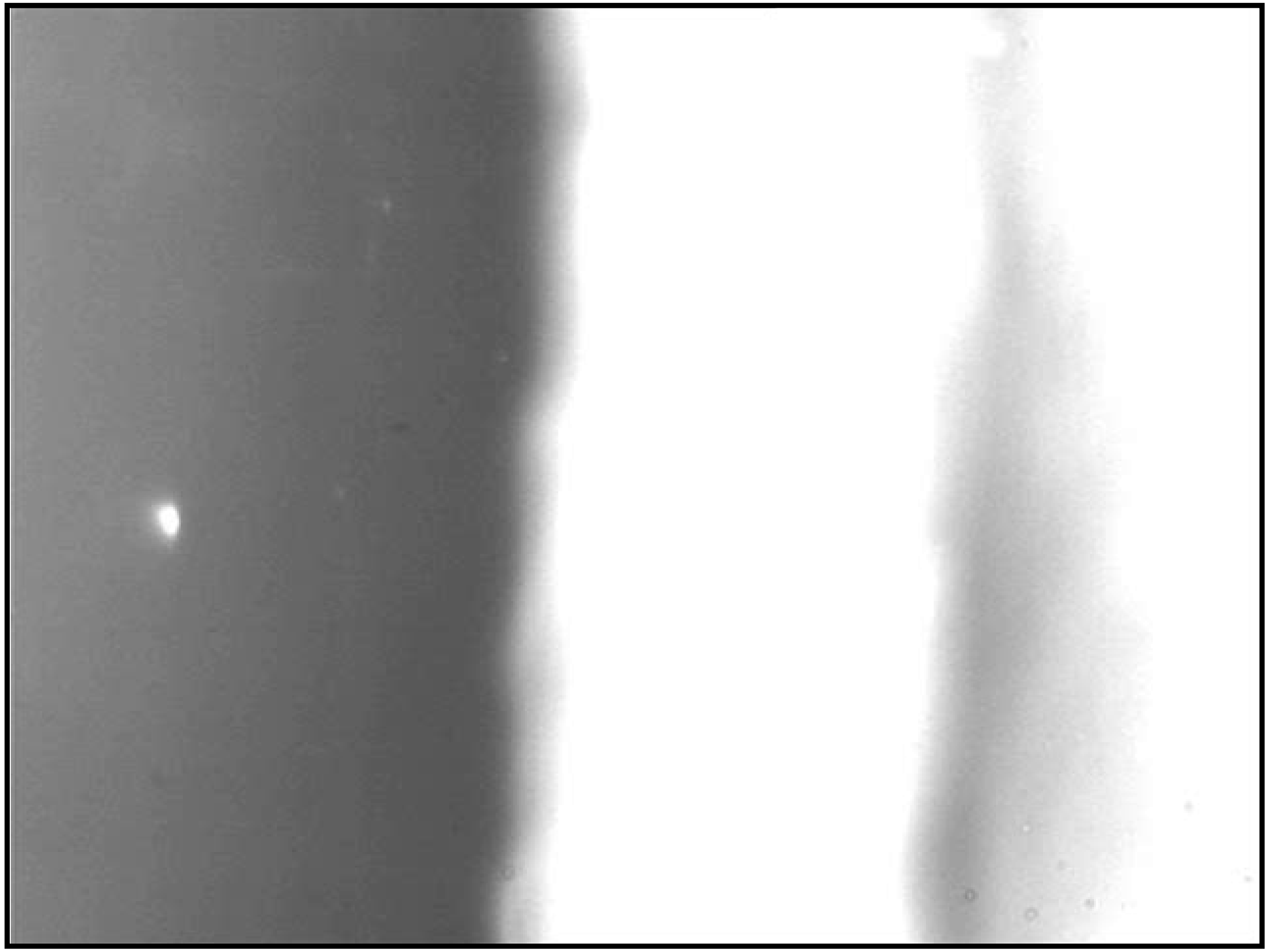

100 μm

Effect of local favored structure on SB nucleation

- $Ni_{60}Nb_{20}Zr_{20}$: amorphous phase with local favored structure

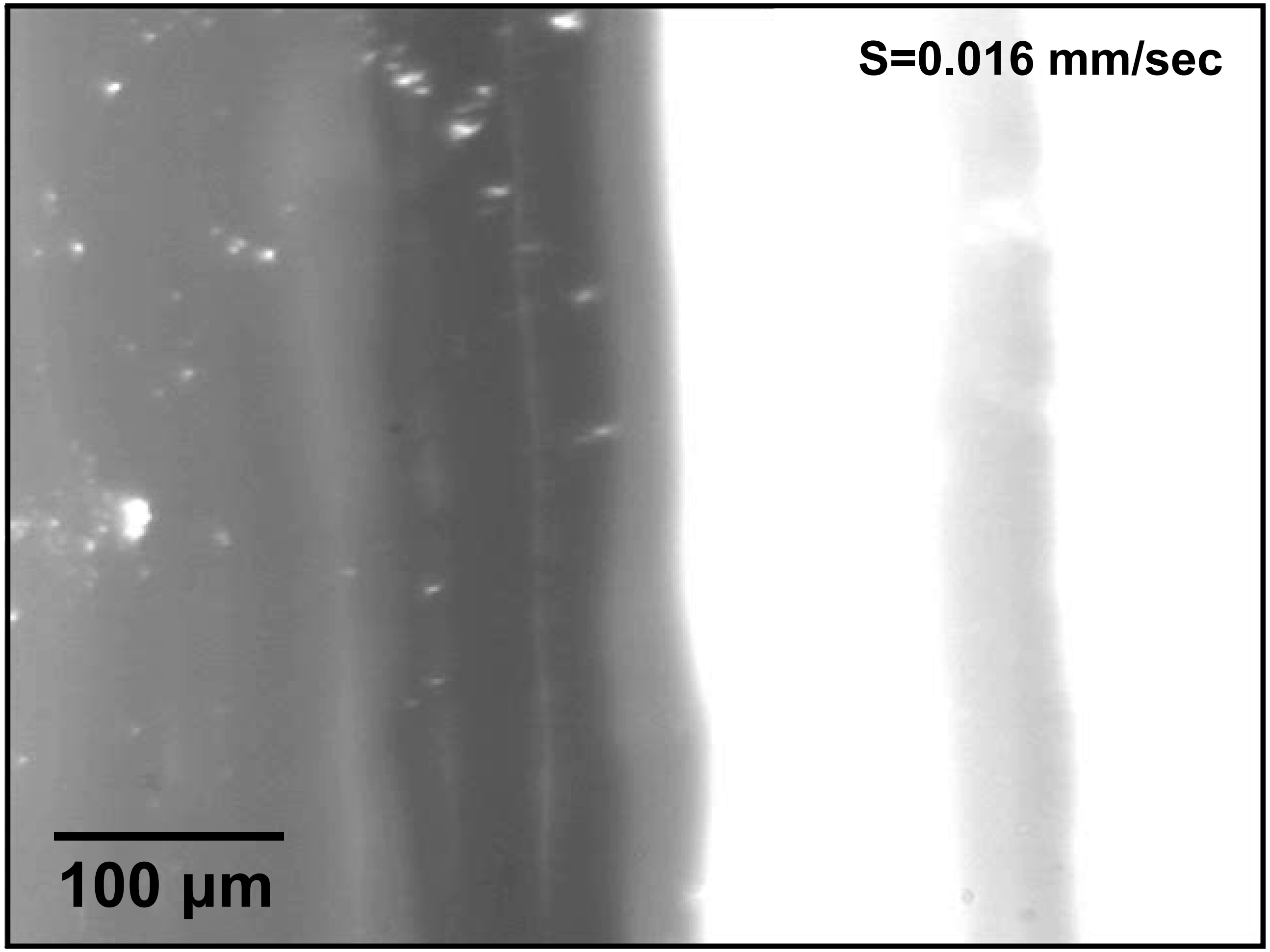

- Increased nucleation sites of shear bands

; evaluate the local heterogeneity in amorphous phase

Tailoring of structural inheterogeneity

- **Alloy design** + **Process control**

atomic scale inhomogeneity generation — Solidification under appropriate conditions

➡ **Enhanced plasticity in $Ni_{60}Nb_{32}Zr_8$, $Ni_{60}Nb_{30}Zr_{10}$ BMGs (σ_{max} : 3.2 GPa, ε_p : 2.5 %)**

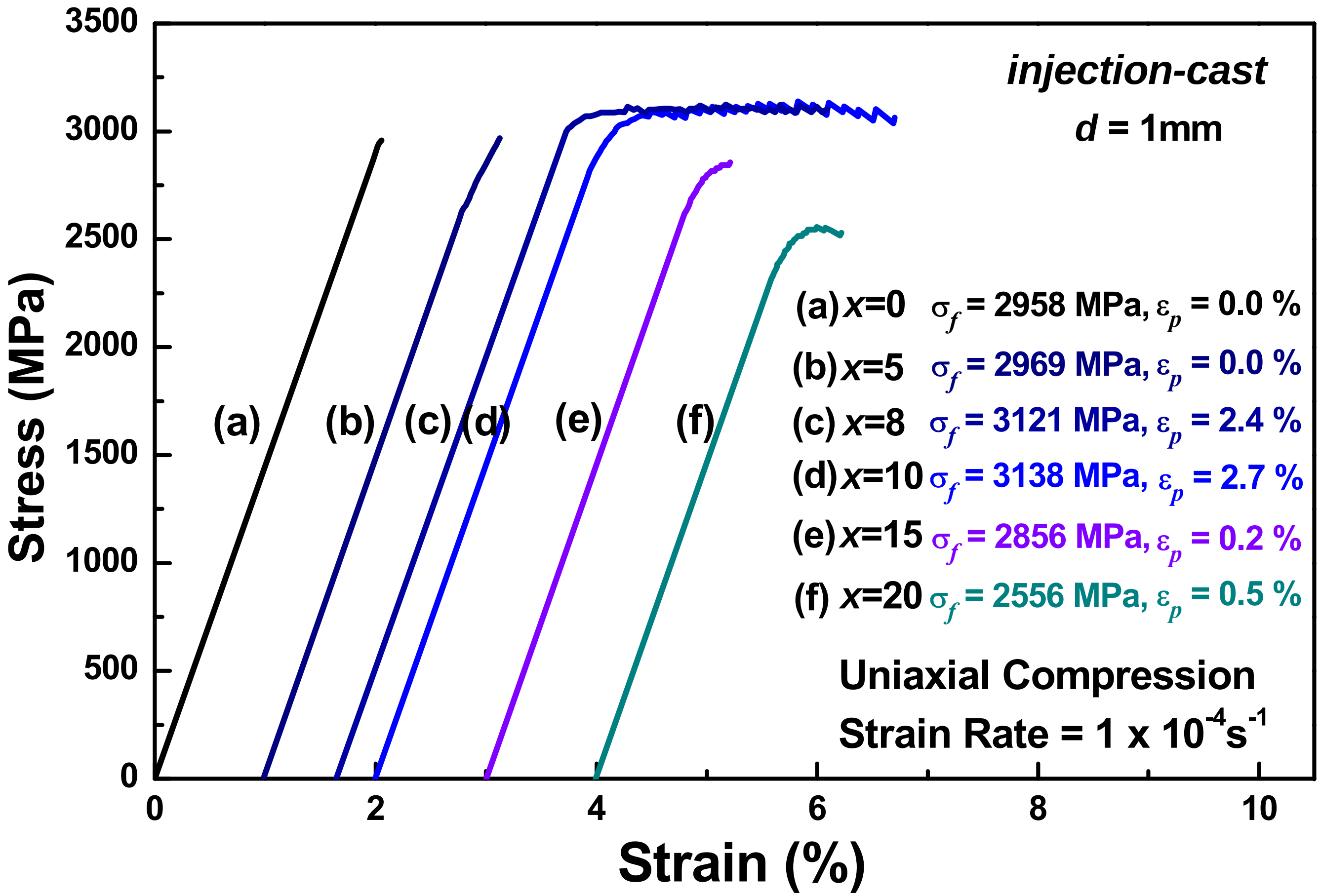

Comparison of Work-hardenability depending on 2nd Phases

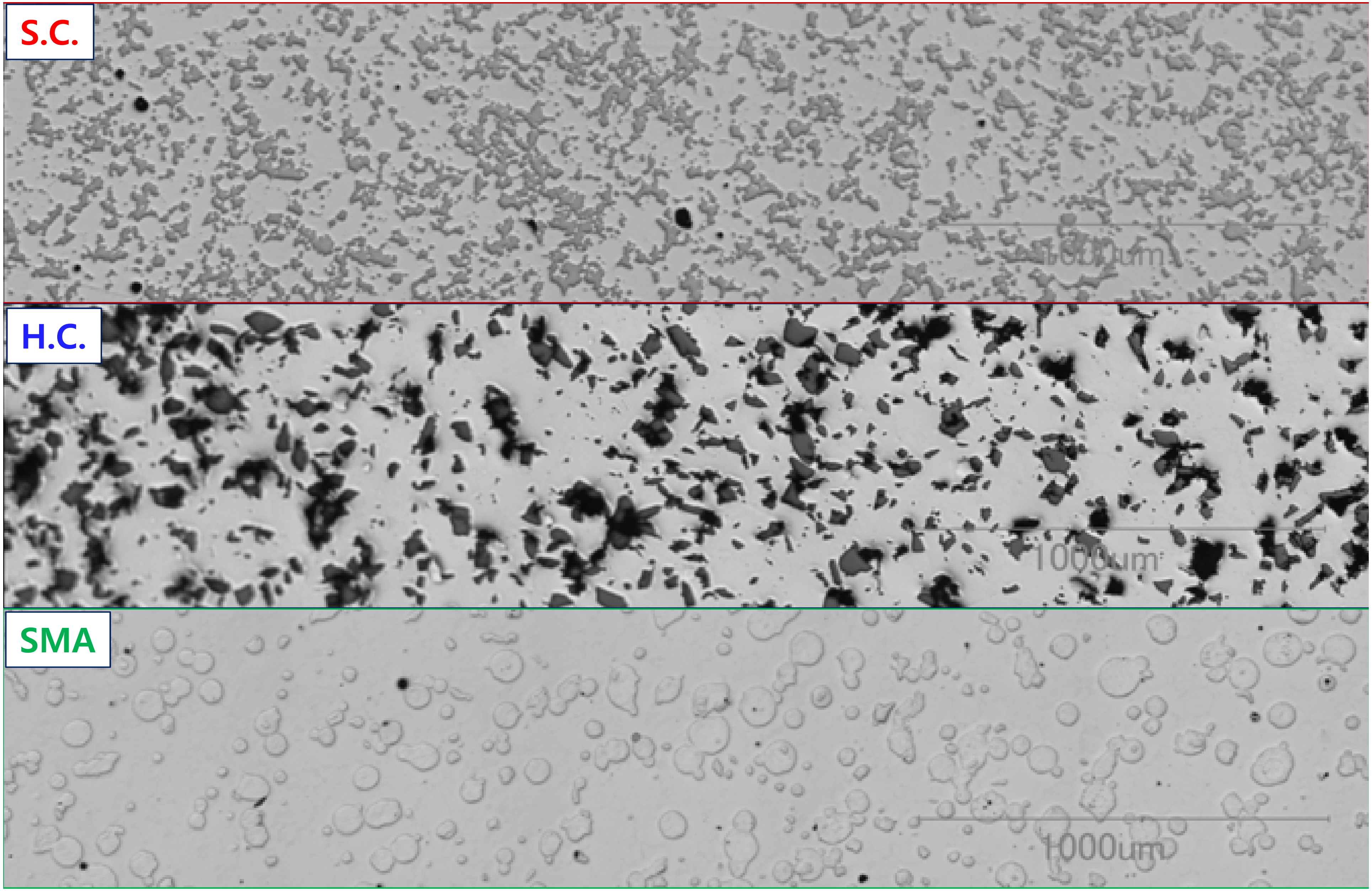

Comparison of Work-hardenability depending on 2nd Phases

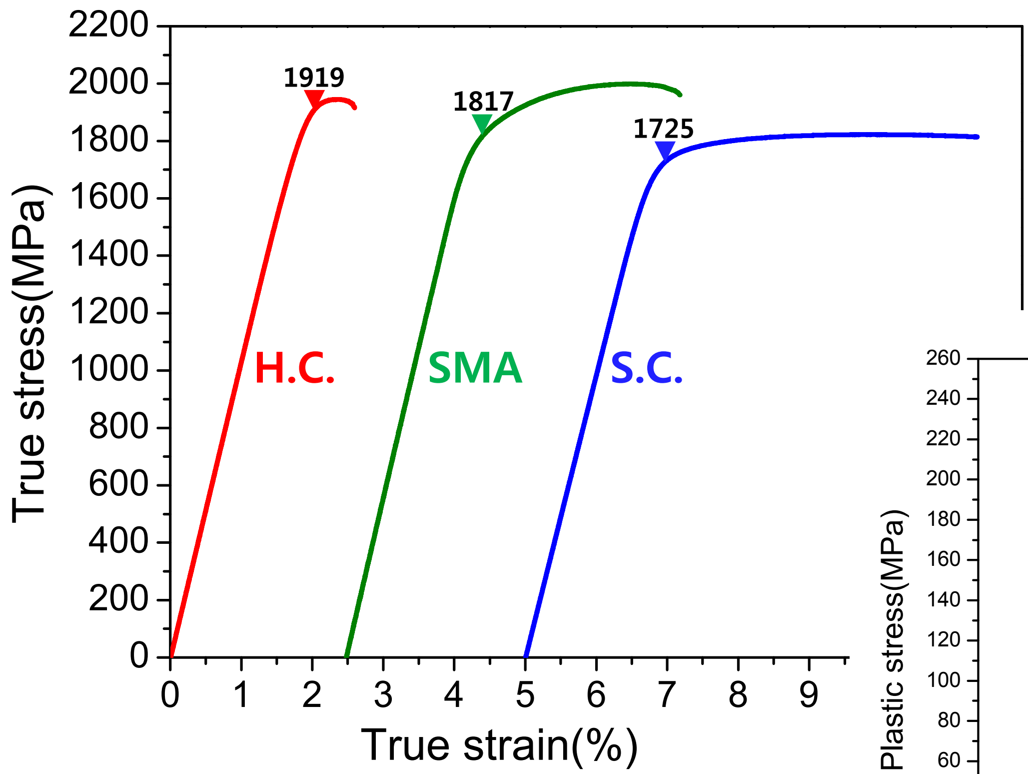

$$\sigma_p = \sigma - \sigma_y$$

$$\varepsilon_p = \varepsilon - \varepsilon_y - \frac{\sigma_p}{E}$$

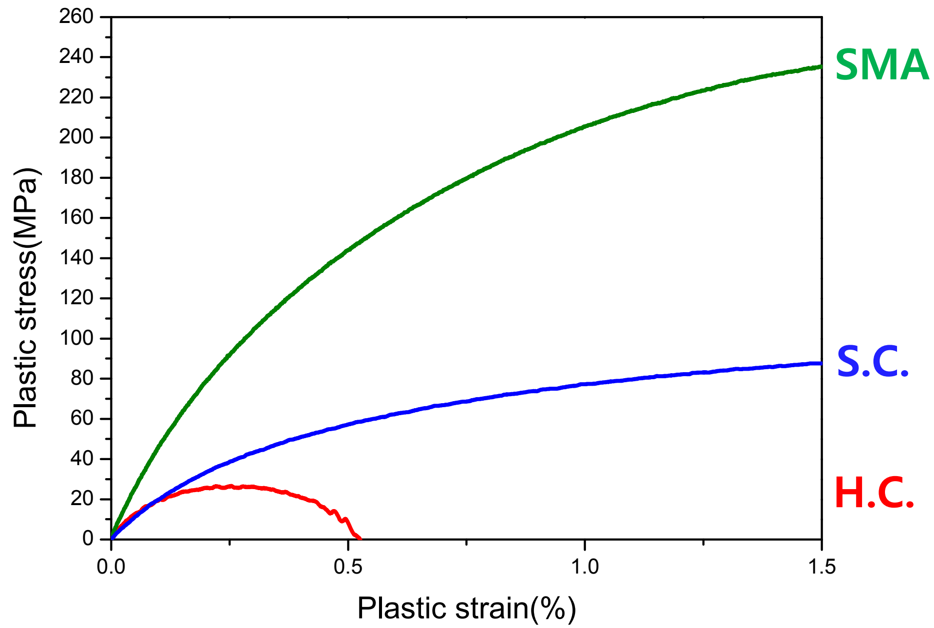

- **SMA : Strain hardening**
- **H.C., S.C. : Strain softening**

Higher strain hardening of SMA, then larger work hardenability of BMGMCs

Strain hardening(2nd) ➡ Work hardening

(SMA > S.C. > H.C.)　　(SMA > S.C. > H.C.)

Mechanism of Work-hardening in BMGC with transformable 2nd phase

"Strain hardening of 2nd phase contributes to work hardening behavior of BMGC."

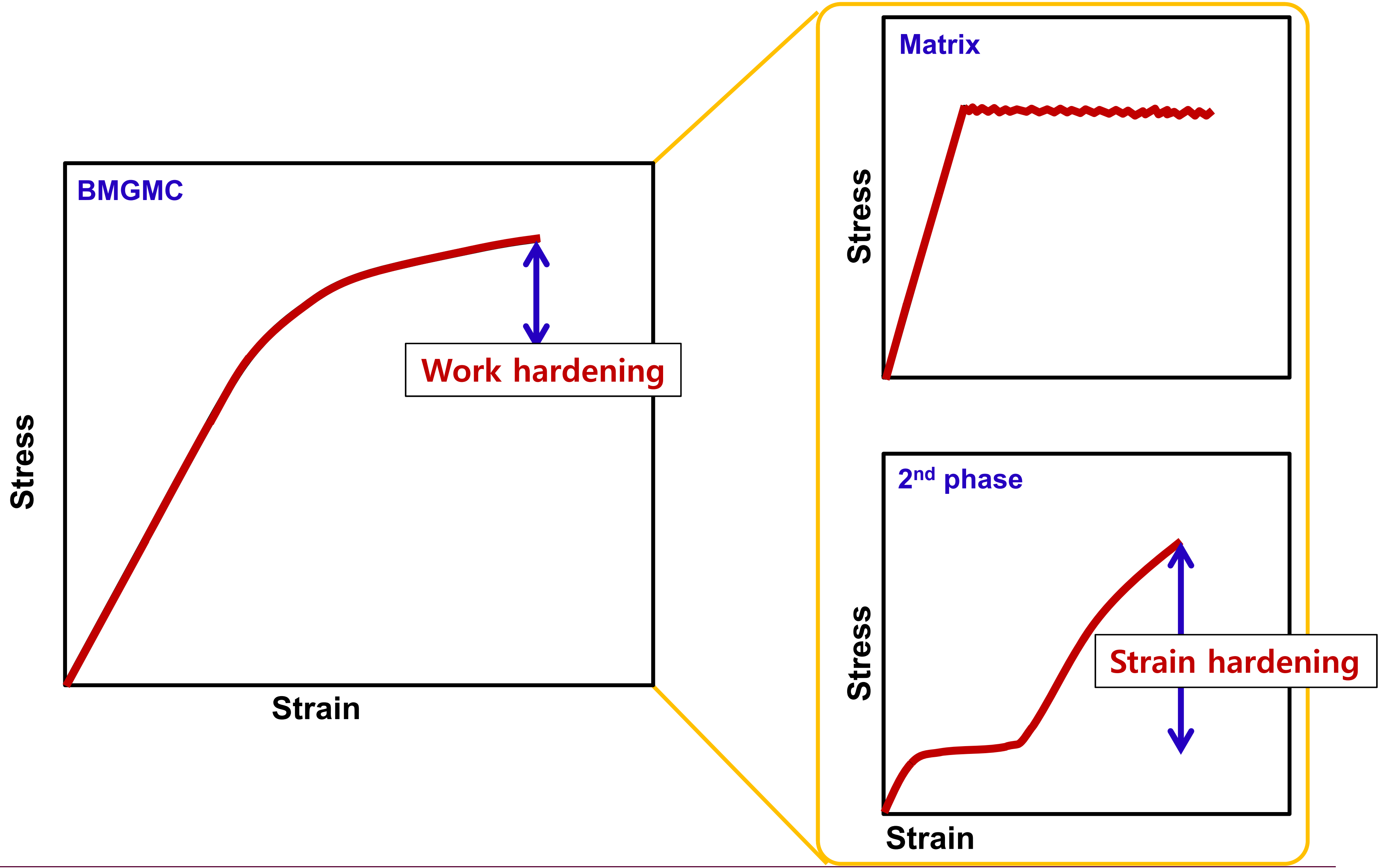

Deformation behaviors of BMGMC under compression depending on 2nd phase

Hard ceramic 2nd phase

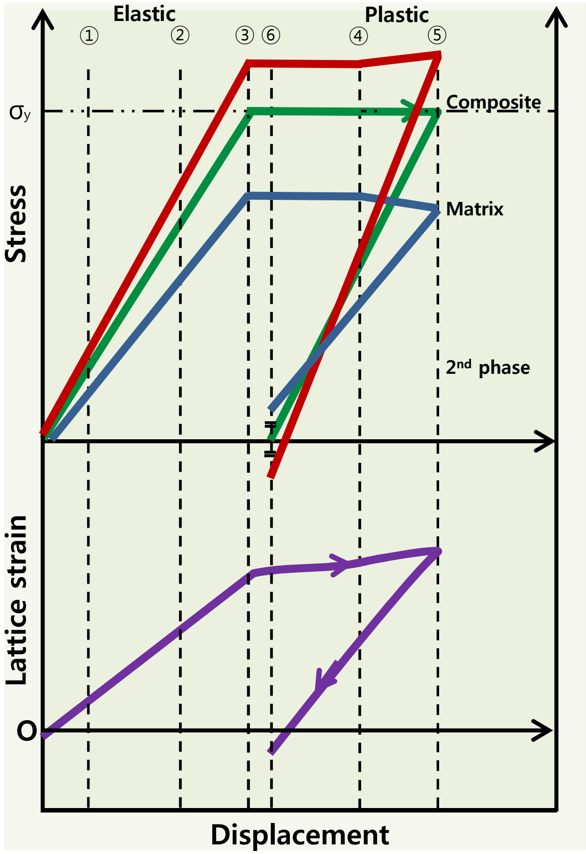

Soft crystalline 2nd phase

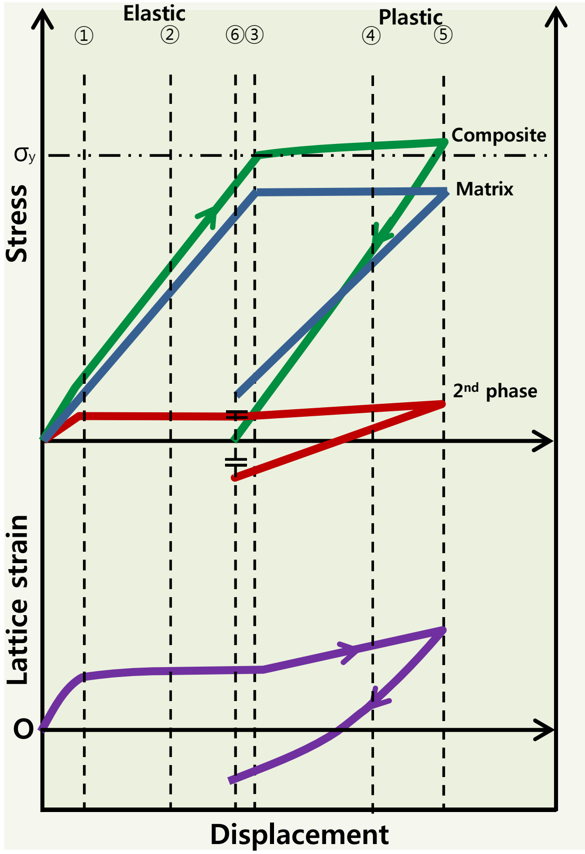

Transformable 2nd phase

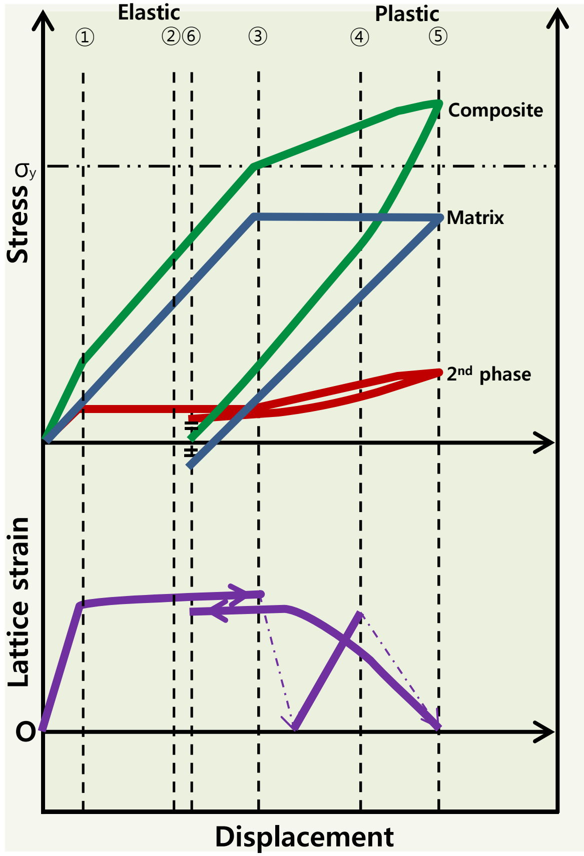

BMGMCs **Strain hardening(2nd)** ➡ **Work hardening**

(SMA > S.C. > H.C.) **(SMA > S.C. > H.C.)**

MATERIALS SCIENCE

10 SEPTEMBER 2010 VOL 329 SCIENCE

Shape Memory Bulk Metallic Glass Composites

Douglas C. Hofmann

Glass-forming and shape memory metals may provide a route to fabricating materials with enhanced mechanical properties.

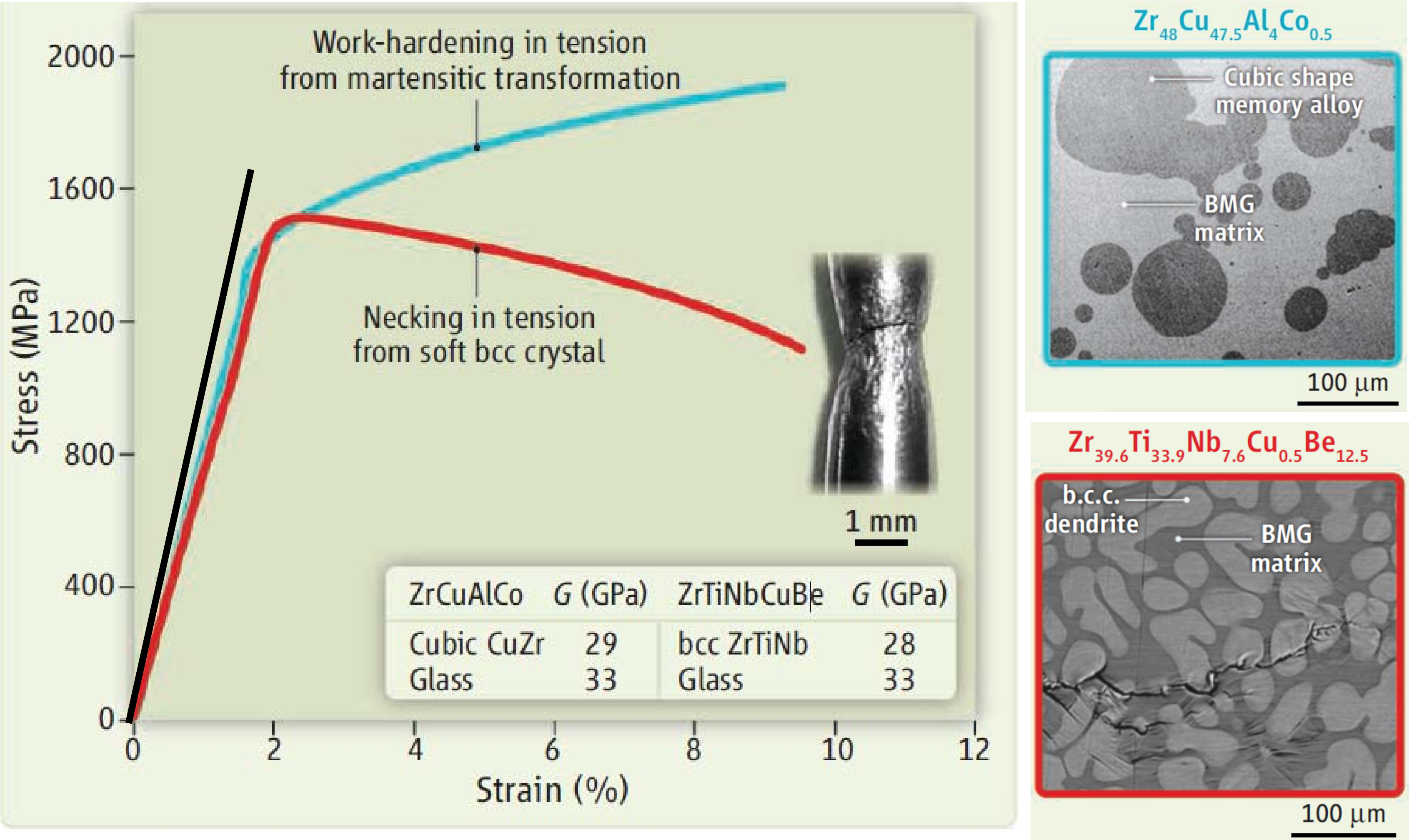

ZrCuAlCo	*G* (GPa)	ZrTiNbCuBe	*G* (GPa)
Cubic CuZr	29	bcc ZrTiNb	28
Glass	33	Glass	33

1) Work softening behavior by ductile secondary phase

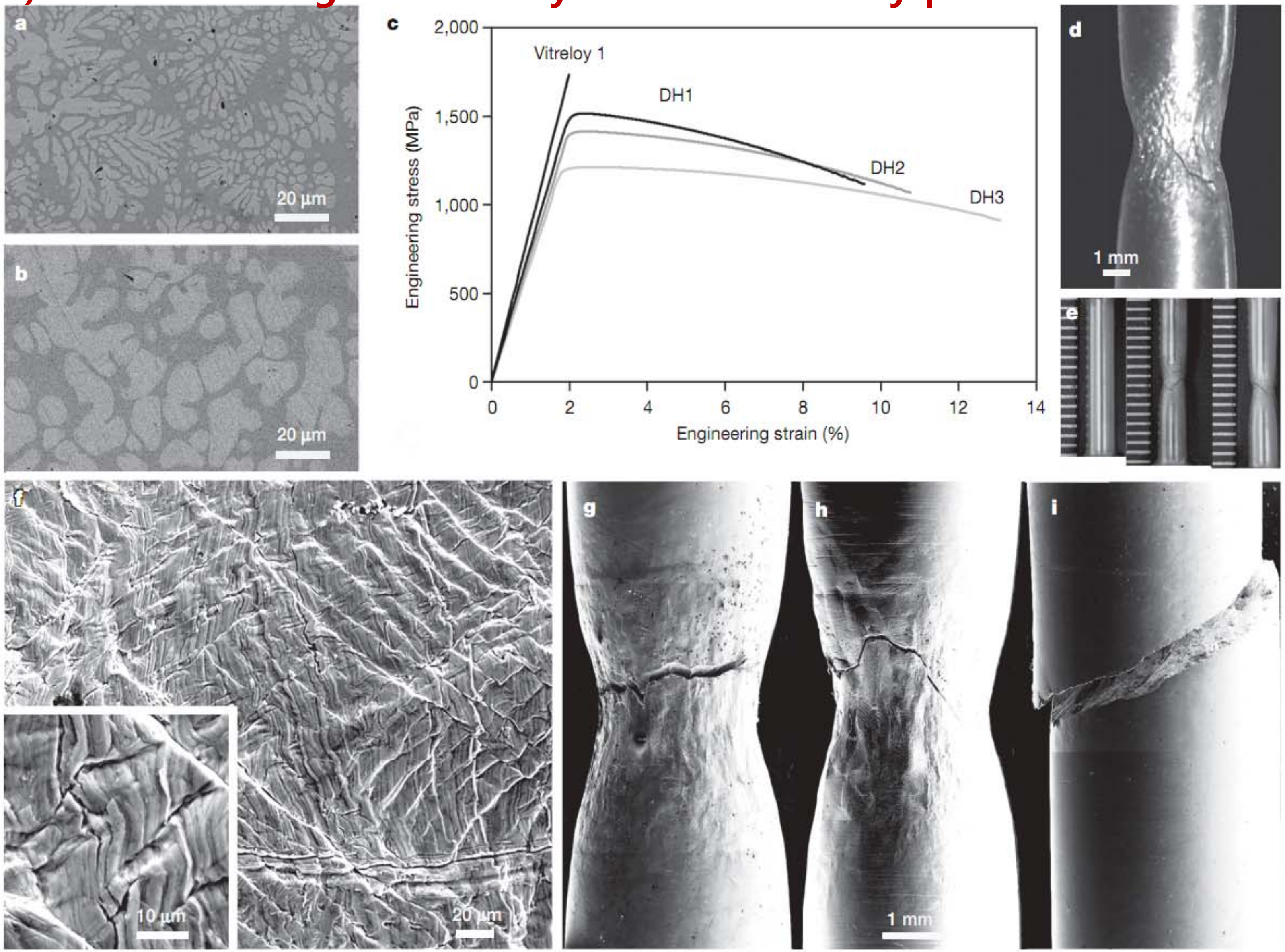

High fracture toughness: > 10 % plastic strain in tensile test

nature materials

Full text access provided to

nature.com ▸ journal home ▸ archive ▸ issue ▸ letter ▸ full text

NATURE MATERIALS | LETTER

Stress-induced phase transformation of secondary phase

Transformation-mediated ductility in CuZr-based bulk metallic glasses

S. Pauly, S. Gorantla, G. Wang, U. Kühn & J. Eckert

Affiliations | Contributions | Corresponding author

Nature Materials 9, 473–477 (2010) | doi:10.1038/nmat2767

Received 17 November 2009 | Accepted 09 April 2010 | Published online 16 May 2010

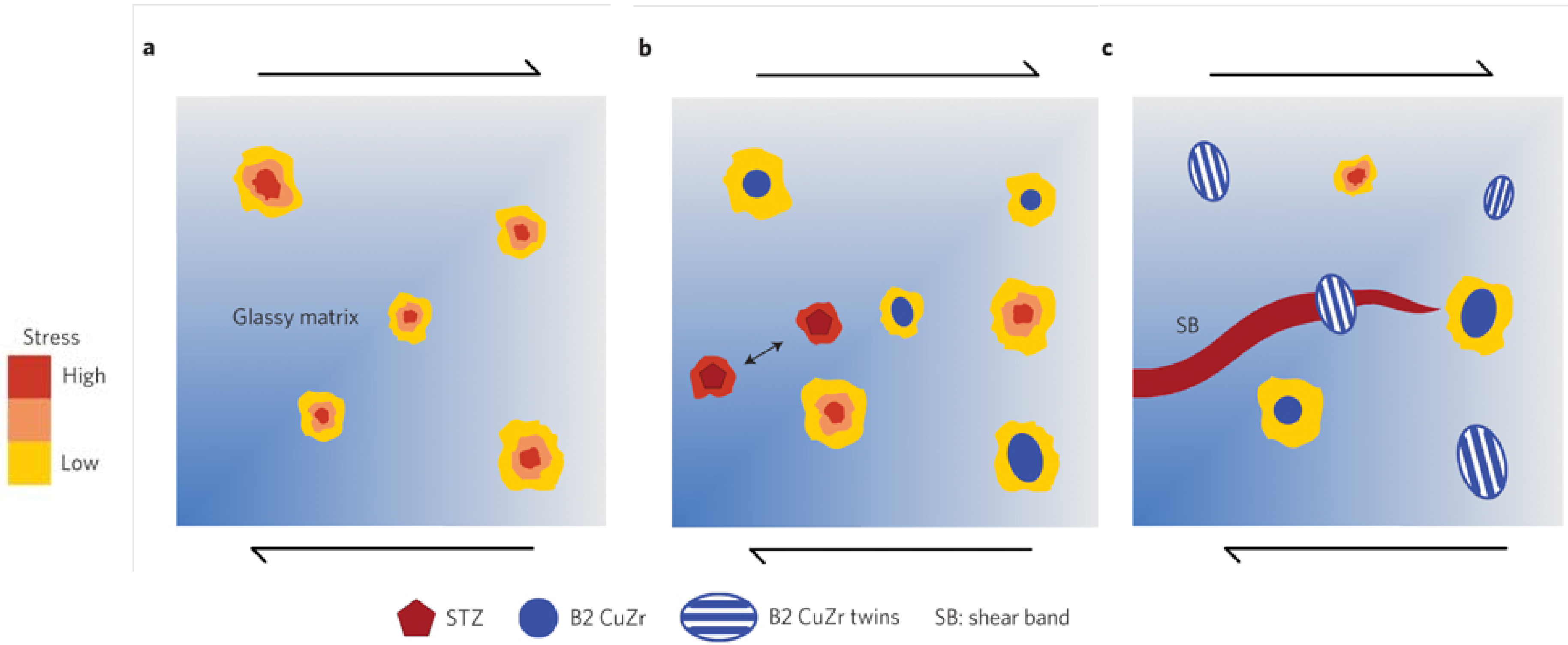

Figure 3: Microstructure of a $Cu_{47.5}Zr_{47.5}Al_5$ specimen deformed to fracture.

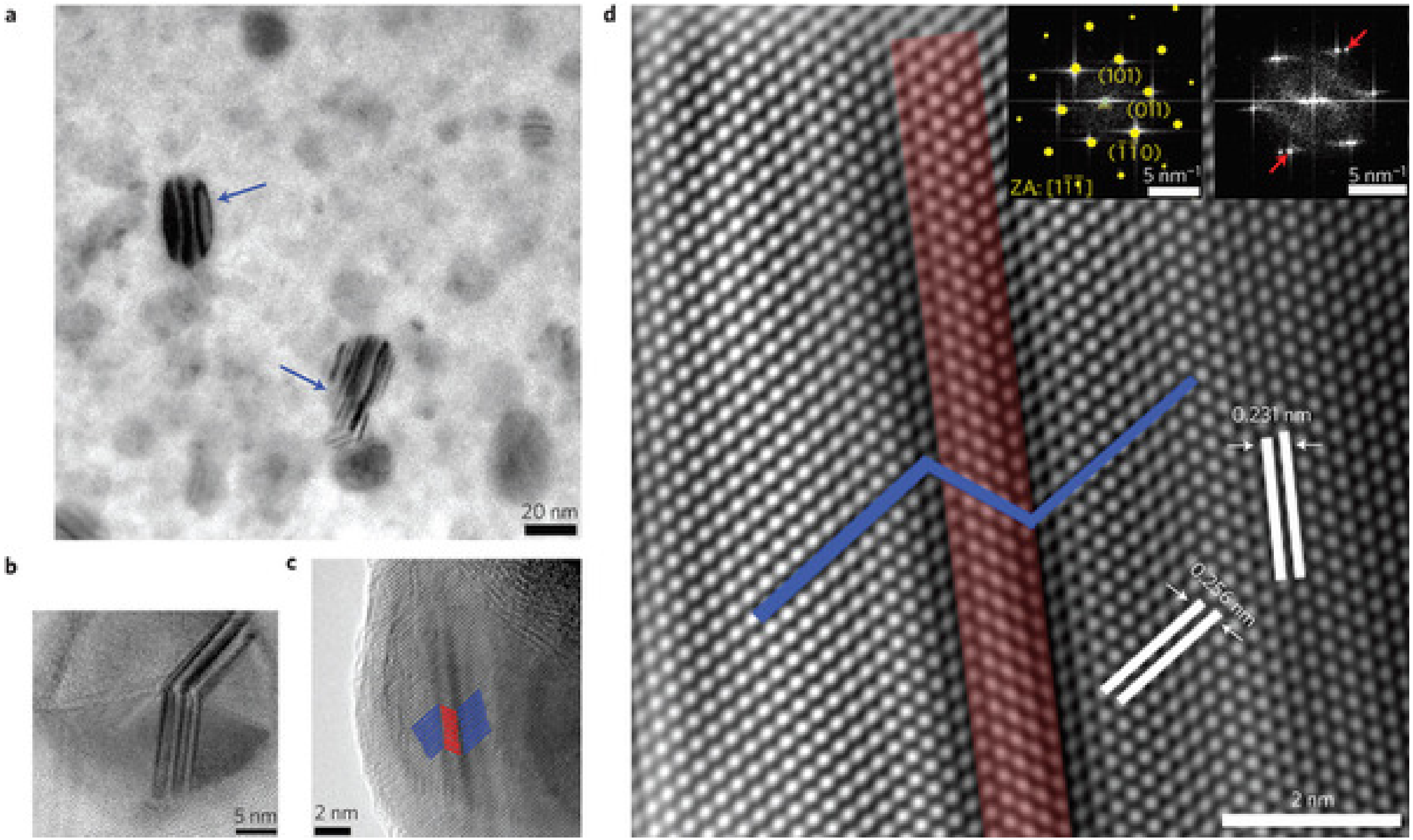

Materials Views
www.MaterialsViews.com

ADVANCED MATERIALS
www.advmat.de

COMMUNICATION

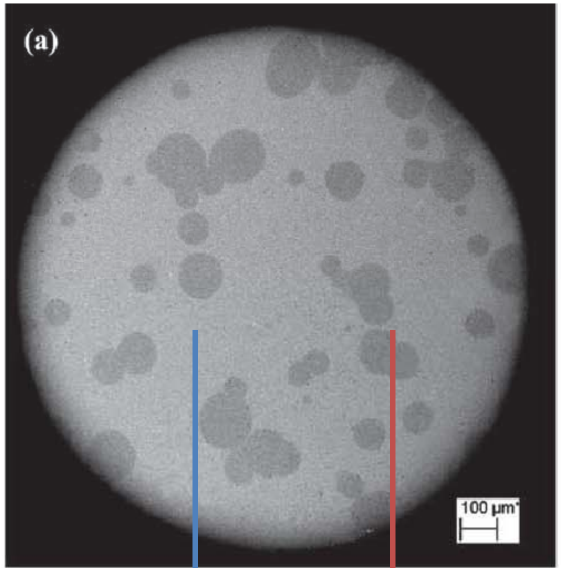

BMG matrix

CuZr B2 Transformation Media

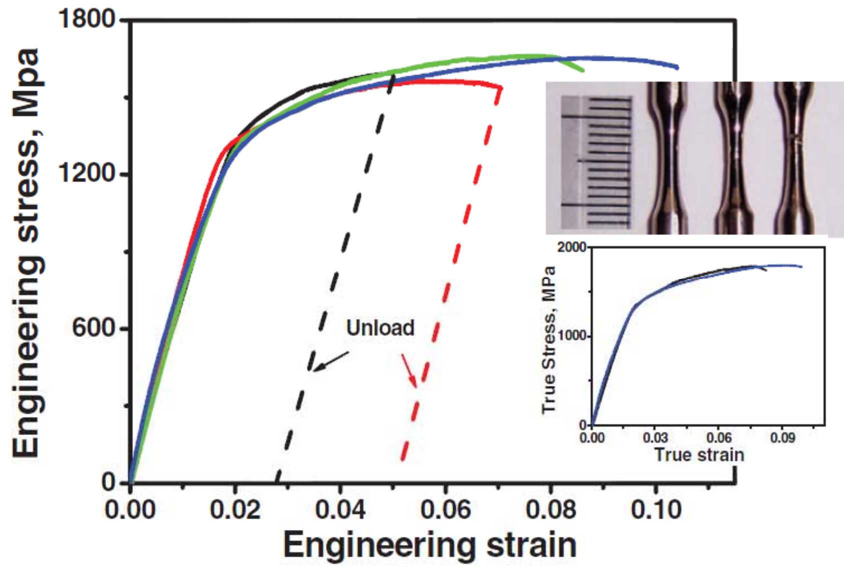

Figure 2. Engineering tensile stress–strain curves of the BMG composites. Dashed lines indicate the unloading process. Top inset shows the outer appearance of the tensile samples pre-strained at the different stages and the lower inset shows the true tensile stress–strain curves, indicating a significant strain-hardening behavior.

Z.P. Lu, et al. Adv. Mater. 2010, 22, 2770–2773

Cu-Zr-Al system